COMPUTER SIMULATION OF CARBURIZATION CORROSION OF NICKEL-BASE SUPERALLOYS

by

Hamid Ghasemi

Thesis submitted to the Faculty of the
Virginia Polytechnic Institute and State University
in partial fulfillment of the requirements for the degree of
Master of Science
in
Materials Engineering

APPROVED:

D. Farkas, Chairperson

J. L. Lytton

J. J. Brown

May 23, 1985

Blacksburg, Virginia

COMPUTER SIMULATION OF CARBURIZATION

CORROSION OF NICKEL-BASE SUPERALLOYS

by

Hamid Ghasemi

D. Farkas, Chairperson

Materials Engineering

(ABSTRACT)

A computer model for diffusion-controlled internal precipitation was used to simulate the corrosion behavior of Ni-based superalloys in carburizing atmospheres. The model is based on Crank-Nicholson finite difference solution of the diffusion equation. The code also includes the ternary cross diffusion effect due to substitutional alloying elements that are preferentially oxidized. The model can treat two sets of boundary conditions corresponding to the presence or absence of a protective oxide scale. It accounts for internal precipitation of corrosion products whenever thermodynamic solubility limits are exceeded. Up to four different carbides can be treated simultaneously. The solubility product is computed for each reaction and the amount of carbon that reacts is removed from the diffusion process. Under non-protective conditions, the predictions of model were compared to carburization profiles obtained experimentally in H_2-CH_4 environment tests. Results are presented for the

formation of Cr, Mo, Ti, W, and Nb carbides in Ni-based superalloys. The predicted corrosion profiles are in qualitative agreement with experimental data.

ACKNOWLEDGEMENTS

The author would like to thank his committee chairperson, Dr. D. Farkas, for her invaluable guidance during the course of this study. In particular, her patience and encouragement during the tedious stage of experimental data acquisition is deeply appreciated. The author would also like to acknowledge the assistance and cooperation of Dr. J. J. Brown, and Dr. J. L. Lytton for participating in the committee.

The author wishes to thank his colleagues in the department for many stimulating discussions on this subject. A warm and sincere thanks is also extended to the secretarial staff of Materials Engineering.

TABLE OF CONTENTS

List of illustrations

List of Tables

1 Introduction

The carburization of Ni-base superalloys is of interest due to the various applications of high temperature alloys that are resistant to carburizing environments. Carburization leads to a sharp decrease in ductility and creep resistance due to grain boundary precipitation of carbides. Applications include high temperature nuclear reactors and coal gasification environments.

In HTGR nuclear reactor materials reaction with impurities in the He coolant gas is a major problem. These impurities may originate from the steam cycle, graphite in the core, degassing of various materials, hydrogen permeation through the walls, among other sources. The impurities include CO, CO_2, and CH_4. In this kind of mixture carburization may occur unless a protective oxide layer is thermodynamic and mechanically stable. The kinetics of the process will be controlled by C diffusion and carbide precipitation. Correct modeling of the kinetics is essential in the selection and design of materials for these applications (1).

In a recent work (3) a computer formalism was developed to predict carburization profiles in alloys. The algorithm was applied to the behavior of Ni-Cr steels and one superalloy. The purpose of the present work is to apply the formalism to a more complex case and analyze the carburization

thermodynamics and kinetics of the Ni-Cr-Mo, Ni-Cr-Ti, Ni-Cr-Nb, and Ni-Cr-W systems where more than one carbide can be formed. In particular, the effect of composition on the distribution of carbides and total C content is analyzed. The predictions of the model are compared to experimental results reported by other investigators on the Ni-Cr-Mo system and superalloys tested in H_2-CH_4 environment for 1.0 carbon activity at 850°C in the present work. The model can be used to predict the carbide penetration depths and maximum carbide level for different alloys. The model can also predict the formation of four different carbides in a system, and obtain the carbon uptake for each system.

2 Review Of Experimental Work

There is extensive work reported in literature regarding the measurement and calculation of carburization profiles in iron base superalloys (1,2). Bongartz (1) has determined the carbon concentration profiles by combustion analysis (LECO-IR12) on layers skin-machined from a cylindrical specimen. Farkas et al. (3) have carburized some preoxidized superalloys and have obtained good agreement with their calculated profiles.

In HTGR, materials reaction with impurities in He coolant gas is a major problem. The impurities are mainly CO, CO_2, CH_4, H_2O, H_2, and O_2. In this kind of mixture, oxidation, carburization, and decarburization may occur. Extensive experimental work has been done in simulated impure He (4-11) using various techniques, such as EPMA, IMMA, radioactive tracer, etc. The materials investigated are mainly nickel-base superalloys containing Cr and other alloying elements such as Mn, Mo, Ti, Al, Co, Nb, Si, W, and Fe. Table (1) shows the composition of some of the alloys tested. The influence of the alloying elements on the corrosion behavior of the alloy is very complex and depends on the environments. For example, in impure He, it is reported that Si has a determental effect (7) whereas for higher oxidation potential it prevents carburization by forming an

Alloy	Cr	Mo	Ti	Al	Co	Nb	W	Fe	Ni
Incoloy 800	20	-	.5	.3	-	-	-	B	32
Hastelloy X	20	9	-	-	2	-	.5	-	B
Inconel 617	20	9	.5	1	12	-	-	2	B
Nimonic PE16	16	4	1.3	1.5	-	-	-	34	B

Table 1. Composition of the alloys studied in atomic percent.

oxide layer (12).

Shikama et al. (13) have studied the corrosion behavior of Inconel 617 in hydrogen base gas mixture (80pct H_2 + 15pct CO + 5pct CO_2). This gas mixture simulates the reducing gas in the direct steel making system that use heat from HTGR in Japan. In temperature range 650 to 1000 C Inconel 617 oxidized to form Cr_2O_3 scale containing Ti oxide. The experimental results have shown that cr and ti were oxidized externally and Al was oxidized internally. Alloys containing Mn may form Mn oxide as the outer scale. Figure (1) shows the schematic structure of the corroded layers according to several investigators (13). This means that Al in the concentration ranges normally present in superalloys does not form a protective layer. On the contrary, it contributes to the intergranular process.

The high oxidation potential here limits the carburization process, and weight gains of specimens were mostly due to the oxidation, and showing the contribution of carburization to the weight gain negligible at 900 C to 1000 C. With the formation and growth of a protective oxide surface scale, carburization would be restrained (13,14). After 100 and a few tens hours exposure, carburization would not be developed any more and the higher concentration of carbon in the near surface region would be obscure because of diffu-

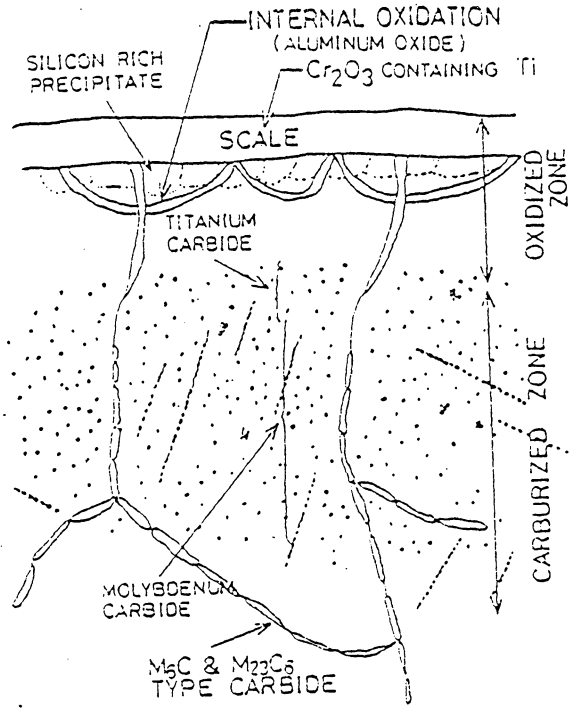

Figure 1. Schematic presentation of the microstructure of the cross section of Inconel 617 exposed to the test reducing gas at 900°C for up to 200 h.

sion. Nickel and iron base alloys which contained Cr and Mn enough to form protective surface oxide scale had resisted being carburized to some extend in the atmospheres where oxidizing potential was relatively high. In these cases carburization did not develop after 100 hours exposure. Carburization of the alloys could not be restrained in the atmosphere which had the high carburizing potential and low oxidizing potential (15). Shikama et al. (13) also determined a parabolic growth law of oxide layer. In carburizing of Hastelloy alloy X, Muraoka et al. (14) reason that the cause of enhancement of carbon penetration into the alloy in helium gas is the fact that the oxidation of a grain boundary enhances the grain boundary diffusion of carbon. They also reported that the grain boundary was selectively oxidized and was depleted in Cr in their test of Hastelloy alloy X.

Typical results also have been reported by Muraoka et al. (14), where carbon penetration profiles were influenced by the Helium gas and oxidation process as shown in Figure (2). The decrease of the carbon concentration at the surface (i.e., uphill diffusion) is attributed to lower carbon solubility in oxide film (mainly Cr_2O_3) than in metal substrate. Comparison of the penetration profiles in vacuo and helium gas indicates the oxygen in helium gas causes

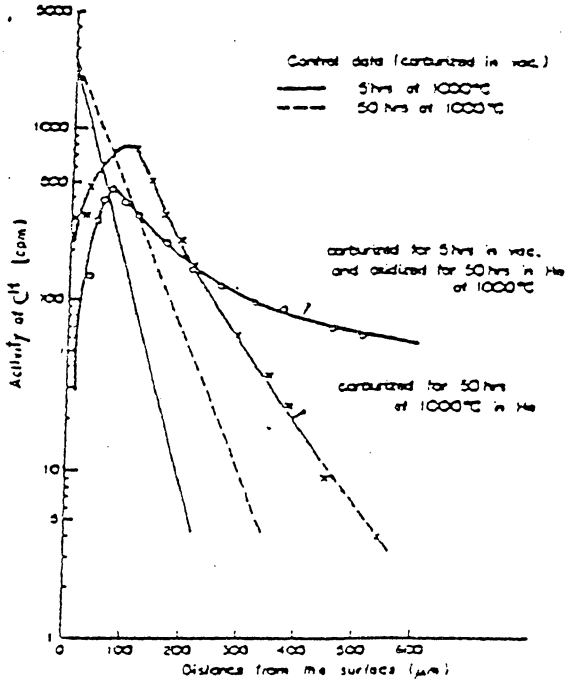

Figure 2. Penetration profiles of C in Hastelloy X.

decarburization at the specimen surface and enhances carbon penetration (diffusion) into the metal substrate.

Muraoka et al. (14) have also carried out diffusion-annealing of specimens over the temperature range 700 to 1100 C for 1 to 100 hours in vacuo. Figure (3) shows these results. In these figures the behavior of the near surface region seem to be due to the precipitation of large amount of carbides which are formed by excess carbon. In these regions the logarithmic concentration decreases with the squares of the distance from the surface, which considered to indicate as domination of volume diffusion in these regions. When grain boundary diffusion is dominant, the logarithmic concentration decreases linearly with distance from the surface. Therefore, in most cases the near surface region is characteristic of volume diffusion, while region far from the surface appears to be controlled by grain boundary diffusion (14).

Hirano et al. (6) have also studied the carburization of some nickel base superalloys in simulated HTGR helium, and thier results suggest that the carburization and decarburization depend strongly on the superalloys and the helium gas. They have reported that the degree of corrosion on Inconel 617 in the simulated HTGR helium depends on the calculated equilibrium oxygen and carbon potential in the

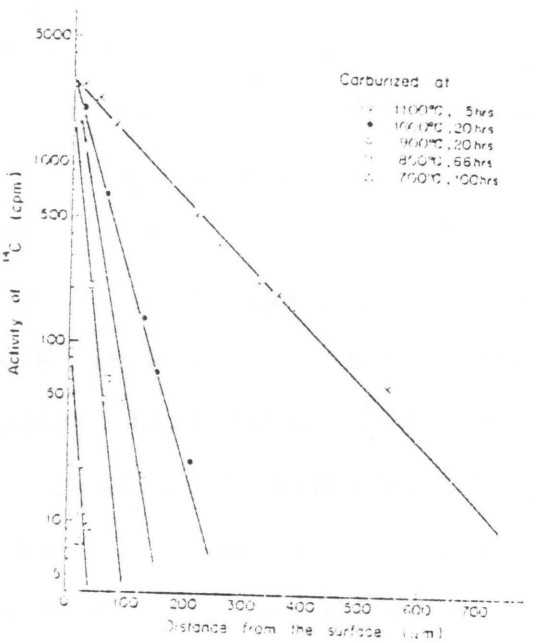

Figure 3. Profiles of C penetration in Hastelloy X at various temperatures.

gases. The depth of internal oxidation and chromium depletion increase with increasing of the equilibrium oxygen potential and the carbon content in the alloy increases with increasing of the equilibrium carbon potential. Their results show that the surface oxide formed does not necessarily act as a barrier for carbon transfer in the simulated HTGR helium. The carbon transfer through the surface oxide layer (mainly Cr_2O_3) may be due to porosity, cracks, or grain boundary transport.

There has not been experimental work reported for environments where oxygen does not contribute to corrosion behavior of nickel base superalloys. The only study has been on the precipitation of carbides in Ni-Cr-Mo system by Raghavan et al. (16). The 11 alloys tested in this study were homogenized at 1523 for 100 hours and subsequently aged at 1123 K (850 C) for 1000 hours to attain equilibrium. Carbides were identified by convergent beam electron diffraction (CBD). The carbides which precipitated in alloys were found to be either the M_6C or the $M_{23}C_6$ type depending upon the alloy composition.

The lattice parameters for M_6C and $M_{23}C_6$ compounds have similar values, hence, it is difficult to distinguish two carbides by electron diffraction except in the [001] orientation (17). In $M_{23}C_6$ carbide, (200) type reflections are

allowed in the zero Laue zone and hence no additional reflection appears in the first order Laue zone.

The ranges of chemical composition of the M_6C and $M_{23}C_6$ carbides are significantly different. The M_6C carbides were essentially Mo with substitution of Cr and Ni, while the $M_{23}C_6$ carbides were rich in Cr with partial substitution of Mo and Ni. The tendency of Mo to M_6C is strong in contrast to the weak tendency of Cr to M_6C. Therefore, the concentration of Cr in this carbide and corresponding austenite was always comparable. Compared to M_6C, the $M_{23}C_6$ carbide has a limited solubility of Mo and Ni. The $M_{23}C_6$ is rich in Cr and dissolved up to 10 at% Mo and 5 at% Ni. The $M_{23}C_6$ carbides were always richer in Cr and Mo compared to the surrounding austenite. This difference in Cr and Mo concentrations could result in the depletion of these elements in the austenite adjacent to the carbides. These results show that the formation of M_6C carbides in the Ni-Cr-Mo system result only in Mo depletion while the formation of $M_{23}C_6$ carbides could result in both Cr and Mo depletion at the carbide/austenite interface.

They also obtained the plot of type of carbide as a function of the austenite composition as shown in Figure (4). It indicates that at a given Cr level, increasing Mo contents promotes the formation of M_6C carbides. The plot

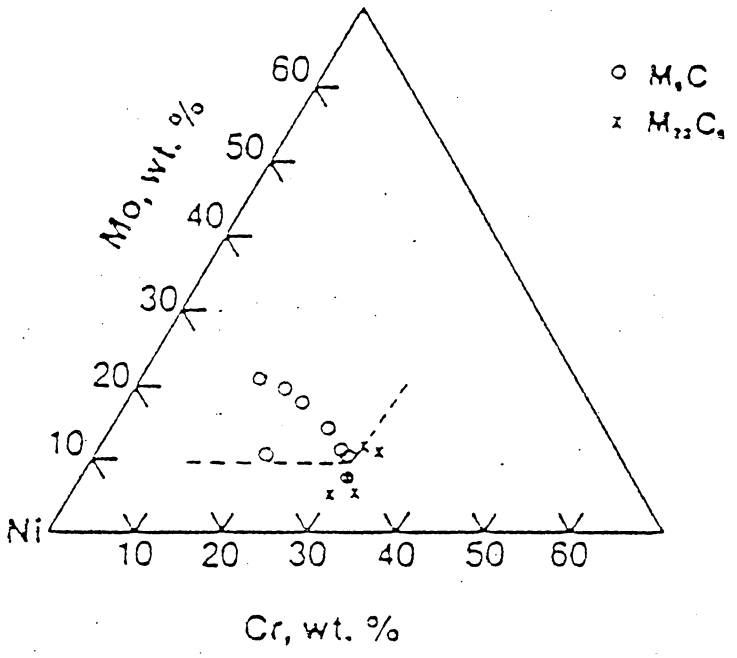

Figure 4. Plot showing the austenite compositions of alloys and the type of carbide.

also shows that when the Cr content of the austenite varies in the range of 15 - 35%, a minimum of 10% Mo is required to promote the formation of M_6C carbides. Below this level, the carbides will be $M_{23}C_6$.

3 Theory

3.1 Diffusion and precipitation kinetics:

The carburization process is a complex interaction between diffusion and carbide precipitation. A change in structure and composition, and physical removal of material may occur as a result of a carburizing reaction, which can degrade a high temperature alloy.

These process of degradation involve: (1) adsorption of carbon on the alloy surface, and (2) the inward diffusion of carbon along grain boundaries and through the bulk materials. Perkins (18) suggests that behavior is governed by the slowest step of these two process and either the surface adsorption or inward diffusion can be rate controlling with respect to degradation. Therefore, surface adsorption or diffusion control could be two approaches for control of carburization. Schnaas and Grabke (19) have shown that the inward motion of carburization front in alloy 800 follows a parabolic rate law:

$$\xi^2 = 2K't \qquad (1)$$

where the rate constant , K', can be expressed by a formalism developed for internal oxidation:

$$K' = \xi D_C C_S / \nu C_M \qquad (2)$$

where,

D_C = Carbon diffusivity

C_S = Carbon concentration on the surface

C_M = Concentration of carbide forming element (Cr,Ti,Mo)

ν = Effective stoichiometric coefficient

ξ = Factor accounting for diffusion cross section blocked by carbide precipitates

The changes that can be produced by controlling the diffusion coefficient of carbon (D_C) are small in comparison with those produced by control of carbon activity at the surface, as means to reduce the rate of carburization. Therefore, The best approach lies in controlling the carbon activity or C_S on the surface of an alloy. From equation (2) a major reduction in the rate of carburization can be achieved by keeping C_S at very low levels on the surface.

One of the means to accomplish a reduced surface concentration of carbon is the formation of oxide layers on the surface (i.e. Cr_2O_3, TiO). This will be discussed later.

The precipitation of carbides slows the progress of carburization by removing a portion of the diffusing carbon, but the carbide forming alloying elements are also removed from the solution resulting in an increased solubility of carbon. This has been extensively studied for the internal

oxidation case. Several theoretical models have been proposed for this influence (1,20,21). Most of these models are analytical treatments.

The model considered in the present work is based on finite difference solution which is the most useful method for solving differential equations such as the diffusion equation. Bongartz et al. (1) developed a numerical solution of diffusion equation that accounted for the chemical reaction where a portion of the carbon which diffuses into the alloy reacts with elements such as chromium to form carbide precipitates. At each time step of the calculation the solubility limit is computed for the precipitation reaction and if the current concentration is higher than this limit the excess is removed from the diffusion process and is added to the precipitated phase. An appropriate amount of the reactive alloying element for carbide formation is also removed from the process.

Goldstein and Moren (2) have demonstrated the application of finite difference techniques for ternary diffusion equations, accounting for cross diffusion effects. Using a similar method in the present work the diffusion modeling of the carburization process is studied by numerical solution of the ternary diffusion equation to compute the effect of an alloying element gradient. This type of gradient has a

cross-diffusion effect on the penetration of carbon

3.2 Ternary Diffusion

Ternary solute impurities may have a important effect on carbon diffusion during the carburization process. If any of the solute impurities are inhomogeneously distributed in the alloy, for example, by grain boundary segregation or by surface or internal oxidation, the carbon flux can be modified by the effect of the off diagonal or cross diffusion coefficient.

In oxidizing-carburizing environment considered in the present work, the mechanism by which ternary alloying elements (i.e., Cr or Ti) may redistributes during carburization is oxidation. Both surface and internal oxidation may occur during the carburization process. The formation of a coherent (protective) oxide layer (i.e., Cr_2O_3) on the surface may act as a barrier to carbon control and acts as a barrier to carbon diffusion. In addition to the protective oxide layer which prevents exchange of carbon between the carburizing gas and the solid, the growth of a non-protective layer can also affect the corrosion behavior due to changes in the surface solubility and cross diffusion effects. Such effects occurs when a non-continuous layer of alloying element oxide (Cr_2O_3 or TiO) cause a depletion zone

of the metallic element (Cr, or Ti) beneath the surface region. The metal depletion could be quite large and the concentration of element M or N in Ni-M-N alloys could approach zero. This makes the surface solubility of Carbon in the alloy much lower than C_S (i.e., the solubility of C in alloy). It also creates a Cr concentration gradient that will have a cross diffusion effect on C penetration.

The diffusion of carbon in ternary Ni-M-Cr alloy, where M is the alloying element such as Mo, Ti, W, and Nb, may be determined with the extension of Fick's second law (22) as:

$$J_i = - D_{ik} C_k \qquad i,k = 1,2,3 \qquad (3)$$

or,

$$J_1 = - D_{11} \partial C/\partial X - D_{12} \partial M/\partial X - D_{13} \partial N/\partial X \qquad (4a)$$

$$J_2 = - D_{21} \partial C/\partial X - D_{22} \partial M/\partial X - D_{23} \partial N/\partial X \qquad (4b)$$

$$J_3 = - D_{31} \partial C/\partial X - D_{32} \partial M/\partial X - D_{33} \partial N/\partial X \qquad (4c)$$

where N is the concentration of Cr.

Combining equation (4) with the continuity equation and assuming that the diffusivities are composition independent, the fick's second law for ternary system becomes:

$$\partial C/\partial t = D_{11} \partial^2 C/\partial X^2 + D_{12} \partial^2 M/\partial X^2 + D_{13} \partial^2 N/\partial X^2 \qquad (5a)$$

$$\partial M/\partial t = D_{21} \partial^2 C/\partial X^2 + D_{22} \partial^2 M/\partial X^2 + D_{23} \partial^2 N/\partial X^2 \qquad (5b)$$

$$\partial N/\partial t = D_{31}\ \partial^2 C/\partial X^2 + D_{32}\ \partial^2 M/\partial X^2 + D_{33}\ \partial^2 N/\partial X^2 \qquad (5c)$$

where C, M, and N denote the concentration of carbon and two alloying elements, respectively. D_{12}, D_{21}, D_{13}, D_{23}, D_{31}, and D_{32} reflects cross diffusion coefficients, or usually refered to as the ternary diffusional interaction. D_{11} is the diffusivity of carbon in the alloy surface, where D_{22}, and D_{33} are the diffusivity of alloying elements in the alloy. As mentioned by Goldstein and Moren (2), the cross-diffusion coefficients are calculated at the surface and considered constant. These coefficients can be calculated from thermodynamics according to Brown and Kirkaldy(23):

$$D_{12}/D_{11} = e_{12}\ N1/(1 + e_{11}\ N1) \qquad (6a)$$

$$D_{13}/D_{11} = e_{13}\ N1/(1 + e_{11}\ N1) \qquad (6b)$$

where N_1 is the mole fraction of carbon. e_{11}, e_{12}, and e_{13} are the thermodynamic wagner interaction parameters which relate the activity coefficient of carbon to the mole fraction of carbon and element 2 and 3 (i.e., M and N respectively) as follows:

$$e_{11} = \partial \ln \gamma_C/\partial C \qquad (7a)$$

$$e_{12} = \partial \ln \gamma_C/\partial M \qquad (7b)$$

$$e_{13} = \partial \ln \gamma_C / \partial N \qquad (7c)$$

It should be noted that if any of these interaction parameters is a negative quantity, the corresponding alloying element would form a more stable carbide than does the base metal (i.e., Nickel), and that the order of increasing magnitude of the $|e|$ follows the order of increasing magnitude of the free energy of formation of the carbide. Similarly the parameter is a positive quantity when the alloying element has a greater affinity for Nickel than either the alloying element for carbon, or Nickel has for carbon.

These calculations are based on a dilute solution model and its validation depends on the kind of alloy and concentration of alloying elements. For example, Farkas and Delgado (24) have shown that this relation can be extended to about 15 percent Cr within the limits of the diffusion coefficient measurement accuracy in Fe-Cr alloys. However, for Ni-base alloys it was found that it can be extended to Cr contents up to 35 wt%.

The addition of oxide forming elements such as Cr and Ti influence both the solubility limits of C in austenite C_S, and the mass fluxes of carbon as predicted by equation (5). These oxides on the surface region cause a depletion zone of oxide forming alloying elements which changes the

effective surface concentration of carbon. This also accounts for the uphill diffusion, already mentioned in chapter 2, when a non-protective oxide layer forms at the surface.

The diffusion of substitutional elements is much slower than interstitial carbon diffusion, therefore, the effect of the carbon concentration gradient on the diffusion of alloying element, as well as the effect of a concentration gradient of one alloying element on the diffusion of the other, can be neglected. Then:

$$D_{21} \approx D_{23} \approx D_{31} \approx D_{32} \approx 0 \qquad (8)$$

The values D_{12} and D_{13} can be calculated according to equation (6). Equation (6) indicates that these cross diffusivities are a strong function of the concentration of diffusing species, carbon (i.e., element 1). They also suggest no strong dependency on the contents [M] and [N] (i.e., concentrations of alloying elements).

3.3 Thermodynamics Of Oxidation-Carburization Reactions

Carburization can occur when an alloy surface comes in contact with solid or gaseous carbon or carbon containing gases such as hydrocarbon or oxides of carbon at elevated temperature. In HTGR materials reaction with impurities in

the coolant is a major problem. The impurities are mainly CO, CO_2, CH_4, H_2O, H_2, and O_2. These impurities react at high temperature and result in complex corrosion, i.e., oxidation and carburization and decarburization. The principal reaction involved on the surface are as follows:

$$CH_4 = C + 2H_2 \quad (9)$$

$$M + CO = C + MO \quad (10)$$

$$2CO = C + CO_2 \quad (11)$$

$$CO + H_2 = C + H_2O \quad (12)$$

$$M + CO_2 = CO + MO \quad (13)$$

$$CO_2 = CO + 1/2O_2 \quad (14)$$

Each of the first four reactions establish a carbon activity (a_C) uniquely defined by the temperature and concentration of reactants and products. Equation (13) is a source of high carbon activity by which CO may be generated (i.e., equation (14)) when a metal is oxidized by CO_2. The CO may then break down to deposit carbon on the surface. Only equation (13) involves a reducing atmosphere. All of the others involve oxygen and can form oxides of reactive alloying elements (i.e., Cr, and Ti).

Shikama et al. (13) have shown that the thermodynamic

stability of oxides and carbides for given oxygen and carbon potentials by Gurry's plot (25). Figures (5), (6), and (7) show these plots for oxides and carbides at 900°C and 650°C, where indicate plots of C content (C/S) verses O content (O/S). These variables can be calculated as follow:

$$O = [CO] + 2[CO_2] + [H_2O] + 2[O_2] \quad (15)$$

$$H = 4[CH_4] + 2[H_2O] + 2[H_2] \quad (16)$$

$$C = [CO] + [CO_2] + [CH_4] \quad (17)$$

$$S = O + H + C \quad (18)$$

If the composition of test reducing gas is as the black dot in figures (5), (6), and (7), the comparison of these plots show that $Cr_{23}C_6$, and TiC are mostly stable at 900°C. In general it can be seen that at low oxygen potential Cr, Al, Mn, and Ti will be preferentially oxidized. They also report the same oxidation behavior at 650°C and 1000°C. Hence, the same oxidation behavior can be expected at 850°C.

T. Hirano et al. (6) have reported that the degree of corrosion on Inconel 617 in the simulated HTGR helium depends on the calculated equilibrium oxygen and carbon potential in the gases. The depth of intenal oxidation and chromium depletion increase with increasing equilibrium oxygen potential and the carbon content in the alloy increases

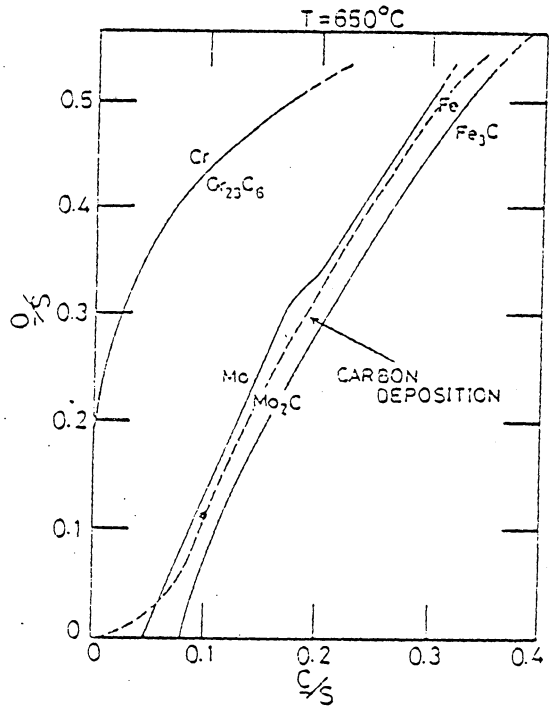

Figure 5. Equilibrium lines between metals and metal carbides at 650°C as function of atomic fraction of oxygen (O/S), and carbon (C/S).

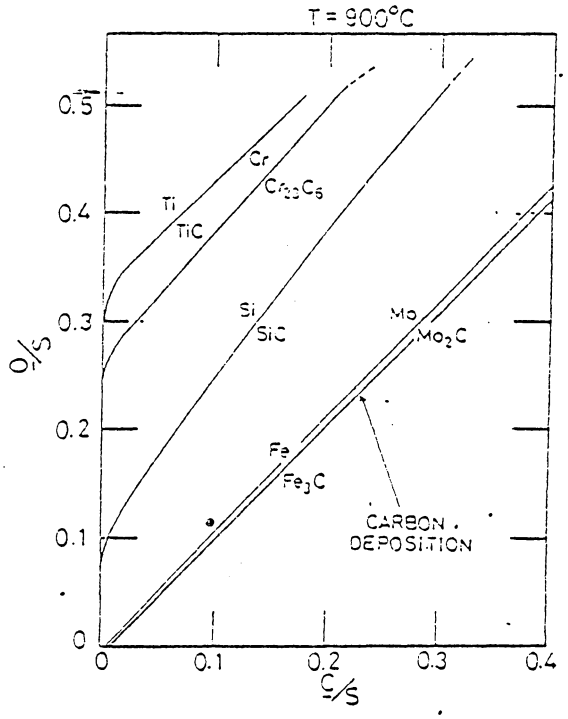

Figure 6. Equilibrium lines between metals and metal carbides at 900°C as function of atomic fraction of oxygen (O/S), and carbon (C/S).

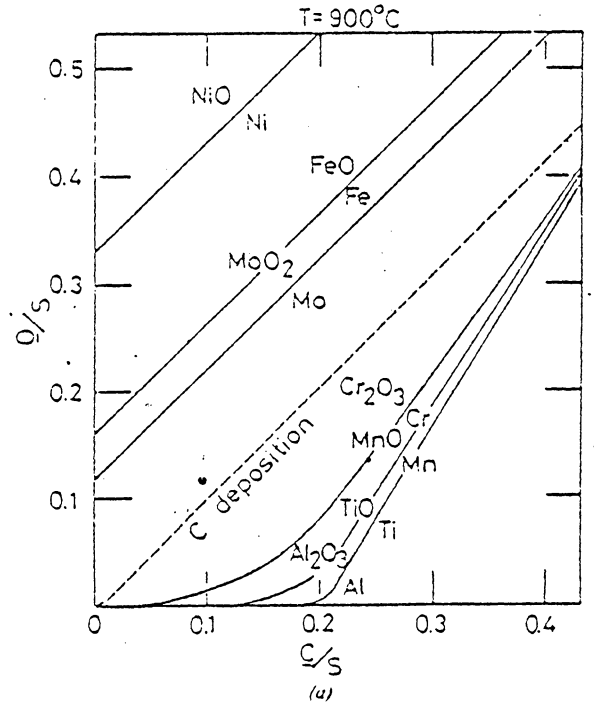

Figure 7. Equilibrium lines between metals and metal oxides at 900°C as function of atomic fraction of oxygen (O/S), and carbon (C/S).

with increasing equilibrium carbon potential. The calculation of the equilibrium activity of C and the partial pressure of O_2 that exist in a gas at any given temperature and pressure can be done by elementary thermodynamics. A knowledge of these activities can be used to estimate how much carbon may dissolve in an alloy and whether or not stable carbides or oxides of any element in the alloy can be formed. Suppose for a $CO:CO_2$ mixture at atmospheric pressure, the carbon activity and the partial pressure of O_2 can be calculated as follows:

$$2CO = C + CO_2 \tag{19a}$$

$$\Delta G = -RT \ln P_{CO_2} a_C/(P_{CO})^2 \tag{19b}$$

then,

$$a_C = (P_{CO})^2/P_{CO_2} \exp(-\Delta G/RT) \tag{19c}$$

For the mixture, the oxygen pressure would be:

$$CO + 1/2O_2 = CO_2 \tag{20a}$$

$$\Delta G = -RT \ln P_{CO_2}/P_{CO} (P_{O_2})^{1/2} \tag{20b}$$

then,

$$P_{O_2} = P_{CO}/P_{CO_2} \exp(-\Delta G/RT) \tag{20c}$$

A knowledge of these activities and pressures can be used to estimate carbon or oxygen dissolution in the alloy

and whether or not carburization or oxidation would be the rate controlling in the alloy. Perkins (18) shows a convenient way to present the results of such calculations in the form of a thermodynamics phase stability diagram (modified Ellingham diagram). Figure (8) shows such diagram where the equilibrium carbon activity (a_C) and oxygen pressure (P_{O_2}) for the formation of a stable carbide and oxide of the Ni-Cr alloy are represented as intersecting horizontal and vertical lines respectively.

The activities and presures in "metal" region can not form stable oxide or carbide of M. This region where the metal will neither carburize or oxidize. However, it can dissolve carbon or oxygen to concentration where the carbon and oxygen activities in the surface will be in equilibrium with the gas phase. When the carbon activities and oxygen pressures are beyond the metal boundary, a carbide or oxide of M can be formed on the surface in equilibrium with the gas phase. The following equation defines the boundary which separates the carbide and oxide stable phase fields.

$$MC + 1/2\ O_2 = MO + C \qquad (21a)$$

The equilibrium constant (K) for this reaction would be:

$$K = \exp(-\Delta G/RT) = a_C\ a_{MO}/a_{MC}\ (P_{O_2})^{1/2} \qquad (21b)$$

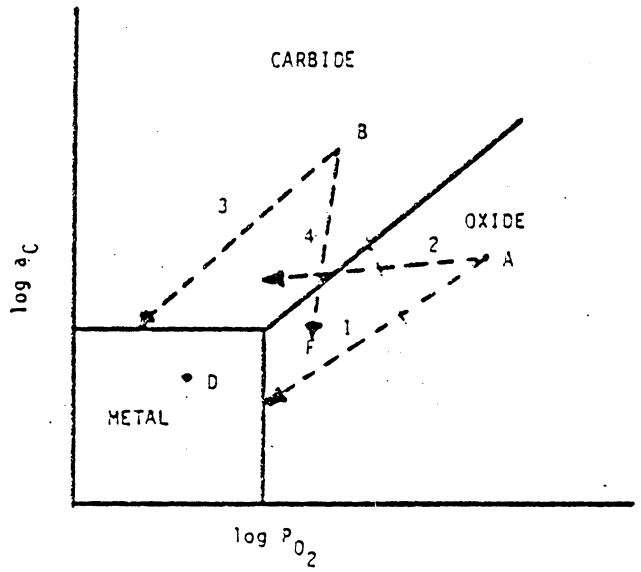

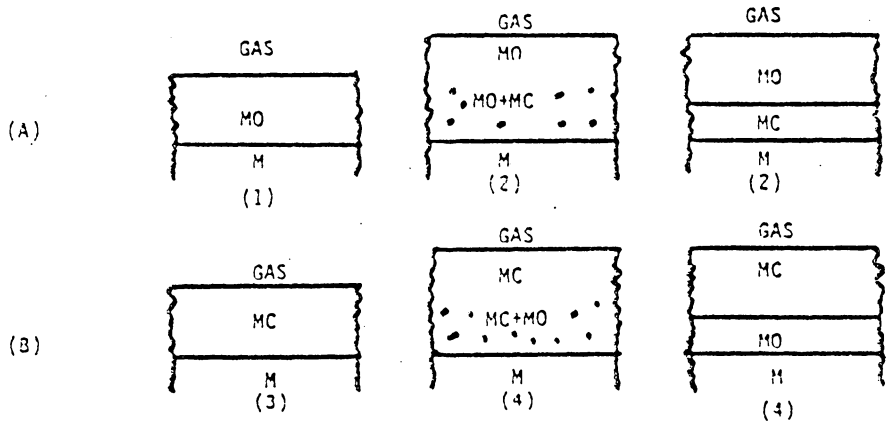

Figure 8. M-C-O phase stability and effect of gas composition and reaction paths on surface scales.

for pure oxide and carbide the last equation reduces to:

$$K = a_C/(P_{O_2})^{1/2} \tag{21c}$$

which gives,

$$\log a_C = -\Delta G/RT \log P_{O_2} \tag{21d}$$

as the equation for the diagonal boundary.

This diagram predicts only the oxide of M in the gas composition of A (shown in fig (8)) on the surface, and no external carbide could be formed. However, an internal carbide case could be formed beneath the oxide scale depending on how the oxygen and carbon activities change in moving through the scale to the oxide/metal interface. If the oxide is protective (i.e., it can be formed in high oxygen, low carbon activity gases), it is a good barrier to the transport of C and O_2, the activities of these element in the scale could fall along a path such as A-1 and only the oxide of the metal would be formed on the surface (i.e., thin Cr_2O_3 in Ni-Cr alloys). This is because of insufficient carbon penetration into the scale to form an underlying carbide case or internal carbides. This behavior represents the ultimate in carburizing resistance.

Now if the oxide is non-protective, it would not be a

good barrier to transport of carbon. Hence, the activities through the oxide scale might change along the path A-2. In this case a_C is sufficiently high for carbide of M to form within the scale or as a carbide case beneath the scale. This results in carbon diffusion beneath the alloy to form chromium carbides in grain boundaries and within the grain.

In the case of a carburizing gas such as gas composition B in figure (8), chromium carbide is the stable phase in equilibrium with the gas on pure Cr or binary Ni-Cr alloys. Depending on whether or not the carbide is a good barrier to the transport of oxygen, the activities of carbon or oxygen on moving through the carbide case could fall according to path B-3 (i.e., for a good carbide barrier), or path B-4 (i,e., for a poor barrier carbide). The path B-3 is the ideal behavior for simple pack or gas carburizing process. This is the case for the experimental section in our work. Here the carbide case would be in stable equilibrium with the underlying metal as well as with the gas phase. Path B-4 could be the case which an oxide might be formed as a continuous layer beneath the carbide case. This underlying oxide scale could then be an effective barrier to continued internal carburization of the alloy. If this oxide case is formed within the carbides case, the oxide would not be continuous and this alloy continues to carburize inter-

nally.

It should be noted that these effects are largely controlled by kinetics, and the available thermodynamic data would not predict the behavior of the scales. For example, for the case of A-1 path where an stable oxide could form on the surface, carbon can penetrate oxide scales along cracks, fissures, and interconnected pores (26,27). However, some behaviors can be predicted when the metal stands in equilibrium with the gas phase. This case is shown in the figure as point D. Here carbon would dissolve in the alloy untill the a_C in the surface is in equilibrium with the a_C in the gas phase, and no carbides or oxides should be formed either on the surface or in the metal.

Equilibrium carbon activities and oxygen pressures can be obtained for complex gas mixture containing CO, CO_2, CH_4, H_2, H_2O, and other gases with the aid of computer programs that calculate the equilibrium gas composition for a given temperature and pressure.

From these compositions the $CO:CO_2$, or $CH_4:H_2$, or $H_2:H_2$ can be used to calculate carbon and oxygen activities in the gas phase. It should be recognize that these ratios can be used to calculate activities only if the given composition of a complex gas mixture is that for an equilibrium mixture.

4 Experimental Procedure

In the present work, mixture of H_2-CH_4 gases were used. Principal reaction that deposits carbon on the surface is:

$$CH_4 = C + 2H_2 \tag{22}$$

This gives the activity of carbon in the gas as:

$$a_C = \exp(-\Delta G/RT)\ X_{CH_4}/P\ (X_{H_2})^2 \tag{23}$$

where, ΔG = free energy of dissociation

R = gas constant

T = temperature (absolute)

X_{CH_4} = mole fraction CH_4

X_{H_2} = mole fraction H_2

P = pressure

It can be seen that relatively small changes in the proportion of hydrogen and methane will result in changes in the carbon activity necessary to evaluate the importance of this parameter. A carbon activity of 1.0 was used for the carburization process at 1 bar atmospheric pressure. This would result to a gas mixture of H_2-$2.7CH_4$ at 850°C.

Four alloys were exposed to the gas mixture at 850°C for up to 200 hours. The chemical composition of the alloys

are shown in table (2). Inconel 600, 601, and X-750 are nickel base superalloys, and Incoloy 800 is a iron base superalloy. The later was included for comparison with nickel base alloys in the carburizing environment. The specimen dimensions were 3 x 13 x 22.2 mm with flat parallel sides. Specimens were ground to 320 grit, and ultrasonic-cleaned in acetone, and were weighted before exposure to the test gas. The gas pressure was 1 bar, and the gas flow was approximately 330 ml/sec in testing.

The corrosion test apparatus used in the present study is shown in figure (9). Four samples could be placed on the sample holder at a time. The furnace was purged with argon till temperature 850°C was maintained before flowing the gas mixture in. The samples were exposed to the gas mixture for 32, 100, and 200 hours each time. The samples were then ultrasonic-cleaned in the acetone and weighted. They were cut with diamond disc across the midsection of their thickness for microstructural studies.

Each sample was then polished and etched. Inconel 600, and 601 and Incoloy 800 were etched by electrolytic phosphoric acid (80ml H_3PO_4, 20ml water), and Inconel X-750 was etched by electrolytic chromic acetic (25g CrO_3, 7ml water, 130ml acetic acid) in a cell voltage of 3-8 volts for 3-5 seconds. The type of etchants used were to show carbide

Alloy	Cr	Mo	Ti	Al	Co	Nb	W	Fe	Ni
Incoloy 800	21	-	.38	.38	-	-	-	45.7	32.5
Inconel 600	15.5	-	-	-	-	-	-	8	76
Inconel 601	23	-	-	1.35	-	-	-	14.1	76
Inconel X-750	15.5	-	2.5	.7	-	1	-	7	73

Table 2. Composition of the alloys studied in weight percent.

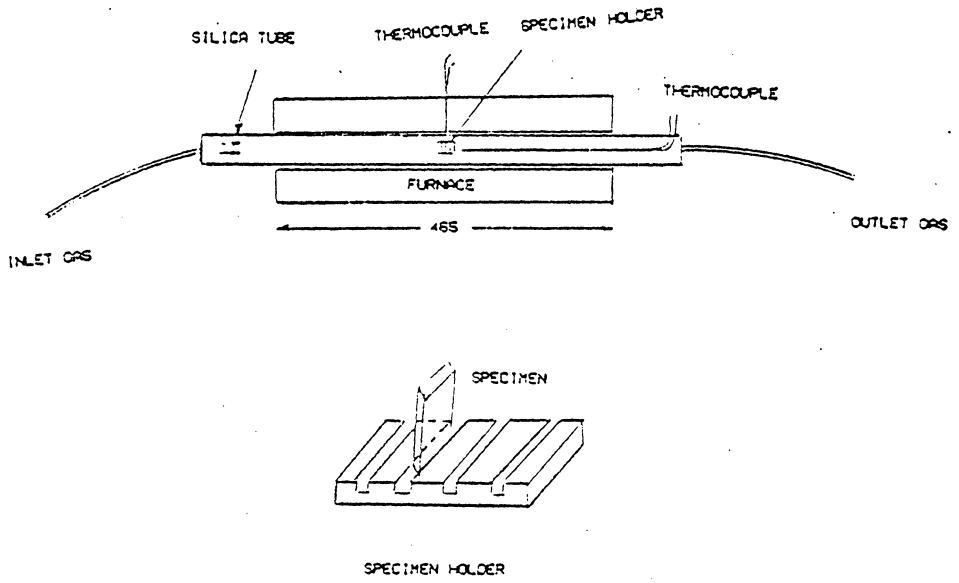

Figure 9. Schematic presentation of apparatus (mm).

precipitants. Micrographs were taken at different magnifications to be used for quantitative image analysis. Image analyzing is a computerized process operated by VAX-2 system at the Spatial Data Analysis Laboratory. The general image processing system, GIPSY, is a coordinated system of over 275 programs written in the programming language RATFOR, that can be used to enhance, manipulate and analysis digital images. These images are divided into 512 x 512 rectangular regions called subimages. Subimaging an image enables the operator to analyze different parts of the image. The GIPSY user's manuals can be obtained from the Spatial Data Analysis Laboratory.

The carburized microstructures were first digitized. The images were then subimaged at several point. Each subimage area was analyzed to account for carbide precipitates. These are the dark areas on the image. First, image histograms were obtained, and, by choosing suitable threshold from these histograms, the area of carbides was obtained at each depth. Choosing a threshold is the most critical part in image analyzing. To obtain the best results, each threshold data should be displayed on the monitor to see how the dark areas are separated from lighter ones, and obtain as close as possible to the original microstructure print.

The data obtained give the fraction of carbide area

present in the image. Then the volume of carbides can be calculated as:

$$V = (P\ L\ W)^{3/2}/(L\ W)^{3/2} = P^{3/2} \tag{24}$$

where P is the fraction area of carbide present, and L, and W are the length and the width of rows and columns (From 512 x 512 rectangular regions) used for analyzing the subimage. Then the percent volume of carbide would be:

$$V(v/o) = V/(1 - V) = P^{3/2}/(1 - P^{3/2}) \tag{25}$$

where (1 - V) would be the volume of the uncarburized region.

5 Simulation Model

5.1 Numerical Methods: Crank-Nicholson Finite Difference Method

Many of the differential equations which result from engineering problems can not be readily solved by analytical methods. Consequently, a knowledge of the methods of obtaining numerical solution of differential equations is important. These methods are used by studying their application to a specific differential equation and its boundary conditions. A numerical solution is always obtained for the differential equation with specific boundary conditions.

The diffusion equation is classified as a parabolic partial differential equation which is a boundary value problem having time-dependent solution. The most useful methods for solving differential equation such as diffusion equation are finite difference techniques.

5.1.1 Binary Diffusion

For a Ni-M-N alloy, the diffusion of carbon in the alloy can be described by Fick's second law:

$$\partial C/\partial t = \partial/\partial X \, (D_{11} \, (\partial C/\partial X)) \qquad (26)$$

for the case Where D is not a function of concentration Equation (22) reduces to:

$$\partial C/\partial t = D_{11}\ \partial^2 C/\partial X^2 \qquad (27a)$$

The diffusion of the alloying elements M and N in the alloy follow the next two equations:

$$\partial M/\partial t = D_{11}\ \partial^2 M/\partial X^2 \qquad (27b)$$

$$\partial N/\partial t = D_{11}\ \partial^2 N/\partial X^2 \qquad (27c)$$

When using a finite difference technique to solve a PDE (plus associated boundary and initial conditions), a network of grid points is first established through out the region of interest occupied by the independent variables. In equation (27), we have one distance coordinate x, and time t as independent variables, and that the respective grid spacing are Δx, and Δt as shown in figure (10). Subscripts i, and n are used to denote that space point having coordinates $i\Delta x$, $n\Delta t$, also called the grid-point (i,n). And U is the dependent variable representing either C, M, N in equations (27).

One of finite difference technique to solve PDE's such as equations (5) and (27) is the Crank-Nicholson finite difference method (28,29). The finite difference equations used in Crank-Nicholson replace the derivatives as follows:

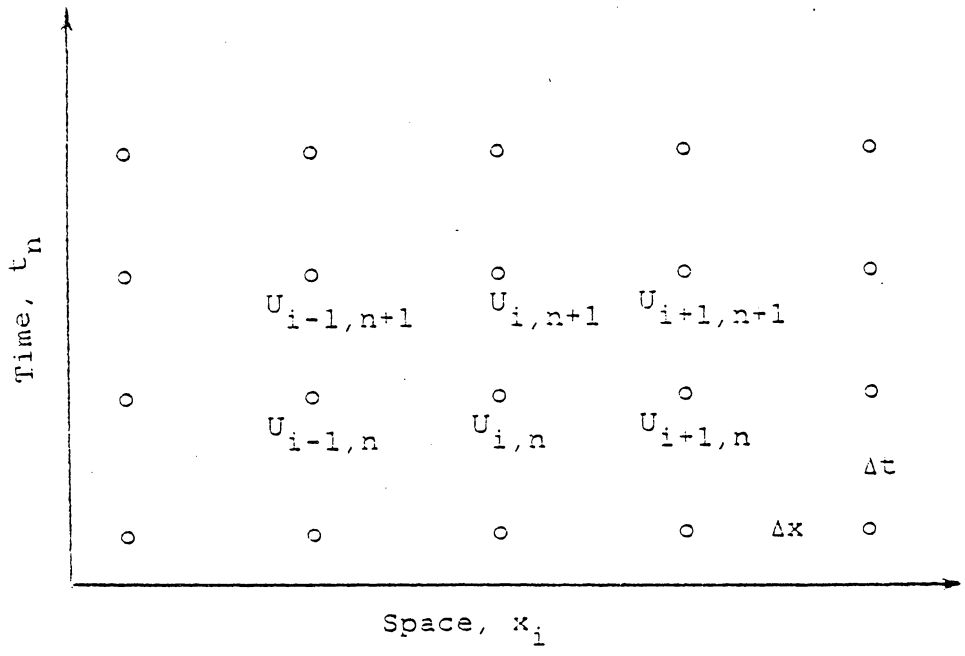

Figure 10. Grid spacing for finite difference model.

$$\partial U/\partial t = (U_{i,n+1} - U_{i,n})/\Delta t \tag{28}$$

$$\partial^2 U/\partial X^2 = (1/2\Delta X^2)\ (U_{i+1,n+1} - 2U_{i,n+1} + U_{i-1,n+1} + U_{i+1,n} - 2U_{i,n} + U_{i-1,n}) \tag{29}$$

These equations are second order-correct with respect to both independent variables x, and t. One better advantage for using this method is its stability over large range of increments of the variables.

At any time step $U_{i-1,n}$, $U_{i,n}$, $U_{i+1,n}$ are known values, and at the next time increment $U_{i-1,n+1}$, $U_{i,n+1}$, $U_{i+1,n+1}$ are unknown values. Substituting equations (28), and (29) into equation (27a), and realizing that U is now element C, carbon, and collecting terms for points n and n+1 on the opposite sides of equation gives:

$$C_{i+1,n+1} - 2C_{i,n+1}\ [-2 - 2((\Delta X)^2/D\ \Delta t)] + C_{i-1,n+1} = C_{i-1,n} + 2C_{i,n}\ [-2 - 2((\Delta X)^2/D\ \Delta t)] - C_{i-1,n} \tag{30}$$

for each of the grid point i.

The same procedure can be applied to equations (27b) and (27c) to obtain the concentration equations for the alloying elements:

$$M_{i+1,n+1} - 2M_{i,n+1}\ [-2 - 2((\Delta X)^2/D\ \Delta t)] + M_{i-1,n+1} = M_{i-1,n} + 2M_{i,n}\ [-2 - 2((\Delta X)^2/D\ \Delta t)] - M_{i-1,n} \tag{31}$$

$$N_{i+1,n+1} - 2N_{i,n+1}\,[-2 - 2((\Delta X)^2/D\,\Delta t)] + N_{i-1,n+1} = N_{i-1,n} + 2N_{i,n}\,[-2 - 2((\Delta X)^2/D\,\Delta t)] - N_{i-1,n} \qquad (32)$$

5.1.2 Ternary Diffusion

The diffusion of carbon in Ni-M-N alloy, when an Oxide scale is formed, was presented in equation (5). We also had:

$$D_{21} \approx D_{23} \approx D_{31} \approx D_{32} \approx 0 \qquad (8)$$

This make questions (5b), and (5c) the same as equations (23b), and (23c) for the binary case. But for the diffusion of carbon in the alloy, we have the cross diffusion effects to consider:

$$\partial C/\partial t = D_{11}\,\partial^2 C/\partial X^2 + D_{12}\,\partial^2 M/\partial X^2 + D_{13}\,\partial^2 N/\partial X^2 \qquad (5a)$$

Equation (5a) is more general for the diffusion of carbon in the alloy. To obtain the binary equation, for which no oxide would be formed, we just need to set the cross diffusivities D_{12}, and D_{13} equal to Zero.

The finite difference solution for this equation fllows:

$$\partial C/\partial t = D_{11}\,(1/2\Delta X^2)\,(C_{i+1,n+1} - 2C_{i,n+1} + C_{i-1,n+1} + C_{i+1,n} - 2C_{i,n} + C_{i-1,n}) + D_{12}\,(1/2\Delta X^2)\,(M_{i+1,n+1} - 2M_{i,n+1} + M_{i-1,n+1}$$

$$+M_{i+1,n} - 2M_{i,n} + M_{i-1,n})$$
$$+ D_{13} (1/2\Delta X^2) (N_{i+1,n+1} - 2N_{i,n+1} + N_{i-1,n+1}$$
$$+N_{i+1,n} - 2N_{i,n} + N_{i-1,n}) \quad (33)$$

In general, applying the finite difference equations (28), and (29) to all grid points i yield tridiagonal matrix of linear equations. The Thomas algorithm solves for new concentrations, e.g. $C_{i,n+1}$, from the the previous ones, e.g. $c_{i,n}$ if the followings are specified:

(1) Initial carbon profile

(2) Appropriate diffusion coefficients

(3) Boundary conditions

The system of linear equations follows:

$$(A)\ (X)_n = (D)_n \quad (34a)$$

where,

$$(X)_n = (C_{i,n}, \text{ or } M_{i,n}, \text{ or } N_{i,n}, ...) \quad (34b)$$

$$(D) = (d^1{}_{i,n}, d^2{}_{i,n}, d^3{}_{i,n}, ...) \quad (34c)$$

where 1, 2, and 3 indicate carbon, and alloying elements M, and N respectively.

$$d^1{}_{i,n} = r11\ (2C_{i,n} - C_{i+1,n} - C_{i-1,n}) - C_{i,n}$$
$$+ r12\ (2M_{i,n} - M_{i+1,n} - M_{i-1,n}) - C_{i,n}$$
$$+ r13\ (2N_{i,n} - N_{i+1,n} - N_{i-1,n}) - C_{i,n} \quad (34d)$$

$$d^2_{i,n} = r22\ (2M_{i,n} - M_{i+1,n} - M_{i-1,n}) - M_{i,n} \qquad (34e)$$

$$d^3_{i,n} = r33\ (2N_{i,n} - N_{i+1,n} - N_{i-1,n}) - N_{i,n} \qquad (34f)$$

the d's are determined at each time increment.

A is a tridiagonal matrix,

$$A = \begin{vmatrix} b & c & 0 & . & . & . \\ a & b & c & 0 & . & . \\ 0 & a & b & c & . & . \\ 0 & 0 & a & b & . & . \\ 0 & 0 & 0 & a & . & . \\ . & . & . & . & . & . \end{vmatrix} \qquad (35)$$

$$a = c = \begin{vmatrix} r11 & r12 & r13 \\ 0 & r22 & 0 \\ 0 & 0 & r33 \end{vmatrix}$$

$$b = \begin{vmatrix} -2r11 - 1 & -2r12 & -2r13 \\ 0 & -2r22 - 1 & 0 \\ 0 & 0 & -r13 - 1 \end{vmatrix}$$

where,

$$r_{ij} = \Delta t\ D_{ij}/2\ \Delta x^2 \qquad (36)$$

The matrix A can be inverted with standard subroutines. The three component concentrations at time step n+1 can be obtained from the concentrations at step n as:

$$(X)_{n+1} = (A)^{-1}\ (D)_n. \qquad (37)$$

5.1.3 Choice of Grid Parameters

Errors are introduced by the truncation of the series (i.e., Taylor series) used to represent the derivatives in the process of replacing the differential equation by finite difference equations. For a numerical solution to be of any value , its solution must converge to the corresponding differential equation when Δx, and Δt are decreased in size. The condition for which the errors will be lessen from one time step to the next suggests that a very restrictive relationship between the size of Δx and that of Δt must be satisfied in order the solutions to PDE to approach that of equation (23). The convergence condition (28) for the choice of grid parameters Δx, and Δt is:

$$\Delta x^2/D\ \Delta t > 2 \qquad (38)$$

However, it should be noted that when reactions (i.e., carbide precipitates) are present in the calculations, the choice of grid size has additional meaning and the resulting profile depends on this size. When a reaction is included, a distance Δx is implicitly assumed to be replenished in diffusing material in time Δt. Therefore, the choice of the ratio $\Delta x^2/D\ \Delta t$ represents the velocity at which this replenishment or distribution occurs. Since the process is diffusioned-controlled and condition should represents the diffu-

sion depth of penetration as a function of time, the correct choice is:

$$\Delta x^2/D\ \Delta t = 4 \tag{39}$$

Bongarts et al. (1) used a value of

$$\Delta x^2/D\ \Delta t = 3 \tag{40}$$

and the results are only slightly different from what is obtained if the relation just given is used.

5.2 Boundary Conditions

Our model can treat two kinds of boundary conditions. The first, constant surface concentration of carbon which corresponds to no oxide growth or a non-protective oxide layer. The second is constant flux J at the surface for the case of an oxide layer growing at the surface which is nearly protective. All our calculations were preformed using constant surface concentration as the boundary condition. However, the second condition is characterized by

$$C_{0,n} = C_{1,n-1} + \Delta x\ J/D_{11} + (D_{12}/D_{11})(M_{1,n-1} - M_{0,n-1}) + (D_{13}/D_{11})(N_{1,n-1} - N_{0,n-1}) \tag{41}$$

where subscript 0 denotes the specimen surface.

The conditions used here are for a plane geometry. The

boundary conditions leading to the construction of carbon and alloying elements profiles are as follows:

1) Constant surface concentrations for both carbon and the alloying elements.

a) For binary diffusion case where there is no oxide formation, the carbon concentration on the surface has been calculated as the solubility limit of carbon in Ni-Cr-C system. This will be shown in the results section.

b) For ternary diffusion calculations where a non-protective oxide layer is formed at the surface, the carbon concentration is the solubility limit of carbon in pure Ni (30). The concentration of alloying elements that form oxides (i.e. Cr and Ti) are equal to zero, since it is assumed that there is a complete depletion of alloying element at the surface of the alloy to oxides.

(2) The diffusion problem is bounded spatially by a constant carbon concentration at the surface of the alloy at grid point i = 2, where:

$$C_{1,n} = C_{3,n} \tag{42}$$

A zero mass transfer boundary at X_{max} = L, that is at grid point i = ID, hence:

$$\partial C/\partial x = \partial M/\partial x = \partial N/\partial x = 0 \tag{43a}$$

and,

$$C_{ID-1} = C_{ID+1} \tag{43b}$$

X_{max} is the maximum distance for carburization, that is half the thickness of sample. Figure (11) shows the composition distribution of carbon and one alloying element (N) in the γ phase. Here $X_{max} = L$ is the total length of grid. Hence:

$$\Delta X = X_{max}/ID-2 \tag{44}$$

5.3 General Procedure for Solving the Differential Equation

For the problem discribed by equation (27) and the boundary conditions just discussed, the value of dependent variable is known at a row of points at each time level, and there are actually an unlimited number of time levels. It is not feasible to solve for all the unknown values of U simultaneously even when a limited number of time levels are considered. Hence, the technique employed is to solve for the unknown values of U at one time level using the known values of U at the previous time level. The values of U at the initial time level, where n = 0, are given as the concentration of element at the surface. These values are used to determine the unknown values of U at the next time level for

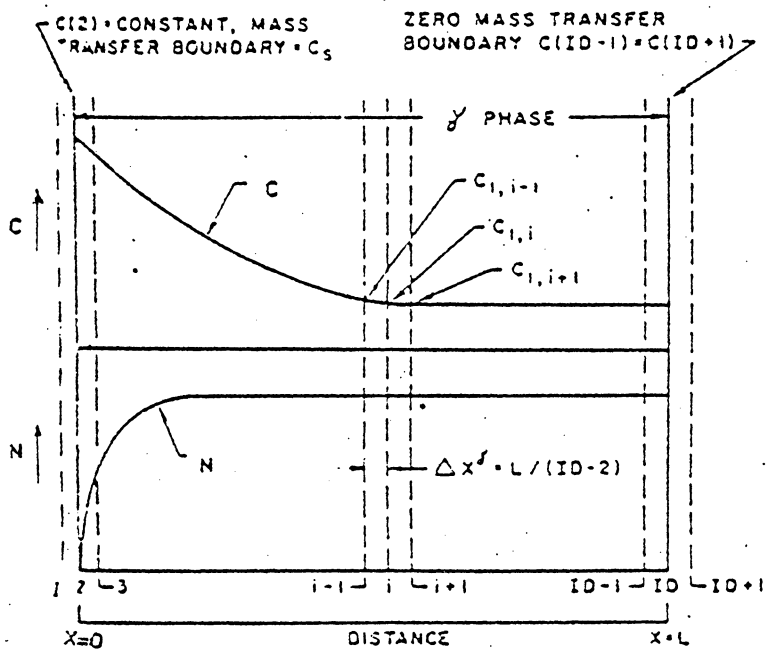

Figure 11. Schematic diagram of the space-composition grid for the numerical model of carburization.

which n = 1. The same procedure is then used to find the values of U for n = 2 from the known values of U at N =1. This procedure is continued for as many time increment as desired. Therefore, the finite difference equations are formulated so that they contain values of U at two consecutive time levels as shown in equations (30), (31), and (32). There the index n shows the time level at which the values of U are known, and n+1 indicates the next time level at which values of the dependent variable are unknown.

5.4 Assumptions for Carbide Formation

The following simplifying assumptions are used through out this model:

(1) The kinetic of precipitation of carbide is much faster than the diffusion process.

(2) Bulk diffusion is dominant and contribution of grain boundary diffusion can be neglected.

(3) No volume changes occur in the lattice during diffusion. This is valid assumption for interstitial diffusion process.

(4) Constant diffusion coefficients are assumed, i.e., the alloying element concentration gradient does not influence C diffusivity in the alloy.

(5) No mixed carbides were considered, since their

energies of formation are not known.

(6) No dissolution of carbides was allowed after they were formed.

These assumptions result in the possibility of forming different carbides at the same penetration depth. For a high Cr content alloy, carbides high in Cr will precipitate first, and as the diffusion process evolves and alloy becomes depleted in Cr, lower carbides will be formed.

The validity of these assumption depends on the alloy and environment. In most cases, these simplifications will not have large effects on the calculated profiles.

The program can treat four different carbides simultaneously. In Ni-N-M system, two for alloying element M which may be a strong carbide former like Mo, Ti, Nb, or W, and two for alloying element N, generally Cr.

The process of internal precipitation of a M_aC_b type carbide can be discribed by the reaction:

$$aM + bC = M_aC_b \tag{45}$$

where C is the carbon and M is the alloying element (M or N in Ni-M-N system). Assuming unit activity for M_aC_b compound, the equilibrium constant K can be derived:

$$K = \exp(-\Delta G/RT) = (\gamma_C)^{-b} (C_{max})^{-b} (\gamma_M)^{-a} [M]^{-a} \tag{46}$$

The solubility limit C_{max} denote the austenite carbon content in equilibrium with the carbide.

$$C_{max}=[\exp(-\Delta G/RT)]^{-1/b} (\gamma_X)^{-1/b} (\gamma_M)^{-a/b} [C_M]^{-a/b} \quad (47)$$

where ΔG^{o} is the standard free energy of formation of the carbide and γM, γC are the activity coefficients of carbon and alloying element in the alloy , respectively. Both the activity coefficients of carbon and the alloying element are considered as a function of the alloying element content. If more than one carbide is envolved these calculations can be carried out for each carbide, and the one that gives the lower value of C_{max} would be the stable carbide at each meshpoint.

At one meshpoint, the concentration of the diffusing carbon is calculated by the finite difference method. Then if the calculated solubility limit (C_{max}) is lower than the current C concentration at that point (calculated by finite difference method), the difference is subtracted from the diffusing carbon as well as an appropriate amount of the carbide-forming element concentration (i.e., M or N). The calculation of C_{max} should satisfy equation (47) for corresponding alloying element. In other word, the concentration soluble in the system according to equation (45) is then determined by equation (47). This is done for each carbide

that is supposed to be formed at each mesh point, and the lowest C_{max} corresponds to the stable carbide at that point. It should be noted that since these calculations are preformed at one Δx and all the time increments at each round, it is possible to form different carbide at different time increments for the same Δx.

Bongarts et. al. (1) did the same calculations, but they first reacted the carbon with element M to form the corresponding carbide, and the remaining carbon then was used for element N to form another carbide at the same space-time grid point. Their program could also treat just two different carbides comparing to four here.

Provision was also made for the case where there was not enough alloying element to precipitate all the excess carbon. In that case, only the possible amount was subtracted. The process was repeated consecutively for the four reaction at each point.

The calculation of carbide stability requires data on the free energies of formations of carbides, and the activities of C and alloying elements in the alloy. These data are required as a function of composition, since the composition of the alloy changes as the precipitation process evolves. The activity of C at the alloy surface is very high for most of the environments of interest and the concentration of C

at the surface can be taken as the terminal solubility.

The formation of mixed carbides were not considered here. However, if mixed carbides are present, a variable carbide composition was included. In this case the free energy of formation of the carbide would also be as a function of this composition.

In reality carbides contain a small amount of nickel. However, as the nickel content of carbide is low, the nickel content of austenite will not change significantly during carbide precipitation, and so the nickel can reasonably be neglected for the purpose of thermodynamic calculations (1). This leads to one alloying element carbide composition which has been used in present work.

It is evident that due to flexibility of the finite difference technique, a carbide composition which varies with the bulk carbon content of the alloy could also be considered if appropriate thermodynamic data were available.

The activity coefficient of carbon in Ni-Cr-C system could be written as:

$$\gamma_C^{Ni\text{-}Cr\text{-}C} = \gamma_C^{Ni}\ \gamma_C^{Cr\text{-}C} \tag{48a}$$

$$\ln \gamma_C^{Ni\text{-}Cr\text{-}C} = \ln \gamma_C^{Ni} + \ln \gamma_C^{Cr\text{-}C} \tag{48b}$$

or,

$$\ln \gamma_C^{Ni\text{-}Cr\text{-}C} = e_{11} N_1 + e_{13} N_{Cr} \quad (49)$$

It is often more convenient to consider the concentration of solutes in terms of weight percentages and to use logarithms to the base ten. Then equation (48a) becomes:

$$\log \gamma_C^{Ni\text{-}Cr\text{-}C} = \log \gamma_C^{Ni} + \log \gamma_C^{Cr\text{-}C} \quad (50a)$$

or,

$$\log \gamma_C^{Ni\text{-}Cr\text{-}C} = e_{11} N_1(wt\%) + e_{13} N_{Cr(wt\%)} \quad (50b)$$

There is a lack of data which accounts for the effects of alloying elements on the activity coefficient of carbon in the respective systems. Hence, the activity coefficient of carbon in Ni-Cr-C system was used for other systems.

5.5 Ternary Diffusion

The formation of oxide on the surface of a sample introduces the depletion of alloying elements that form oxide at the surface, and cause the uphill diffusion of carbon near the surface. The metal depletion could be quite large and the concentration of the alloying element (i.e., M, or N) in the Ni-M-N system could approach zero (2). The alloys considered in the calculations are:

(1) Ni-Cr-C

(2) Ni-Cr-Mo

(3) Ni-Cr-Ti

(4) Ni-Cr-Nb

(5) Ni-Cr-W

In our ternary calculations, thin relatively incoherent oxide layers are assumed to be formed on the surface of the alloys. The concentrations of the alloying elements that form oxides (i.e., Ti, Cr) are therefore considered to be zero at the surface.

In case of Ni-Cr-Ti alloy, two kind of oxides would be formed such as, Cr_2O_3, and TiO on the surface. For other alloys, Cr_2O_3 was the only oxide allowed to form in our ternary diffusion model.

Five diffusion coefficients, D_{11}, D_{12}, D_{13}, D_{22}, and D_{33} are necessary to describe the ternary diffusion problem. D_{11}, D_{22}, and D_{33} are measures of the effect of the concentration gradient of a given component on its own flux; whereas, D_{12}, and D_{13} reflects cross diffusion effects. Other ternary coefficients described in equation (5) such as, D_{21}, D_{23}, D_{31}, and D_{32} could be set equal to zero, since diffusion of substitutional elements is much slower than interstitial carbon diffusion by a factor of 10^{-4}. Therefore, the effect of the carbon concentration gradient on the diffusion of alloying element, as well as, the effect

of concentration gradient of one alloying element on the diffusion of the other, can be neglected. Hence:

$$D_{21} \simeq D_{23} \simeq D_{31} \simeq D_{32} \simeq 0 \qquad (8)$$

The value of D_{11} was assumed to be average diffusion coefficient of carbon in Ni-base alloys. D_{22} was taken as the diffusivity of the alloying element other than Cr in Ni, and D_{33} was the diffusivity of Cr in Inconel-600.

The cross diffusion coefficients D_{12}, and D_{13} were calculated from equation (6):

$$D_{12}/D_{11} = e_{12}\, N1/(1 + e_{11}\, N1) \qquad (6a)$$

$$D_{13}/D_{11} = e_{13}\, N1/(1 + e_{11}\, N1) \qquad (6b)$$

Equation (6a) calculates the diffusion coefficient ratio D_{12}/D_{11} which considers the formation of TiO, and equation (6b) considers the effect of Cr_2O_3. N_1 is the mole fraction of element 1 or carbon, and considered to be the maximum solubility of carbon in pure nickel (C_S), since the concentration of the alloying element would be zero at the surface.

When a gradient of alloying element occurs close to surface, the effect of cross coefficient on carbon diffusion would only be important close to the surface. Therefore, the cross coefficients are calculated at a point where the

carbon content approaches C_S.

It should be noticed that the values of the diffusion coefficient ratios depends on the unit of concentration, although it is a non-dimensional quantity. Therefore, it depends on the calculation of interaction parameters (i.e., e's). The equations (6) can be used as it is if mole fraction is the unit for calculation of interaction parameters. But, if weight fraction is the unit, equation (6) should be modified. The modification has been done by Wada (31) as:

$$D_{12}/D_{11} = (M_1/M_2)\ e_{12}\ N1/(1 + e_{11}\ N1) \qquad (51a)$$

$$D_{13}/D_{11} = (M_1/M_3)\ e_{13}\ N1/(1 + e_{11}\ N1) \qquad (51b)$$

where, M_1, M_2, and M_3 are the atomic weights of carbon and alloying elements, respectively.

6 Results

6.1 Thermodynamic Stability of Carbides

Several investigators have measured the free energy of formation of Cr carbides. A recent study is presented by Small and Ryba (31). There is a large difference between the values reported by different investigators. Comparison with experimental studies of carbide stability (16) suggests that the data of Small and Ryba result in Cr_7C_3 being stable for Cr contents higher than those observed experimentally. In the present work the free energy of formation of Cr carbides were estimated as shown in table (3). These values are taken from Kleykamp (32), Small and Ryba (31), and Kulkarni and Worrell (33) for Cr_3C_2, Cr_7C_3, and $Cr_{23}C_6$, respectively. Table (3) also shows the energy of formation of other carbides that can be formed in Ni-Cr-Ti, Ni-Cr-W, Ni-Cr-Mo, and Ni-Cr-Nb systems.

The activity coefficient of carbon in Ni-Cr system could be obtained from equation (49), and (50). The activity coefficient of carbon in pure Ni has been calculated by (41):

$$\log \gamma_C^{Ni} = e_{11} N_1 = 2.25 \qquad (52)$$

PARAMETER	VALUE		REFERENCE
ΔG° (Cr_3C_2)	-67.4	KJ/mol	32
ΔG° (Cr_7C_3)	-143	KJ/mol	31
ΔG° ($Cr_{23}C_6$)	-402	KJ/mol	33
ΔG° (Mo_2C)	-58	KJ/mol	38
ΔG° (Mo_6C)	-54.2	KJ/mol	39
ΔG° (TiC)	-171.9	KJ/mol	41
ΔG° (WC)	-35	KJ/mol	41
ΔG° (NbC)	-125.6	KJ/mol	41
$\log \gamma_C$	$2.25-4.45N_{Cr}$		34
γ_{Cr}	$.7+5.3N_{Cr}$		35
γ_{Mo}	17		36
γ_{Ti}	5.3×10^{-4}		36
γ_{Nb}	0.1		37
γ_W	23.5		36
C_S (+)	$25.4 \times 10^{(2.25-4.45N_{Cr})}$		34
C_S (*)	.143 wt%		30

Table 3. Data for carburization studies. (+) Non-oxidizing conditions, (*) Oxidizing conditions, N_{Cr} is in atom fraction.

The activity of carbon in Ni-Cr system could be extrapolated from the data by Lobl et al. (34) at 850°C. Substituting these values in equation (50) result the values for e_{13}. An average e_{13} was calculated as:

$$e_{13} = -4.45 \tag{53}$$

This gives an equation for the activity coefficient of carbon in the system:

$$\log \gamma_C^{Ni\text{-}cr} = 2.25 - 4.45\ N_{Cr} \tag{54a}$$

or,

$$\gamma_C^{Ni\text{-}cr} = 10^{(2.25 - 4.45\ N_{Cr})} \tag{54b}$$

The activity coefficient of Cr in the system can be extrapolated from the data given by Tousek et al. (35) at 850°C,

$$\gamma_{Cr} = 0.7 + 5.3\ N_{Cr} \tag{55}$$

where N_{Cr} is the atomic fraction of Cr.

The activity coefficients of alloying elements in nickel base superalloys can be obtained from the work of Williams (36), where he gives the activities for such element as Mo, Ti, and W. Activity data for niobium in the respective system could not be found. However, on the basis

of data from the iron-niobium, chromium-niobium, and nickel-niobium systems, Spencer (37) has estimated the activity coefficient of niobium to be approximatly 0.1. These activities are tabulated in table (3).

The calculation of the maximum solubility of carbon in Ni-Cr can be carried out based on the maximum solubility of carbon in nickel (30), and the measured activity of carbon in Ni-Cr alloys,

$$\gamma_C^{Ni\text{-}Cr}/\gamma_C^{Ni} = S_C^{Ni}/S_C^{Ni\text{-}Cr} \tag{56a}$$

then,

$$S_C^{Ni\text{-}Cr} = S_C^{Ni}\ (\gamma_C^{Ni}/\gamma_C^{Ni\text{-}Cr}) \tag{56b}$$

where,

$$\gamma_C^{Ni} = 178 \tag{57a}$$

$$S_C^{Ni} = 0.143 \tag{57b}$$

This results in an equation for solubility of carbon in the system as:

$$C_S = 25.4 \times 10^{(2.25 - 4.45N_{Cr})} \tag{58}$$

From these data and data on the activity of carbon, the calculations of the thermodynamic stability of carbides can be carried out using equation (47). In Ni-Cr system three

carbides could be formed as follows:

$$3Cr + 2C = Cr_3C_2 \quad (59a)$$

$$7Cr + 3C = Cr_7C_3 \quad (59b)$$

$$23Cr + 6C = Cr_{23}C_6 \quad (59c)$$

Substituting the data given in tables (3) for each reaction in equation (47), for different contents of chromium, would result in three set of values for C_{max}. The lowest C_{max} calculated at a content of chromium for the three reactions, would correspond to the carbide stable for that Cr concentration. The calculated data indicate that, in Ni-Cr alloys Cr_7C_3 is stable with respect to $Cr_{23}C_6$ up to 16 wt% Cr. In addition, Cr_3C_2 is stable with respect to Cr_7C_3 up to 12 wt% Cr. A similar calculation for MO_2C - MO_6C shows that MO_2C is stable up to 10.5 wt% Mo. The data for the Mo carbides were taken from references (38) and (39). $Cr_{23}C_6$ carbides were found to be stable with respect to Mo_6C for Cr contents higher than 32 wt% and Mo contents higher than 10.5 wt%. The stability regions predicted for the different carbides in Ni-Cr-Mo system are shown in the ternary diagram of figure (12). The predictions are in agreement with the observations of Raghavan et al (16). MO_6C carbides have been also observed in studies of carburization behavior of Inco-

Experimental

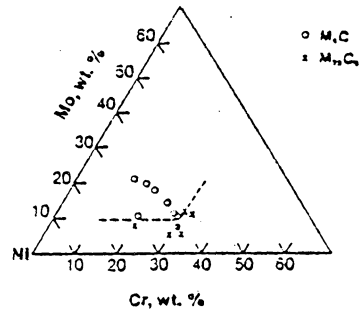

Calculated

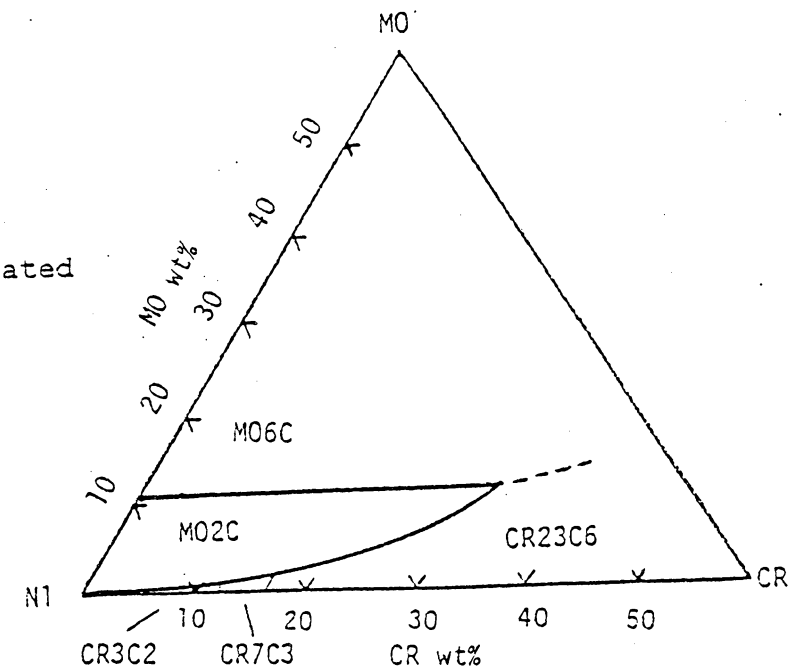

Figure 12. Plot showing stability regions for different carbides. Fig (4) is also shown for comparison.

nel 617 and Hastelloy C (17,40).

A similar calculation for WC-W_2C also shows that WC is stable up to 19.2 wt% W. $Cr_{23}C_6$ carbides were found to be stable with respect to WC for Cr contents lower than 41 wt%, and W contents lower than 19.2 wt%. Other alloying elements such as, Ti, and NB would form only one carbide as TiC, and NbC.

However, carbides of the types Cr_3C_2 , Cr_7C_3 have not been observed in Ni-base systems. This may in principle be due to their solubility limit of C in the alloy surface region being lower than the required C contents for these higher carbides.

These results show that Cr_3C_2 should be formed for Cr content less than 12 wt% Cr. If Cr oxide is formed at the surface the maximum amount of C in the alloy would be 0.143 wt% and the only carbides that could be formed are $Cr_{23}C_6$ and Cr_7C_3. The formation of a non-protective Cr_2O_3 layer is taken into account in the present calculations under oxidizing conditions.

6.2 Estimation of Diffusivity Parameters

The cross diffusivity D_{12} considered the formation of TiO_2 at the surface, and it can be calculated according to equation (6a). e_{12} is the thermodynamic wagner interaction

parameter which relates the activity coefficient of carbon to the mole fraction of Ti as:

$$e_{12} = \partial \ln \gamma_C / \partial [Ti] \Big|_{[Ti]=0} \qquad (60)$$

There was a lack of data on the activity coefficient of carbon in Ni-Cr-Ti system. Hence, an approximation was used to calculate e_{12} in Ni-Ti system. Equation (60) indicates that e_{12} is the slope of a plot of $\ln \gamma_C$ against the concentration of titanium (i.e., [Ti]) at constant N_C. Figure (13) shows such a plot. For pure Ti the activity of carbon in titanium carbide was calculated as follows:

$$Ti + C = TiC \qquad (61)$$

which is the reaction to form TiC. The equilibrium constant for the reaction would be:

$$K = a_{TiC} / \gamma_{Ti} [Ti] \gamma_C N_C \qquad (62)$$

for a pure carbide, $a_{TiC} = 1.0$

The average Ti concentration in superalloys is about 2 at%. This also satisfies equation (62) since the equation predicts the dilute solution of Ti in the system. The activity coefficient of Ti is listed in Table (3) as:

$$\gamma_{Ti} = 5.3\ 10^{-4} \qquad (63)$$

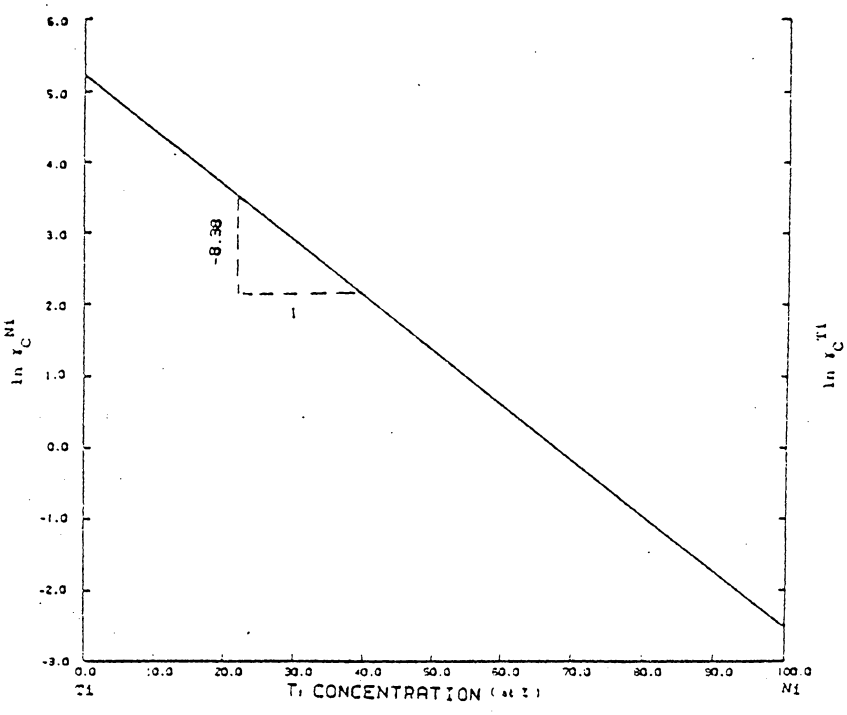

Figure 13. plot for calculation of interaction parameter e_{12}.

The energy of formation of TiC is also listed in Table (3), then the equilibrium constant for the reaction is:

$$K = 9.8\ 10^{7} \tag{64}$$

N_C is the mole fraction of carbon in pure Ti (30):

$$N_C = 0.012 \tag{65}$$

Substituding these values in equation (62) gives,

$$\gamma_C = 0.0802 \tag{66}$$

then,

$$\ln\gamma_C^{Ti} = -2.5 \tag{67}$$

The activity coefficient of carbon in nickel was (41):

$$\ln \gamma_C^{Ni} = e_{11}\ N_1 = 5.18 \tag{68}$$

The line constructed for these two points given in figure (13), gives an approximation of the activity of carbon in Ni-Ti. However, we are interested in dilute solution of Ti in Ni, therefore, for small amount of Ti we could expect a first order equation for the line. Hence, at 2 at% Ti, the slope of line would be:

$$e_{12} = -8.38 \tag{69}$$

substituting these values in equation (6a), and using D_{11} =

$1x10^{-8}$:

$$D_{12} = -9.3x10^{-11} \quad (70)$$

Equation (51b) can be used to calculate D_{13} since the calculation of e_{13} was based on weight fraction as units:

$$M_1/M_3 = 12/52 = 0.23 \quad (71)$$

Hence,

$$D_{13} = -1.98\ 10^{-11} \quad (72)$$

D_{11}, D_{22}, and D_{33} are measures of the effect of the concentration gradient of given component on its own flux. D_{11} was estimated as the diffusivity of carbon in Inconel 617 (3). D_{22} was considered as the diffusion of element M in Ni-M system. D_{33} was estimated as diffusivity of Cr in Inconel 600 (42). The diffusivity data are tabulated in table (4).

6.3 Input Parameters

The formalism described requires the input of the following parameters:

(1) Maximum diffusion distance in cm (half of the thickness of the sample, X_{max} = .153 cm)

(2) Carburization time in hours.

(3) Diffusivity of carbon, D_{11}.

(4) Cross diffusivity D_{12}, zero for binary diffusion.

PARAMETER	VALUE	REFERENCE
$D_C = D_{11}$	$1x10^{-8}$ cm^2/sec	3
$D_{Cr} = D_{33}$	$1.98x10^{-13}$ cm^2/sec	42
$D_{Mo} = D_{22}$	$2.35x10^{-11}$ cm^2/sec	44
$D_{Ti} = D_{22}$	$2.5x10^{-10}$ cm^2/sec	43
$D_{Nb} = D_{22}$	$1x10^{-12}$ cm^2/sec	45
$D_W = D_{22}$	$1.3x10^{-14}$ cm^2/sec	46
$D_{C-Cr} = D_{13}^*$	$-1.98x10^{-11}$ cm^2/sec	-
$D_{C-Ti} = D_{12}^*$	$-9.3x10^{-11}$ cm^2/sec	-

Table 4. Diffusivity data for the alloys studied. (*) Oxidizing conditions.

(5) Cross diffusivity D_{13}, D_{13} was zero for binary diffusion.

(6) Diffusivity of alloying element (Mo, Ti, Nb, or W), D_{22}.

(7) Diffusivity of Cr in the alloy, D_{33}.

(8) Maximum solubility of carbon on the surface. For binary diffusion this was obtained using equation (58). And for ternary calculations this was the maximum solubility of carbon in Ni (0.143 wt%).

(9) Concentration of alloying element at the surface, zero if alloying element formed oxide at the surface.

(10) Concentration of Cr at the surface, which was also zero for ternary diffusion calculations.

(11) The bulk carbon concentration; this was assumed to be zero.

(12) The bulk concentration of alloying element.

(13) The bulk concentration of Cr.

(14) For a M_aC_b Carbide, the reaction parameters were input as follows:

(a) Equilibrium constant of the carbide.

(b) Coefficient b in the M_aC_b carbide.

(c) Coefficient a in the M_aC_b carbide.

Four carbides could be considered in the program. A listing of the program is included in the appendix.

6.4 Carburization in Non-oxidizing Conditions

The carbide precipitation distribution in Ni-Cr alloys was calculated for different Cr contents at 850°C. Figures (14) through (29) show the results for 10 and 20 wt% Cr, and two different alloying element contents for 100 hours of exposure. The alloying element contents and concentration of Cr represent the concentrations generally found in Ni-base superalloys.

These figures show that TiC, Mo_2C, Mo_6C, and NbC were found to be more stable than Cr carbides which form only when the alloys deplete in solute elements. The alloys with 10 wt% Cr formed Cr_3C_2 as the stable Cr carbide. The alloys with 20 Wt% Cr formed $Cr_{23}C_6$ as the stable Cr carbide. All the stable carbides formed at the surface. In Ni-Cr-Mo system, the alloys with 6 wt% Mo formed Mo_2C as the stable carbide, and the alloys with 15 wt% Mo formed Mo_6C as the stable Mo carbide. In Ni-Cr-W system, the alloys with 20 wt% Cr, $Cr_{23}C_6$ was more stable carbide than WC, but in the alloy with 10 Cr, WC was the most stable carbide.

The comparison of these carbon profiles suggests that the carbon penetration depth increases with increasing Cr content while the surface carbon concentration, C_S, decreases. In Ni-Cr-Mo, and Ni-Cr-Nb systems, increasing the

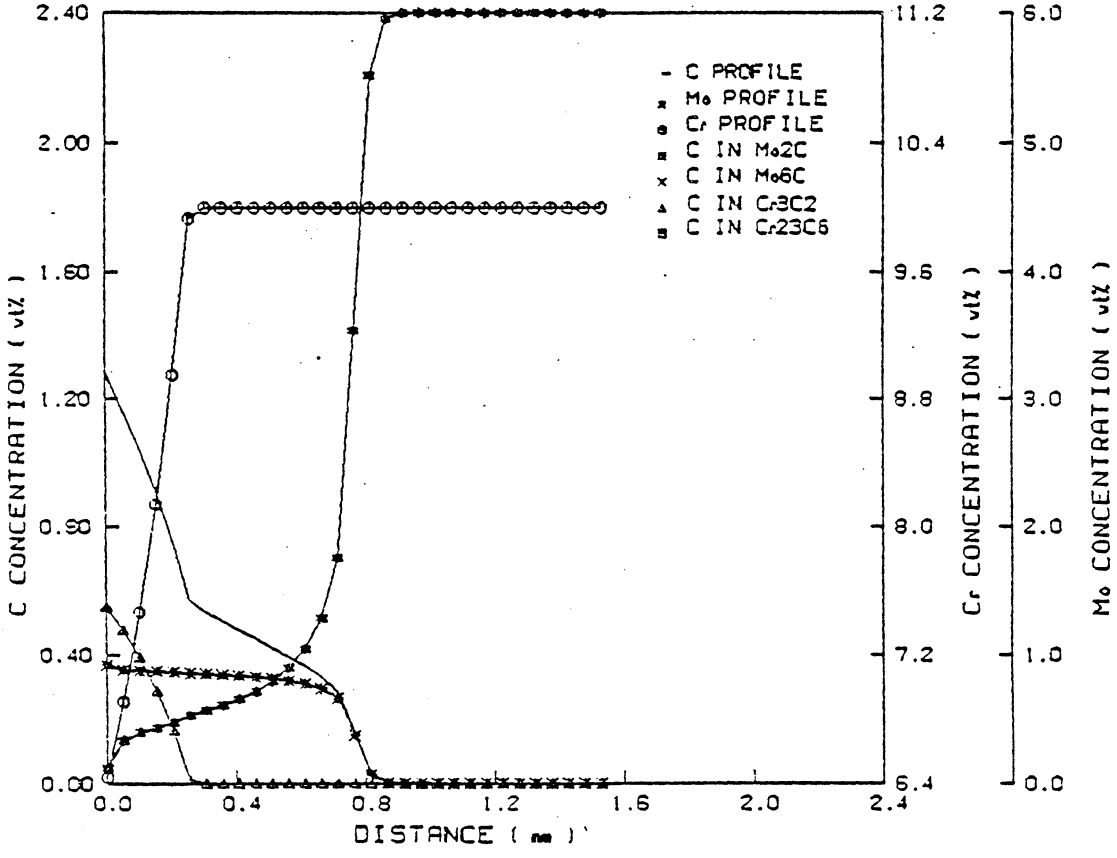

Figure 14. Carburization profiles of Ni-10Cr-6Mo alloys, 100 hrs, 850°C, non-oxidizing condition

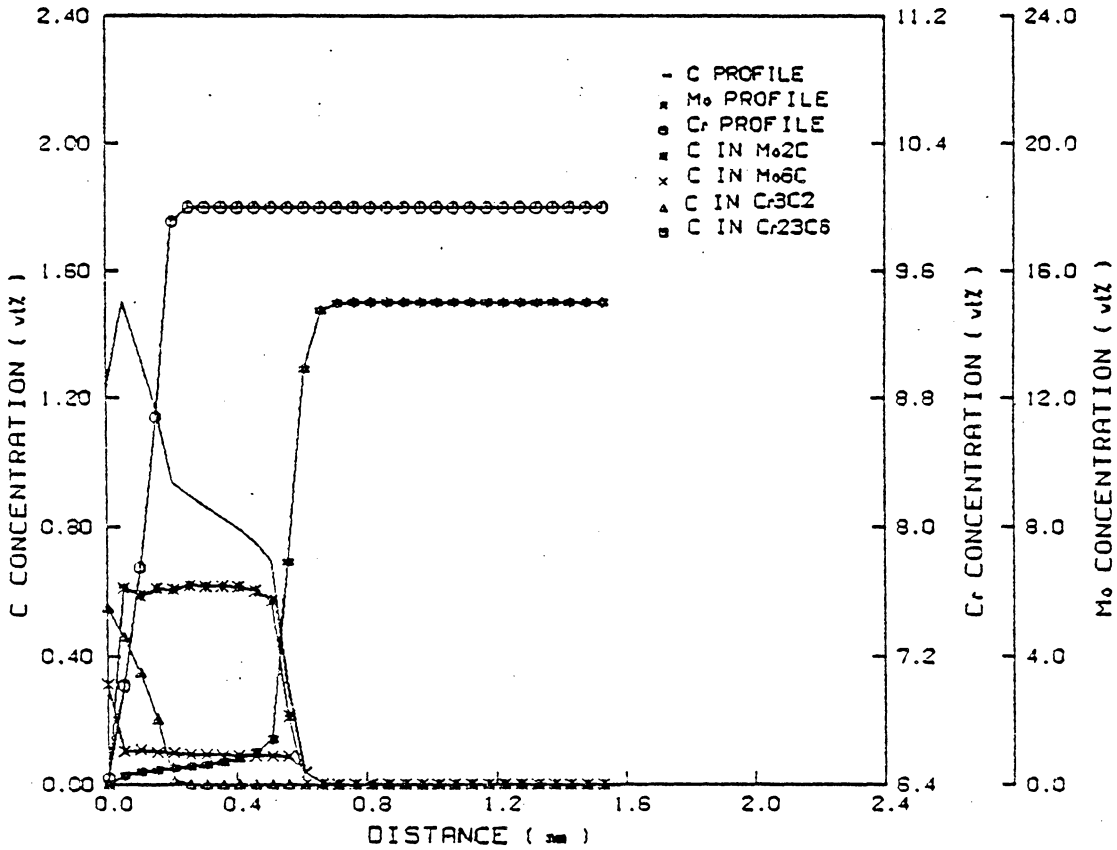

Figure 15. Carburization profiles of Ni-10Cr-15Mo alloys, 100 hrs, 850°C, non-oxidizing condition.

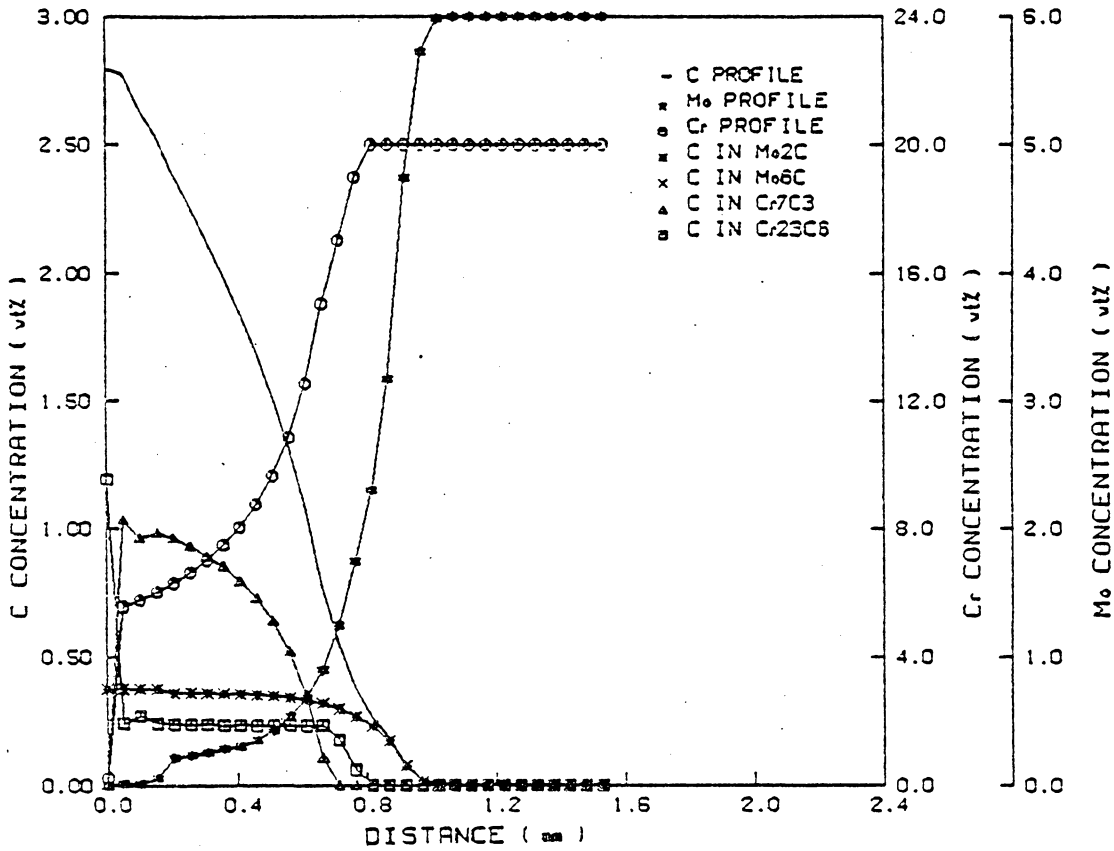

Figure 16. Carburization profiles of Ni-20Cr-6Mo alloys, 100 hrs, 850°C, non-oxidizing condition.

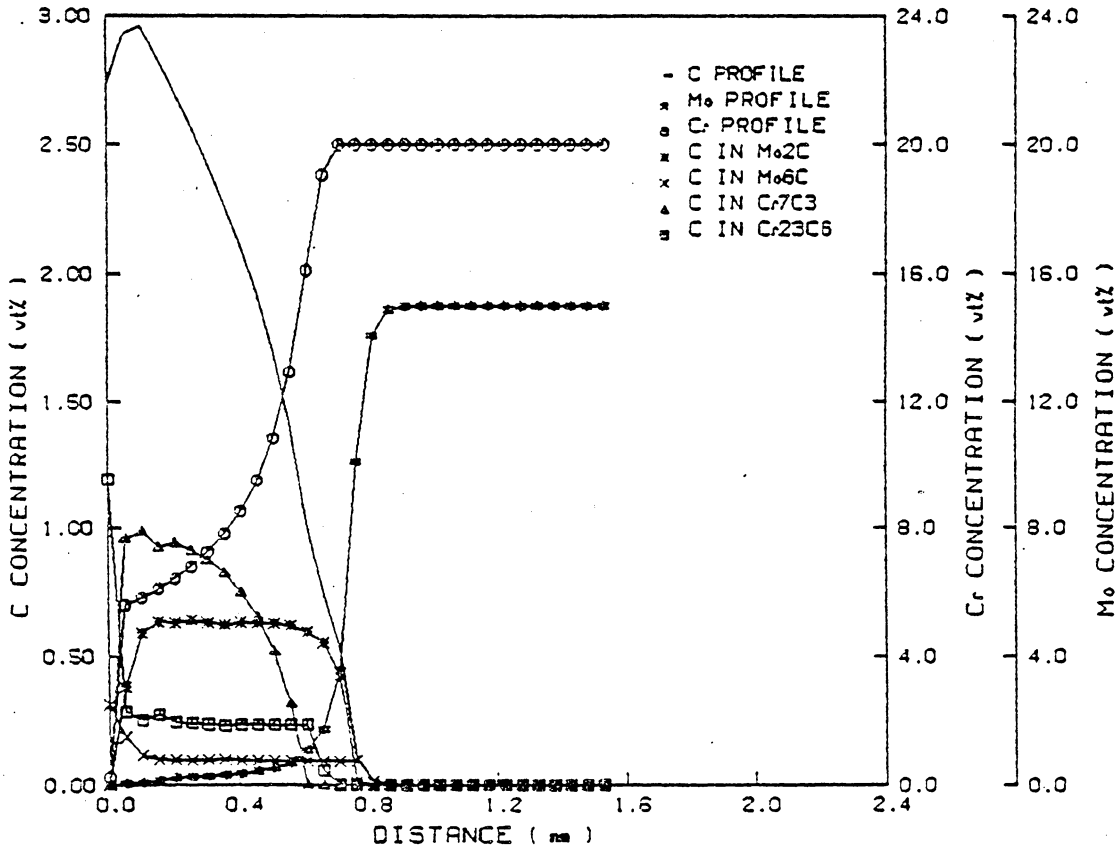

Figure 17. Carburization profiles of Ni-20Cr-15Mo alloys, 100 hrs, 850°C, non-oxidizing condition.

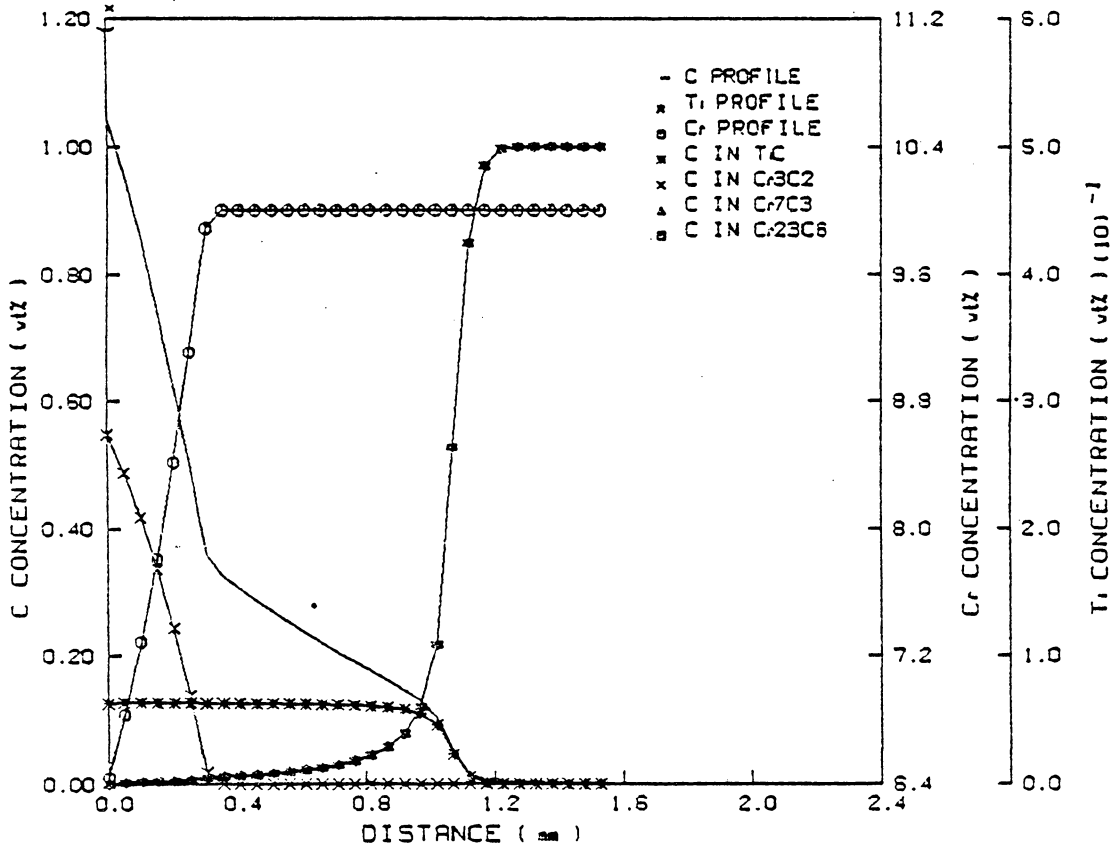

Figure 18. Carburization profiles of Ni-10Cr-.5Ti alloys, 100 hrs, 850°C, non-oxidizing condition.

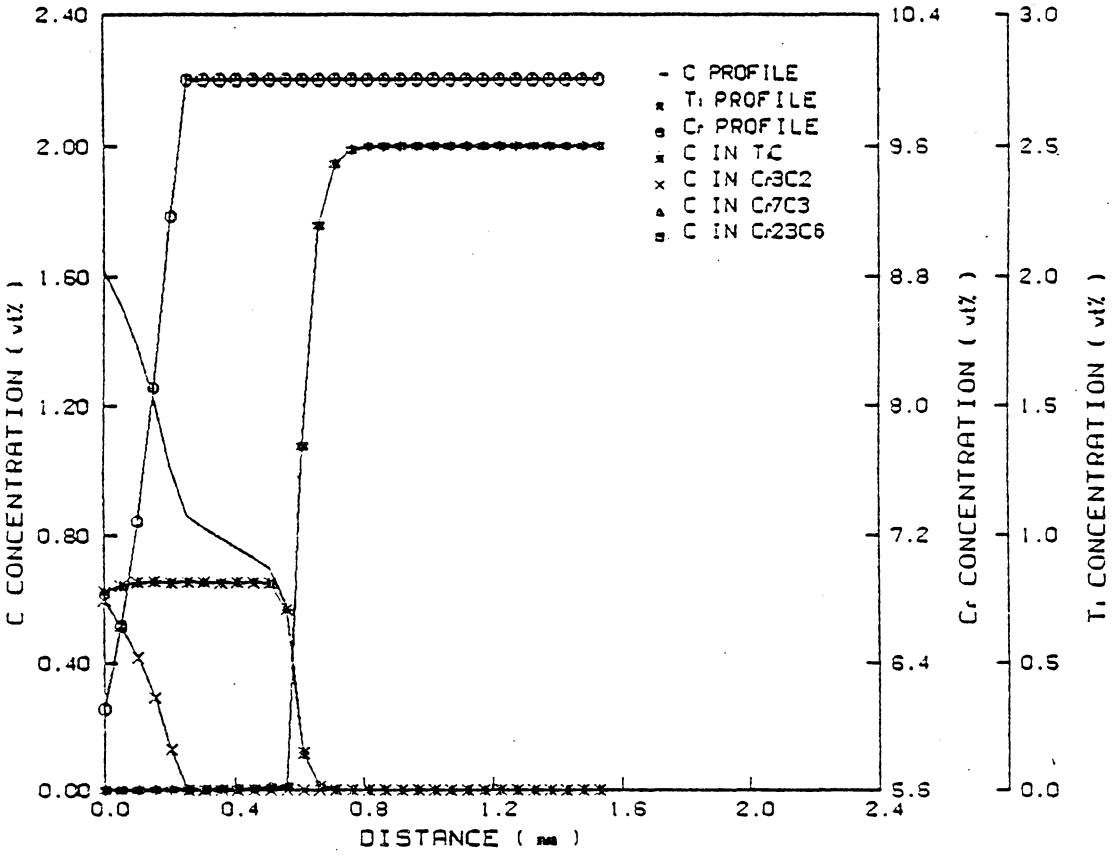

Figure 19. Carburization profiles of Ni-10Cr-2.5Ti alloys, 100 hrs, 850°C, non-oxidizing condition.

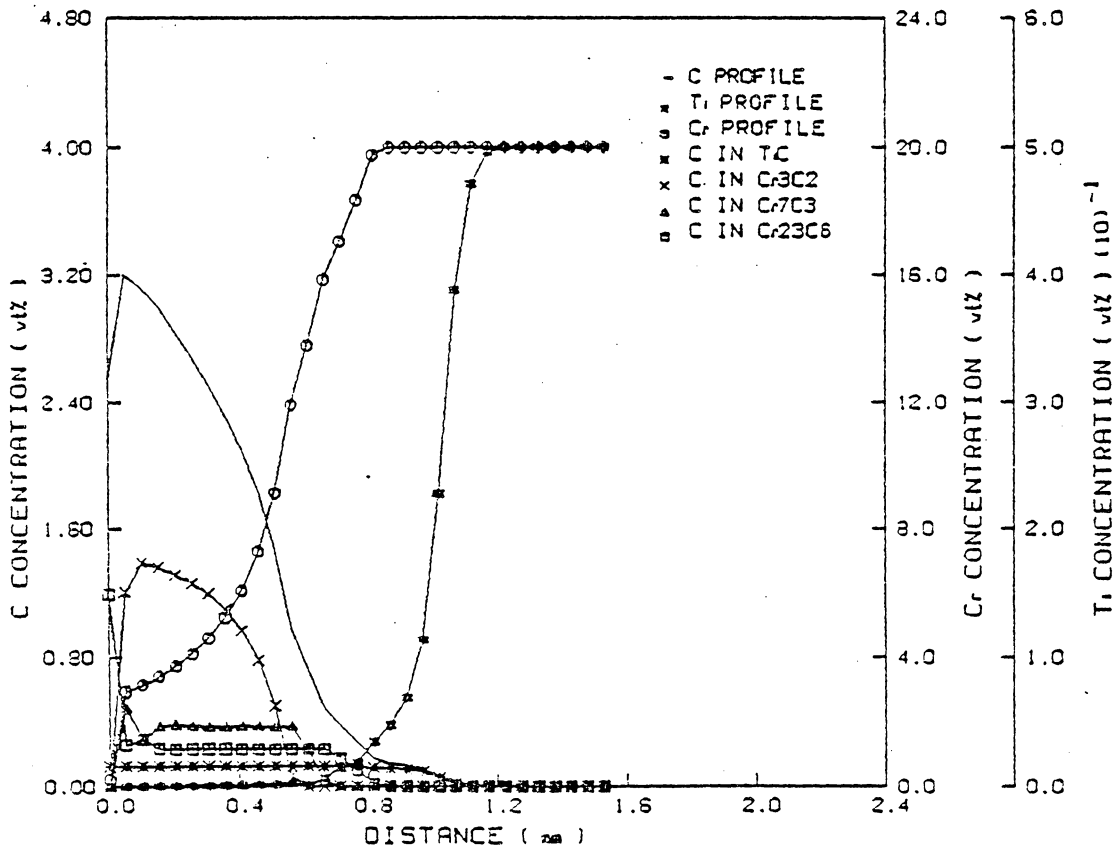

Figure 20. Carburization profiles of Ni-20Cr-.5Ti alloys, 100 hrs, 850°C, non-oxidizing condition.

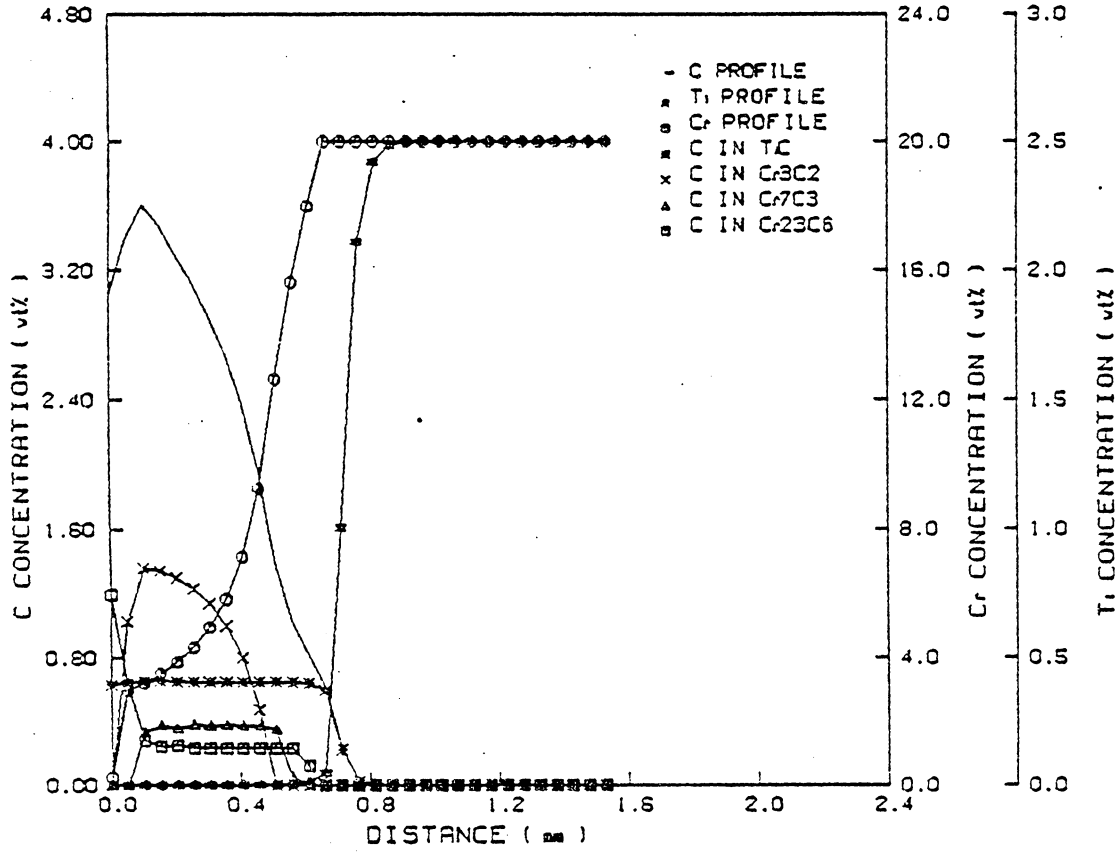

Figure 21. Carburization profiles of Ni-20Cr-2.5Ti alloys, 100 hrs, 850°C, non-oxidizing condition.

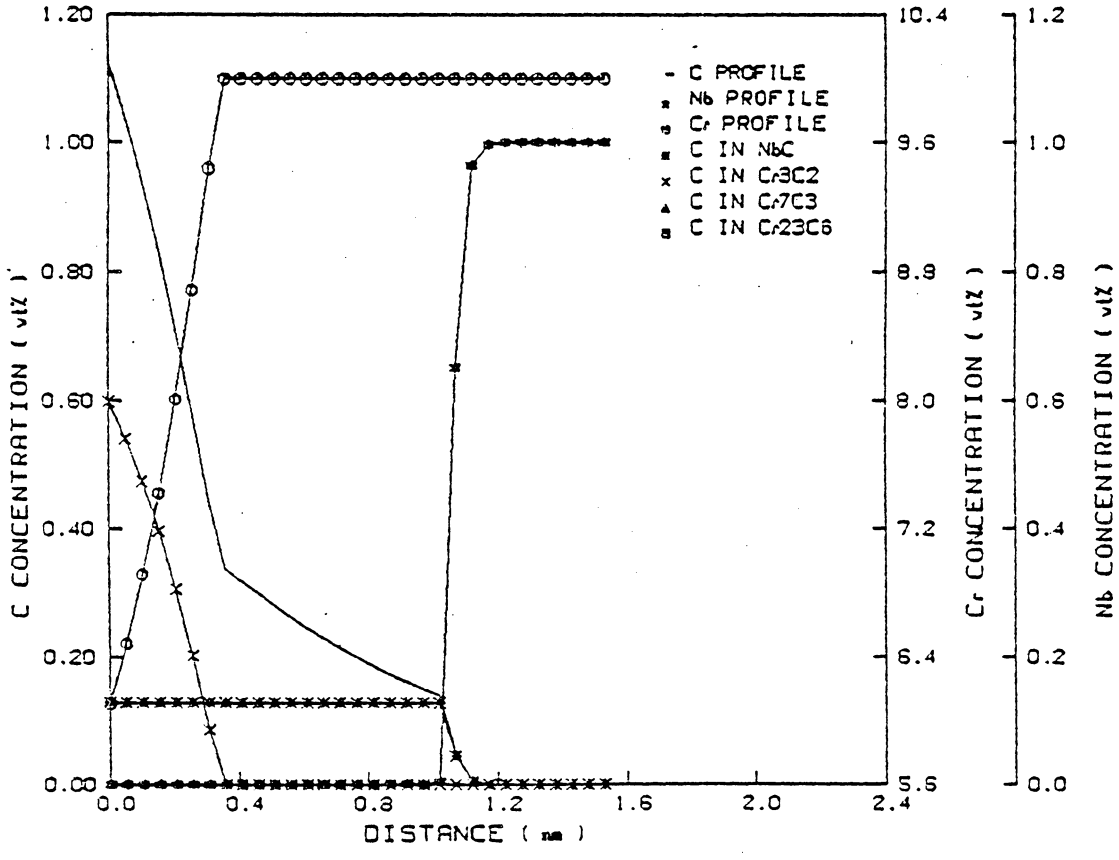

Figure 22. Carburization profiles of Ni-10Cr-1Nb alloys, 100 hrs, 850°C, non-oxidizing condition.

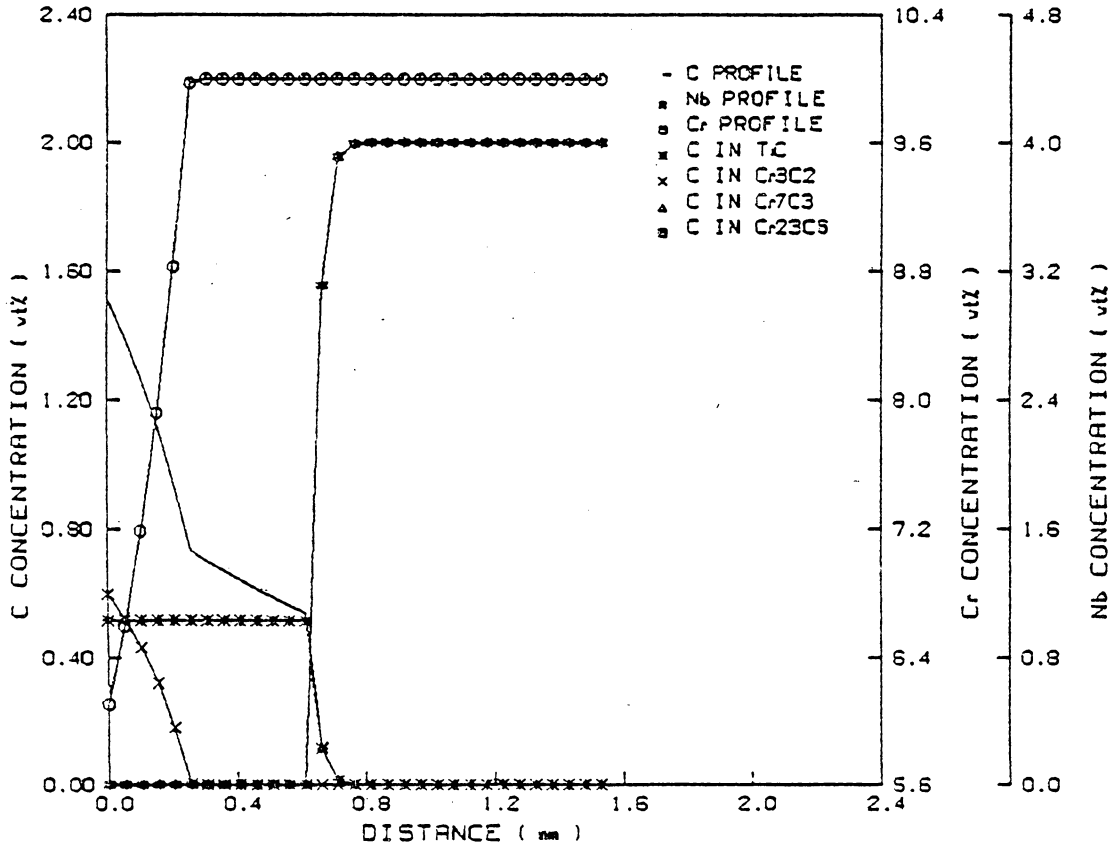

Figure 23. Carburization profiles of Ni-10Cr-4Nb alloys, 100 hrs, 850°C, non-oxidizing condition.

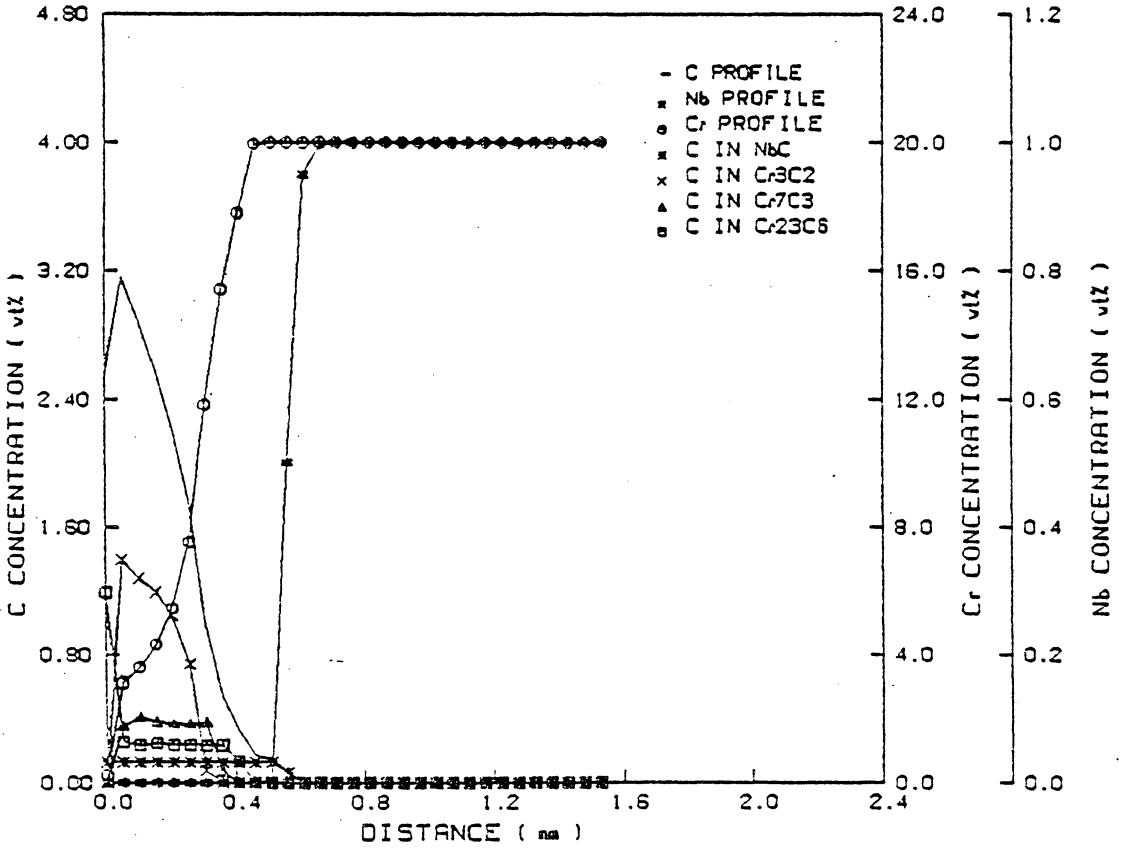

Figure 24. Carburization profiles of Ni-20Cr-1Nb alloys, 100 hrs, 850°C, non-oxidizing condition.

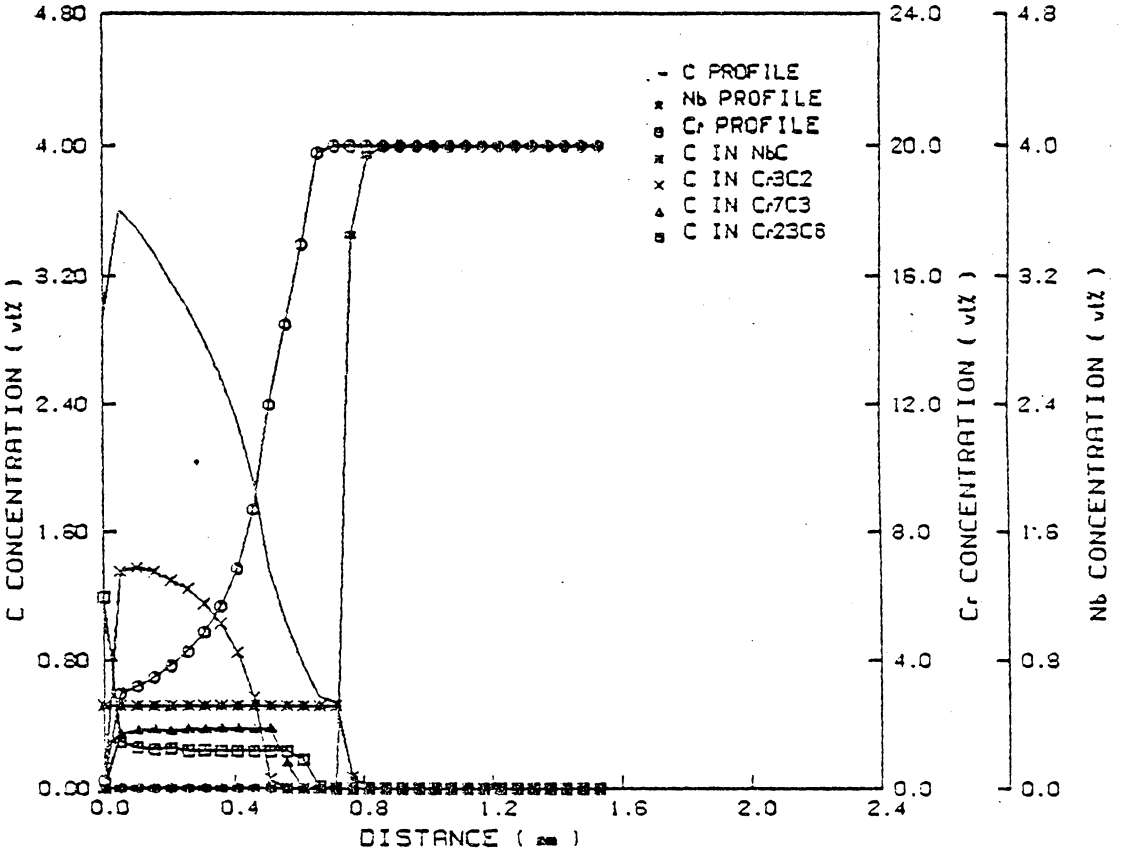

Figure 25. Carburization profiles of Ni-20Cr-4Nb alloys, 100 hrs, 850°C, non-oxidizing condition.

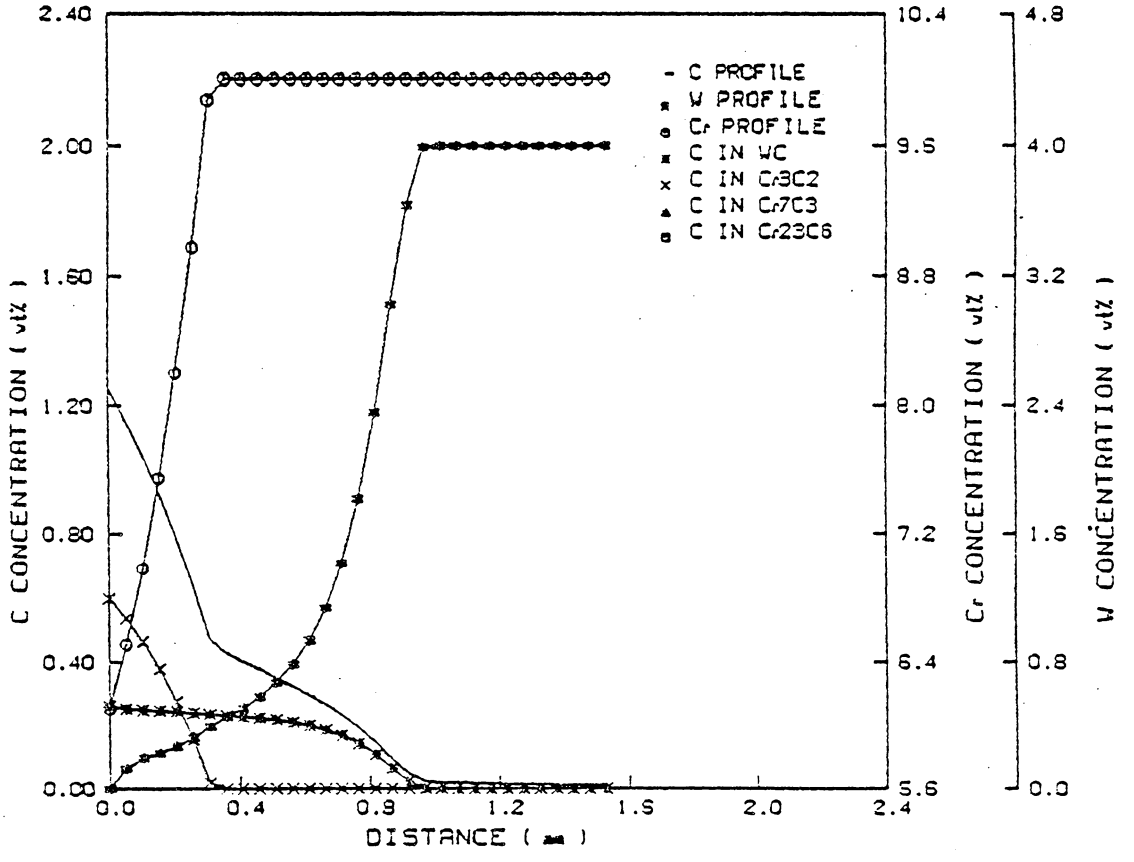

Figure 26. Carburization profiles of Ni-10Cr-4W alloys, 100 hrs, 850°C, non-oxidizing condition.

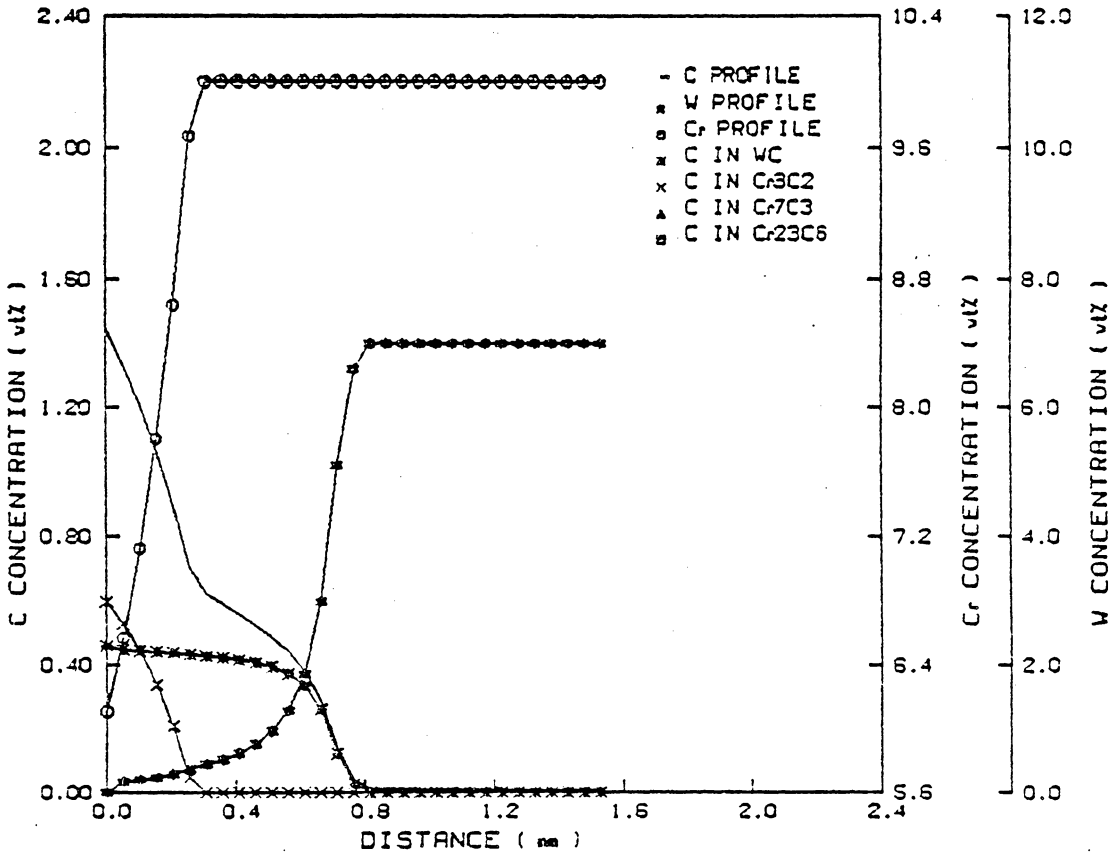

Figure 27. Carburization profiles of Ni-10Cr-7W alloys, 100 hrs, 850°C, non-oxidizing condition.

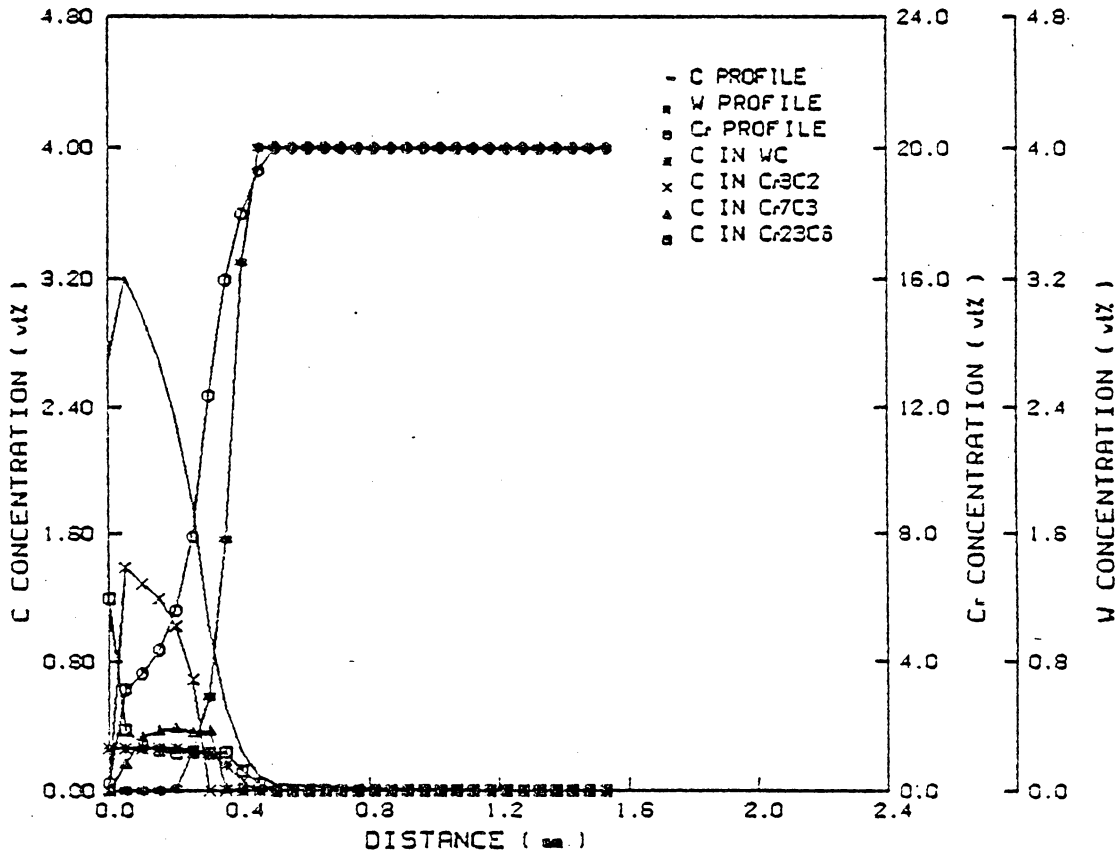

Figure 28. Carburization profiles of Ni-20Cr-4W alloys, 100 hrs, 850°C, non-oxidizing condition.

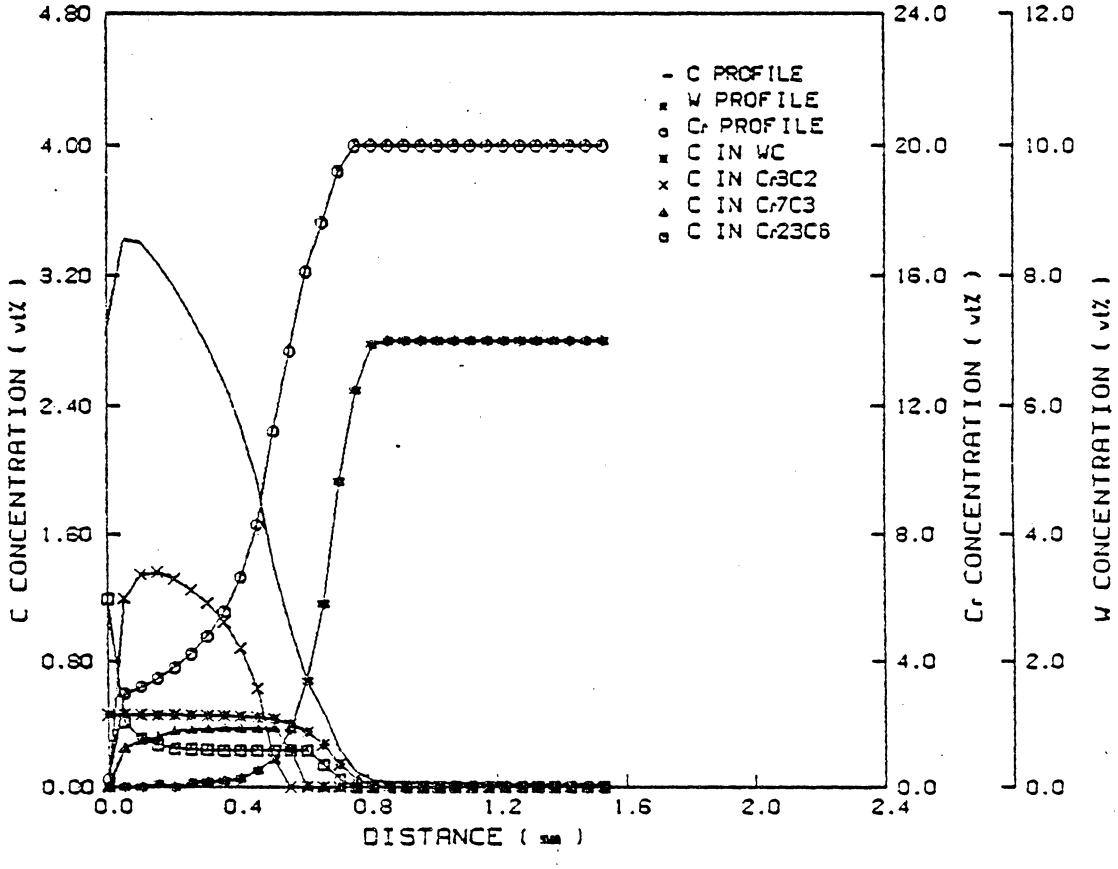

Figure 29. Carburization profiles of Ni-20Cr-7W alloys, 100 hrs, 850°C, non-oxidizing condition.

solute element content (i.e., Mo, or Nb) increase the surface carbon concentrations, while in Ni-Cr-Ti, and Ni-Cr-W systems, increasing the alloying element content decreases C_S.

Figures (30) through (33) show the corrosion behavior of the alloys, that is total carbon uptake as a function of carburization time for 10, 20,and 30 wt% Cr and different alloying elements, for 100 hours at 850°C. These plots show that as the chromium content increases, the carbon uptake increases sharply.

6.5 Carburization in Oxidizing Conditions.

Figures (34) through (49) show results for ternary diffusion calculation for the same alloys calculated in non-oxidizing condition. These calculations simulate the case where a non-protective oxide layer is formed at the alloy surface. This layer still allows fast carbon transfer from the gas phase but results in depletion of the elements that form oxides beneath the surface. The saturation concentration of C at the surface decreases sharply with Cr depletion. Note that the ternary cross diffusion effect was considered in this case. The effect of the cross diffusivities was significant. They raise the value C_S, for instance, in Ni-20Cr-2.5Ti, they raise the C_S value from 0.143 wt% at the

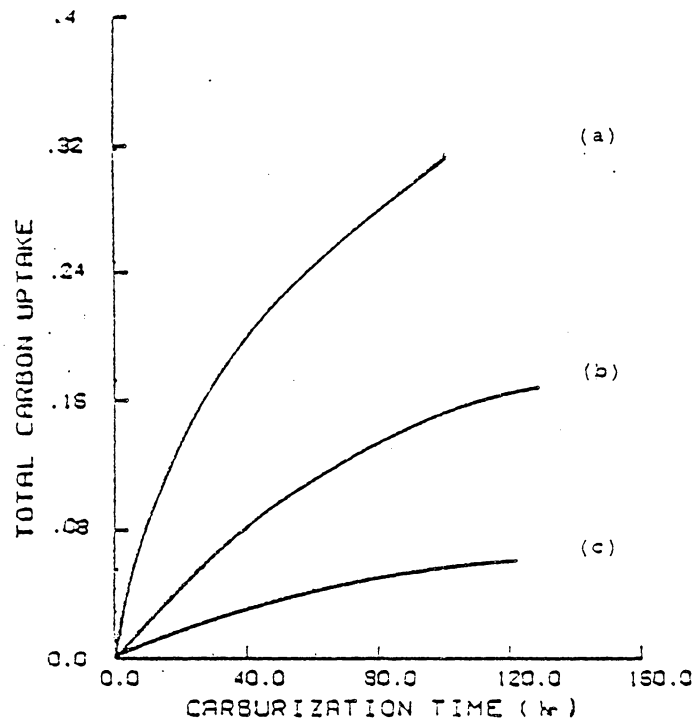

Figure 30. Total carbon uptake as a function of time, non-oxidizing condition. (a) Ni-30Cr-15Mo, (b) Ni-20Cr-15Mo, (c) Ni-10Cr-15Mo

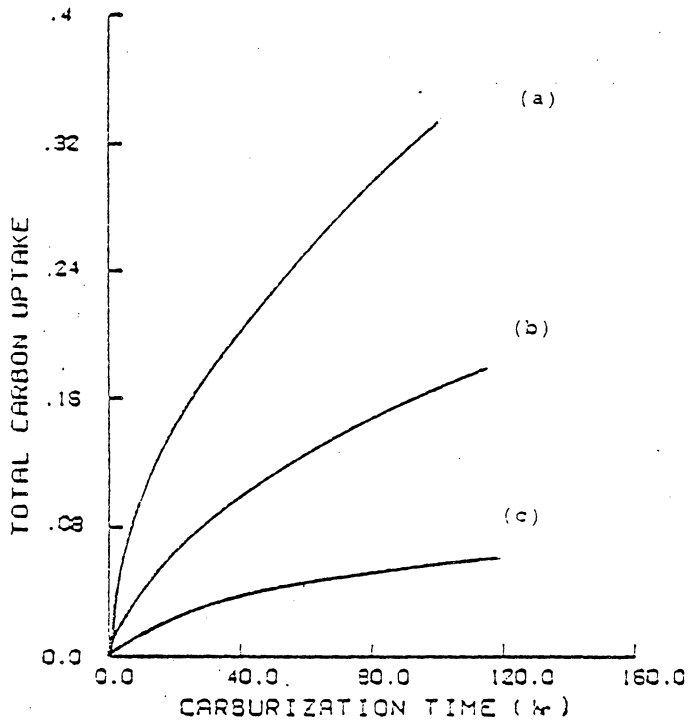

Figure 31. Total carbon uptake as a function of time, non-oxidizing condition. (a) Ni-30Cr-2.5Ti, (b) Ni-20Cr-2.5Ti, (c) Ni-10Cr-2.5Ti

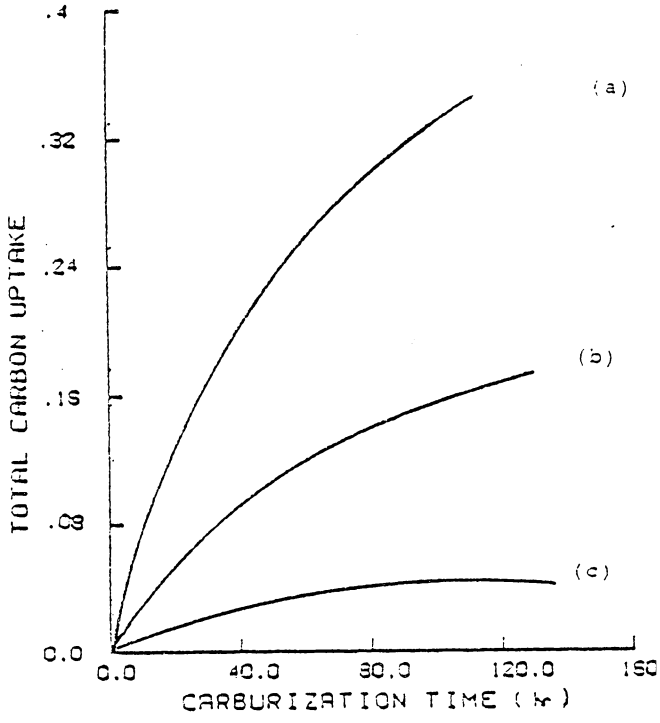

Figure 32. Total carbon uptake as a function of time, non-oxidizing condition. (a) Ni-30Cr-1Nb, (b) Ni-20Cr-1Nb, (c) Ni-10Cr-1Nb

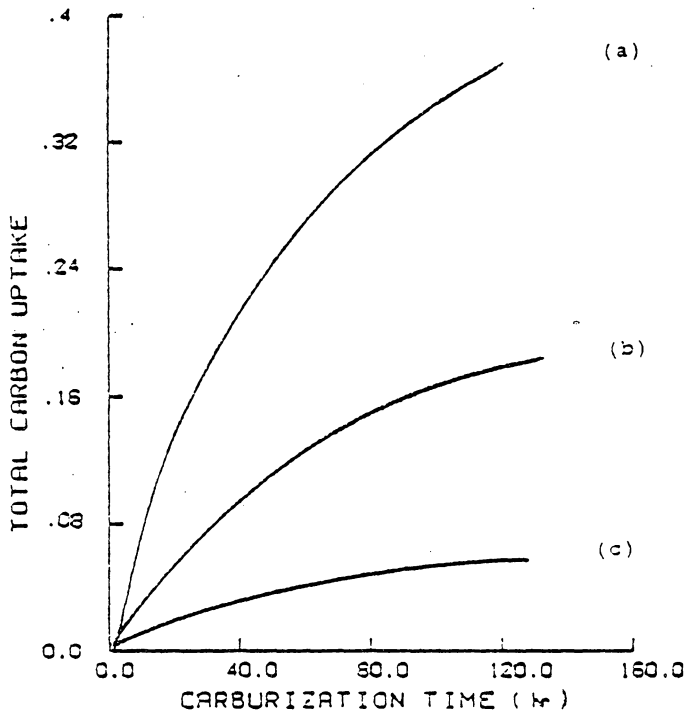

Figure 33. Total carbon uptake as a function of time, non-oxidizing condition. (a) Ni-30Cr-4W, (b) Ni-20Cr-4W, (c) Ni-10Cr-4W

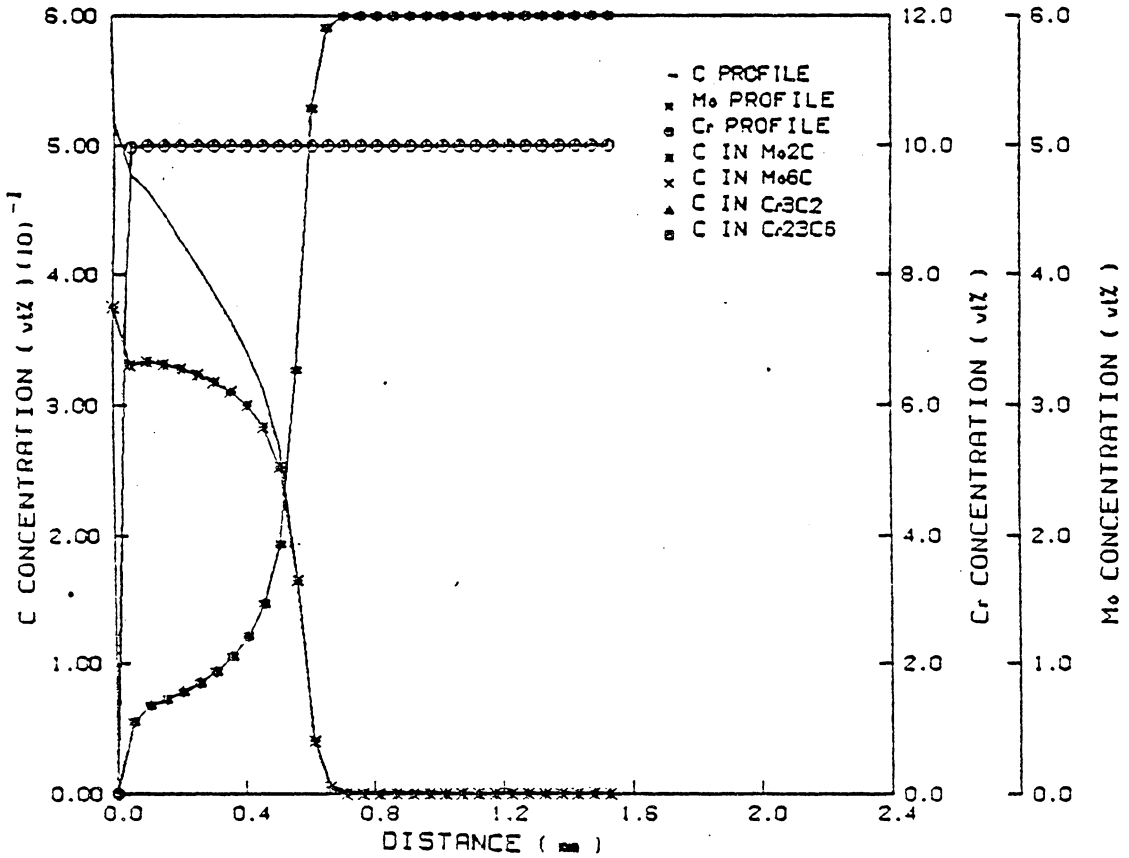

Figure 34. Carburization profiles of Ni-10Cr-6Mo alloys, 100 hrs, 850°C, oxidizing condition.

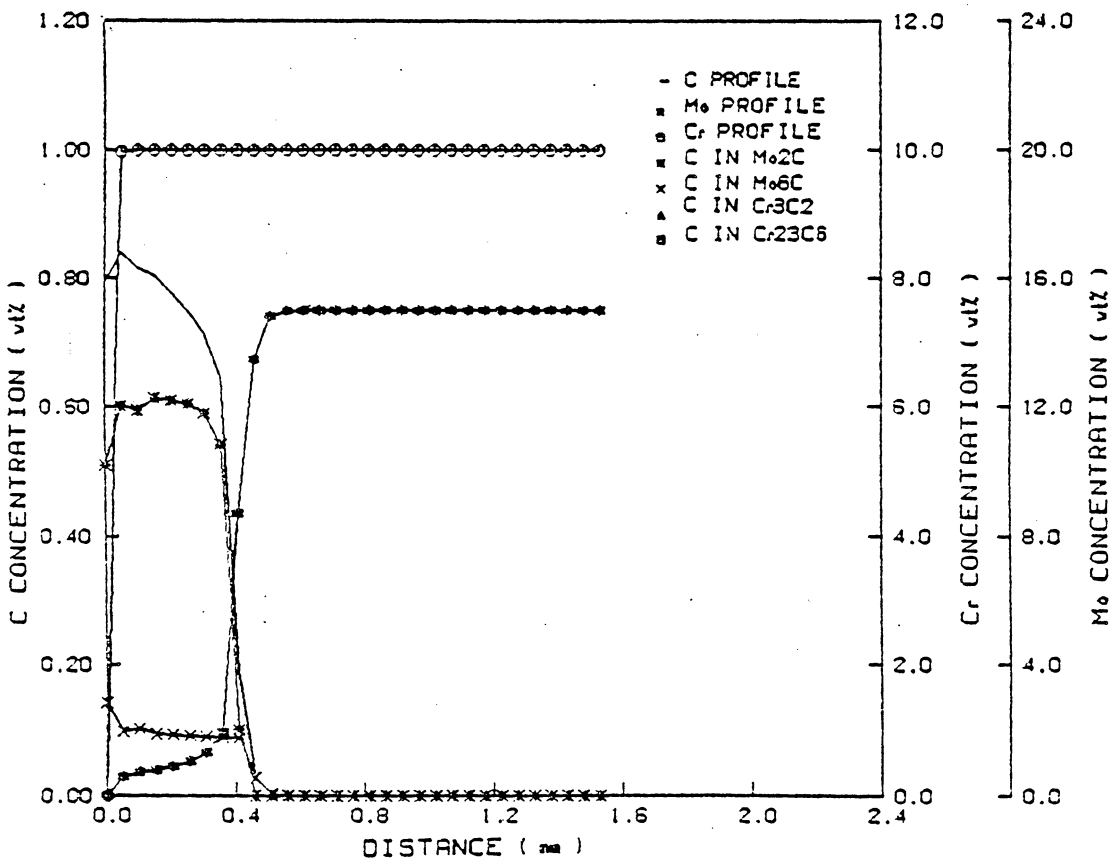

Figure 35. Carburization profiles of Ni-10Cr-15Mo alloys, 100 hrs, 850°C, oxidizing condition.

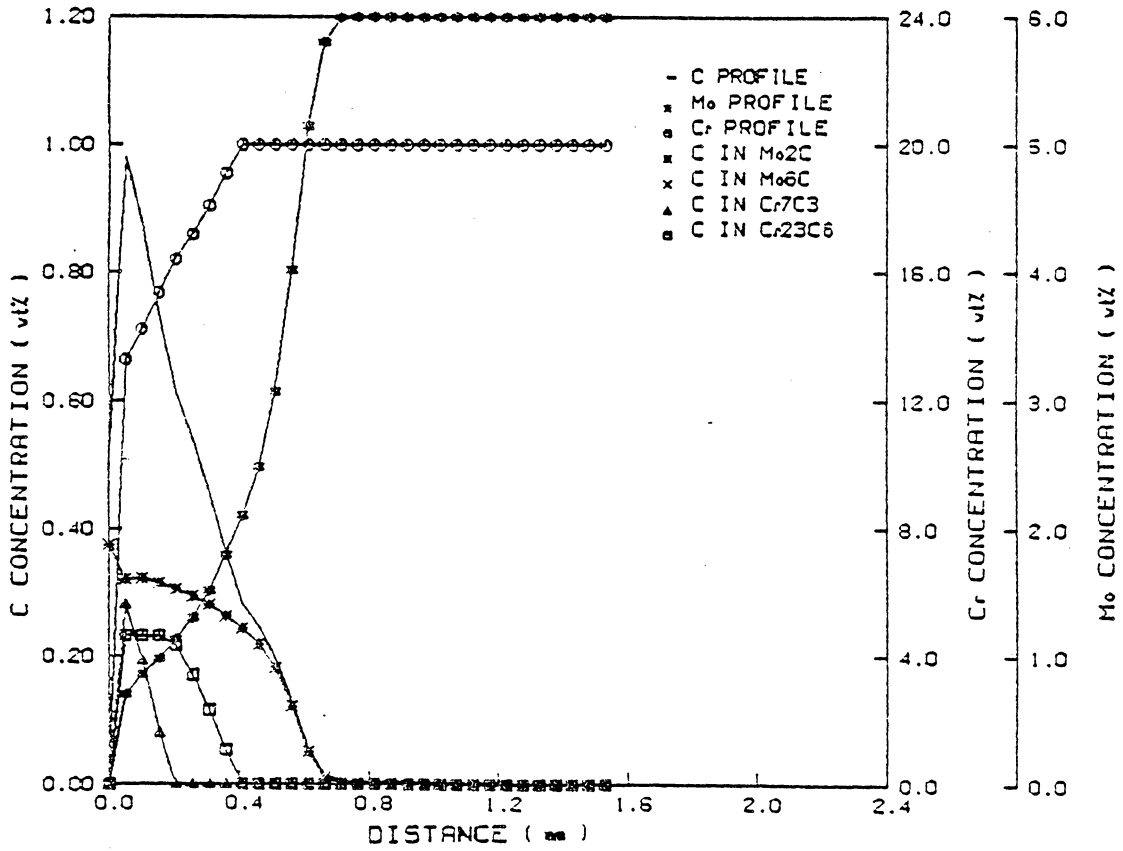

Figure 36. Carburization profiles of Ni-20Cr-6Mo alloys, 100 hrs, 850°C, oxidizing condition.

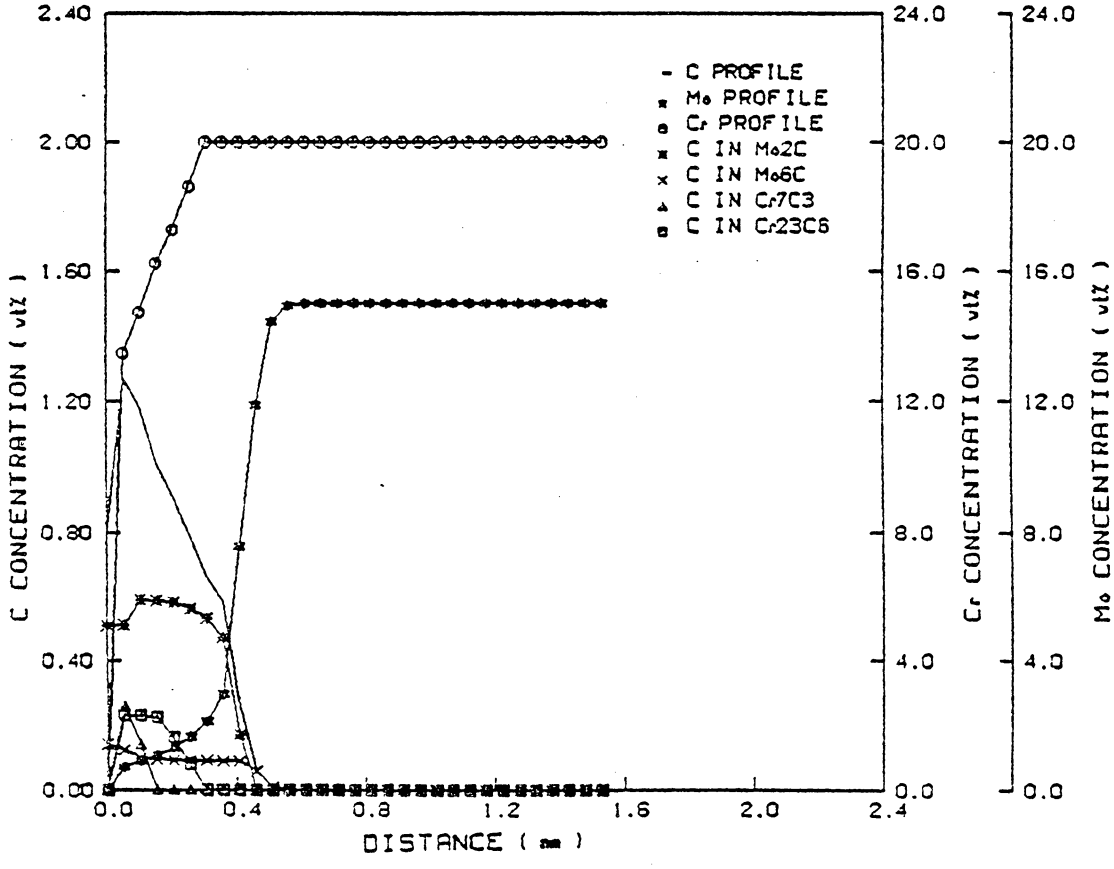

Figure 37. Carburization profiles of Ni-20Cr-15Mo alloys, 100 hrs, 850°C, oxidizing condition.

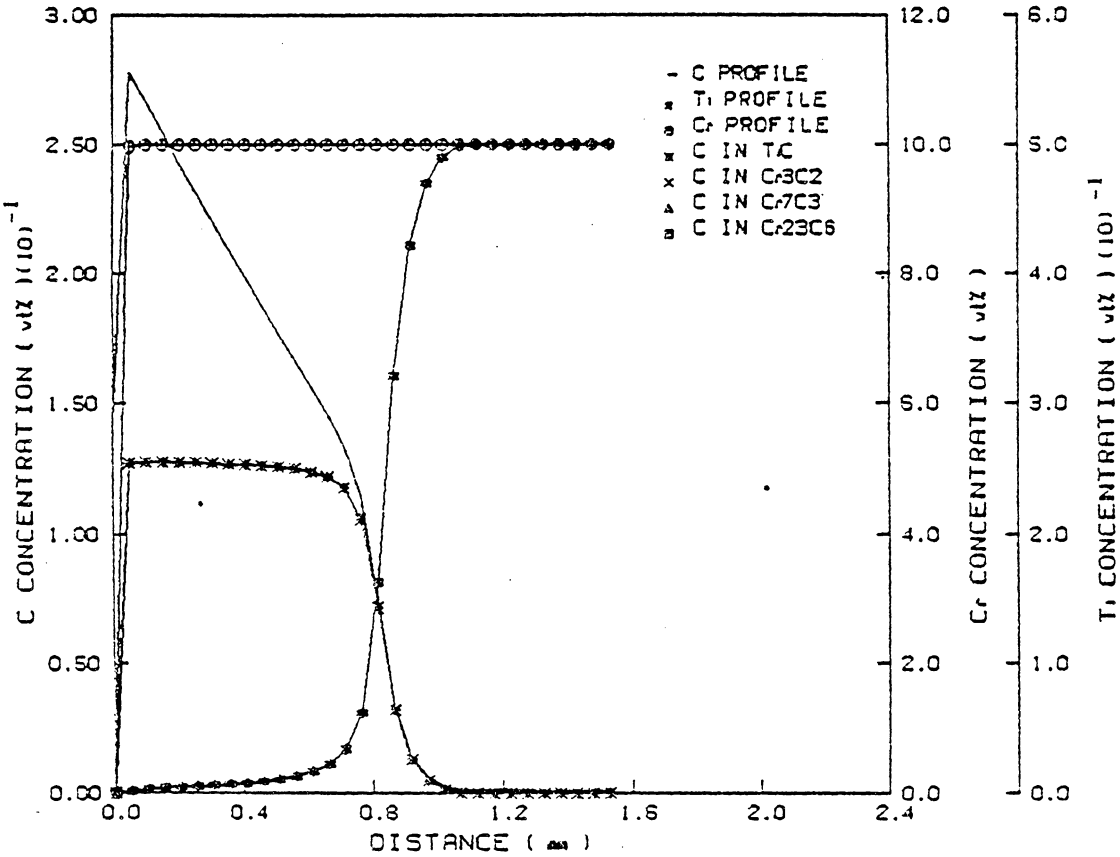

Figure 38. Carburization profiles of Ni-10Cr-.5Ti alloys, 100 hrs, 850°C, oxidizing condition.

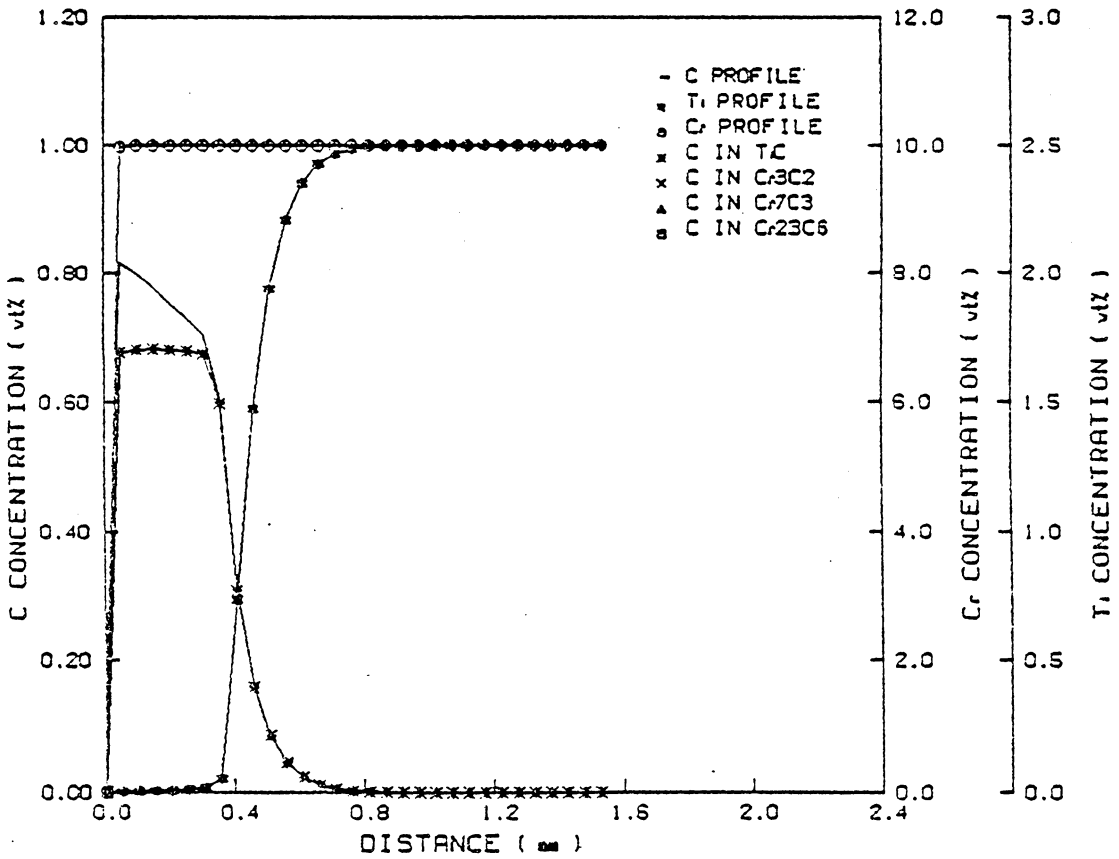

Figure 39. Carburization profiles of Ni-10Cr-2.5Ti alloys, 100 hrs, 850°C, oxidizing condition.

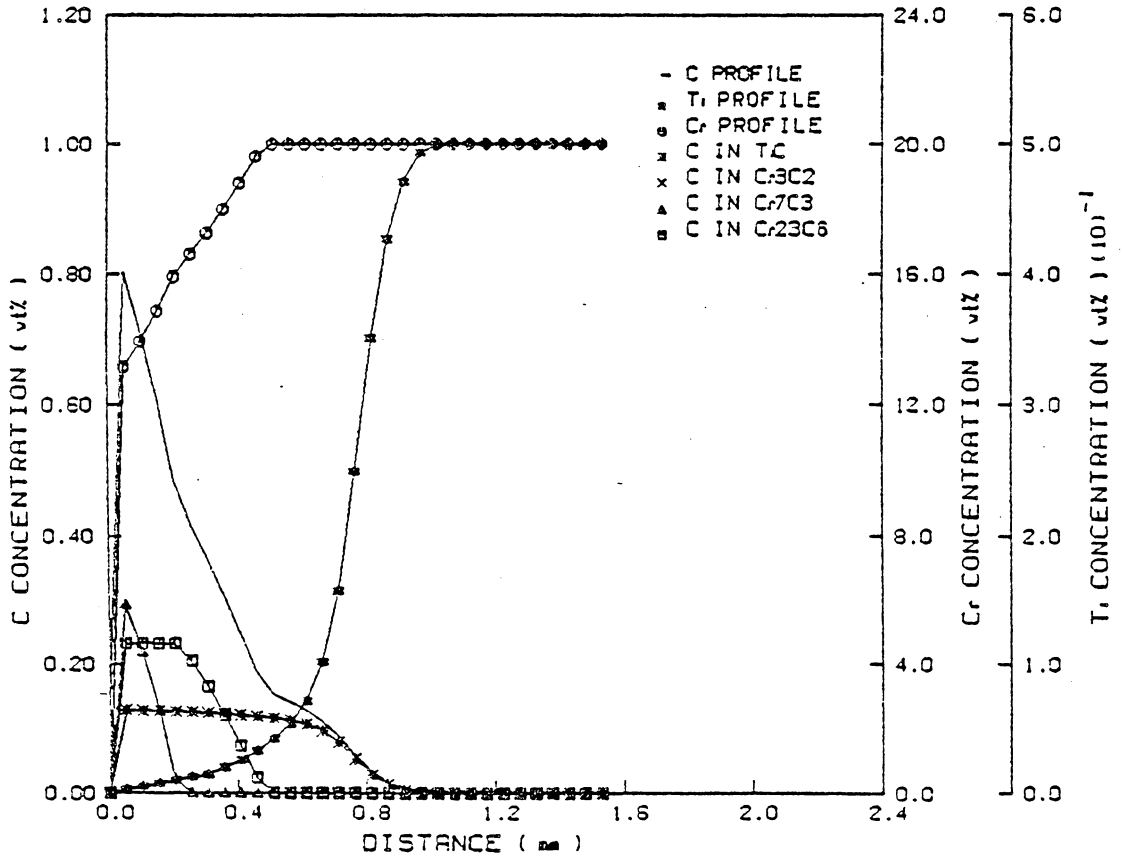

Figure 40. Carburization profiles of Ni-20Cr-.5Ti alloys, 100 hrs, 850°C, oxidizing condition.

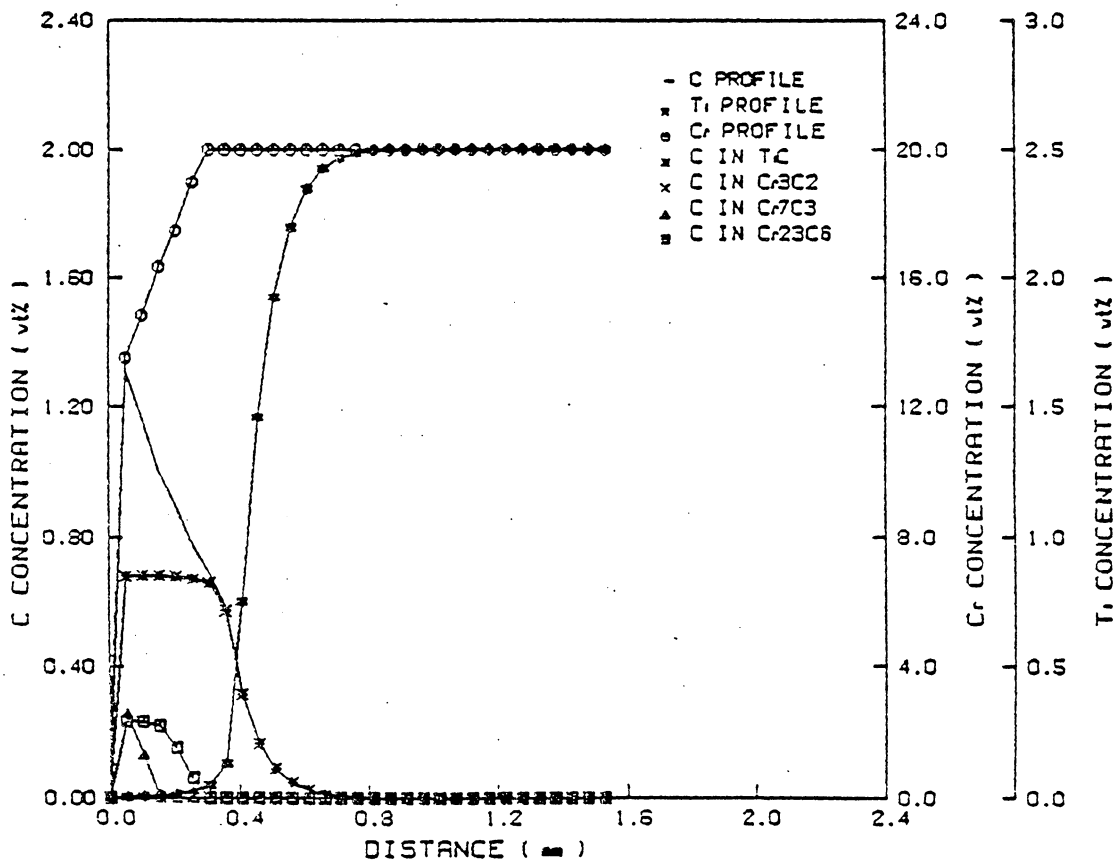

Figure 41. Carburization profiles of Ni-20Cr-2.5Ti alloys, 100 hrs, 850°C, oxidizing condition.

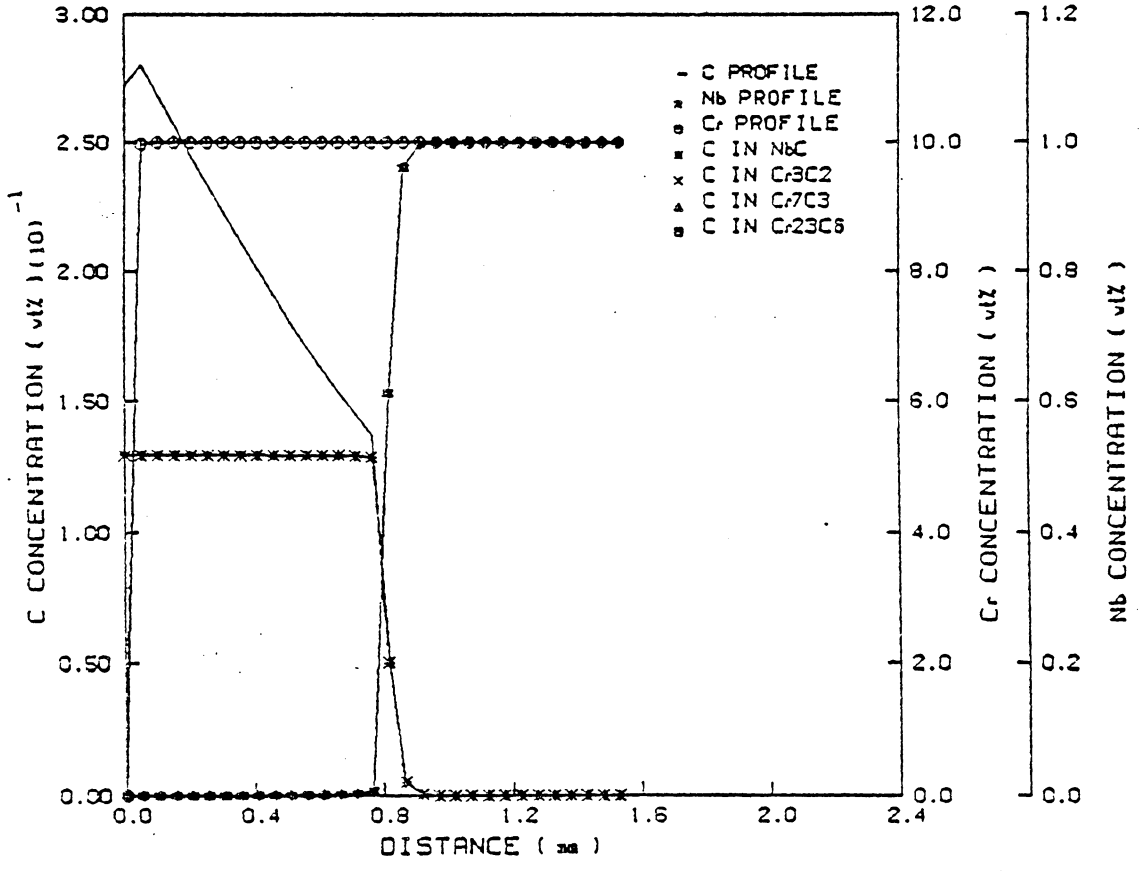

Figure 42. Carburization profiles of Ni-10Cr-1Nb alloys, 100 hrs, 850°C, oxidizing condition.

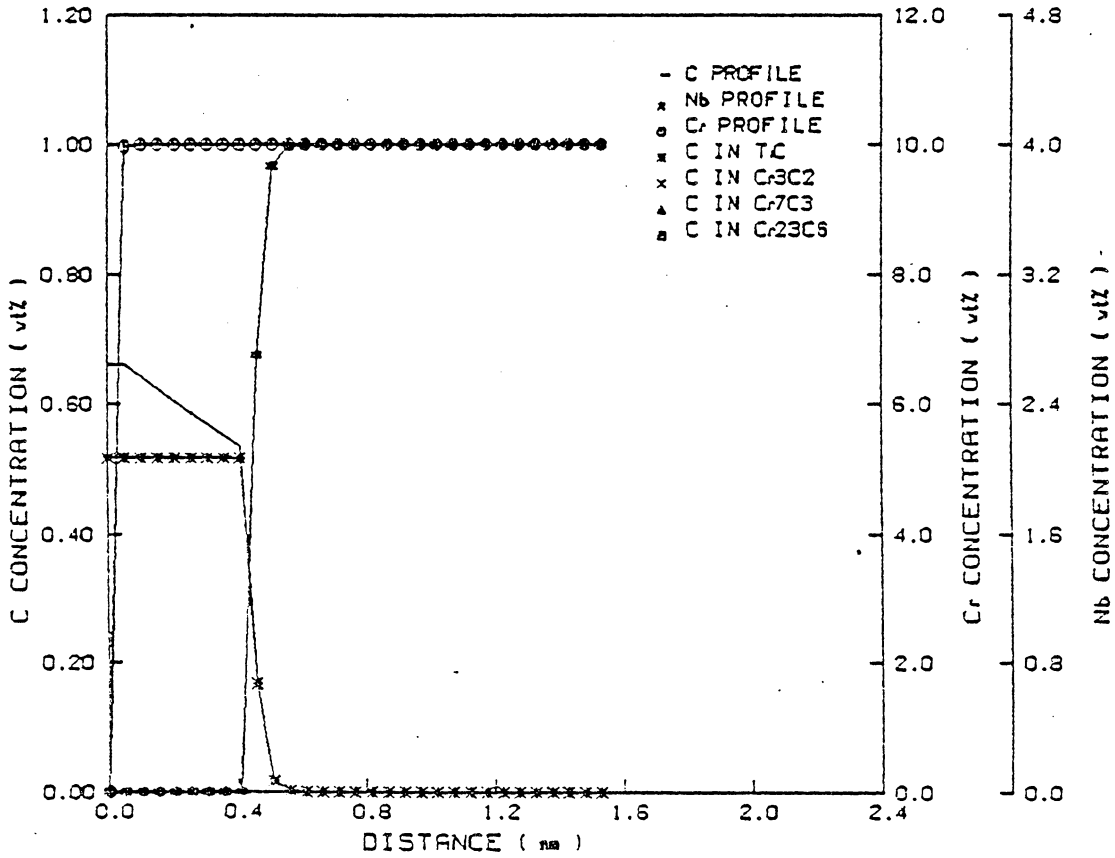

Figure 43. Carburization profiles of Ni-10Cr-4Nb alloys, 100 hrs, 850°C, oxidizing condition.

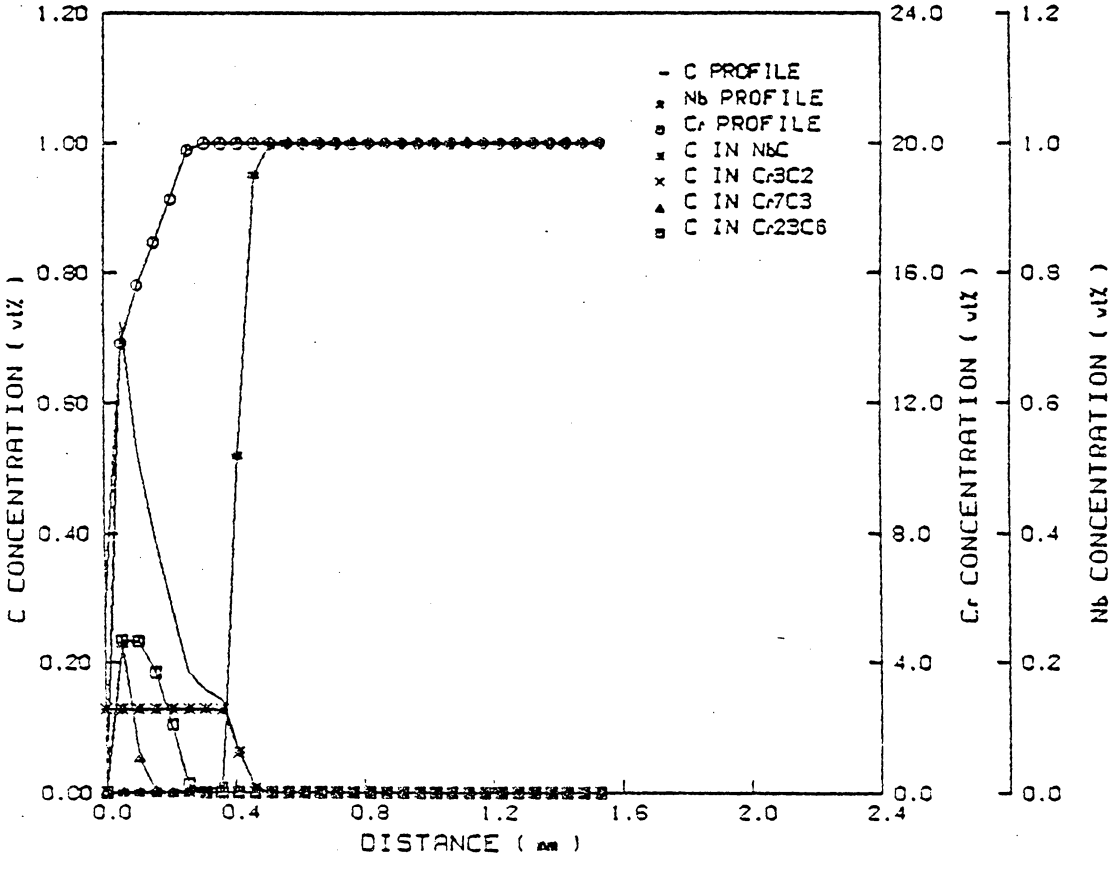

Figure 44. Carburization profiles of Ni-20Cr-1Nb alloys, 100 hrs, 850°C, oxidizing condition.

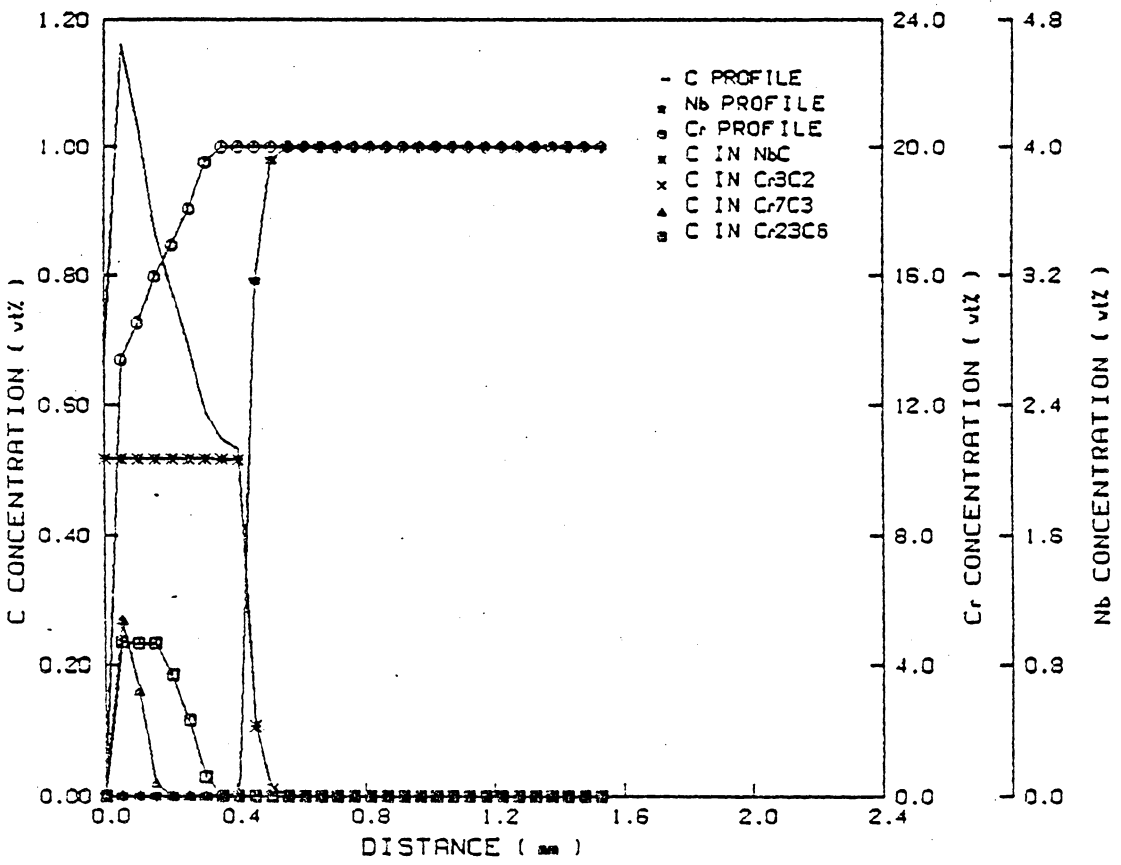

Figure 45. Carburization profiles of Ni-20Cr-4Nb alloys, 100 hrs, 850°C, oxidizing condition.

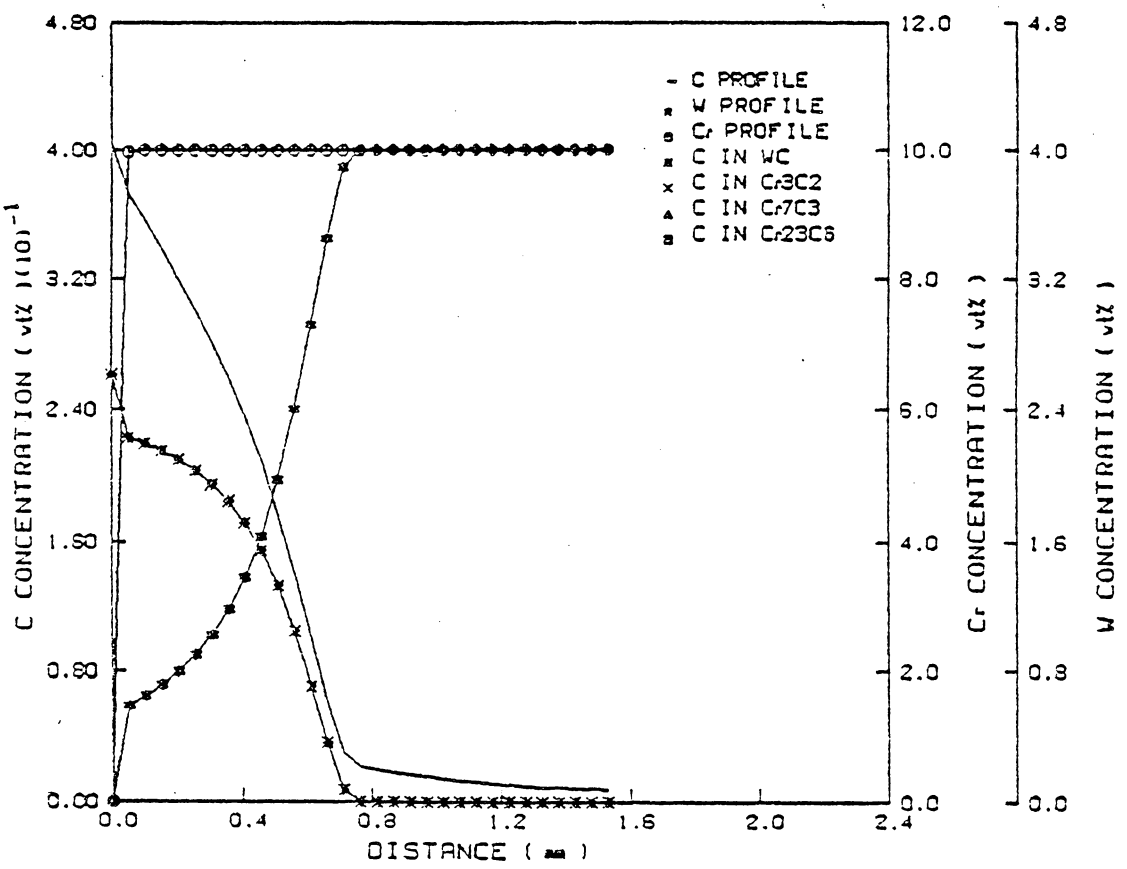

Figure 46. Carburization profiles of Ni-10Cr-4W alloys, 100 hrs, 850°C, oxidizing condition.

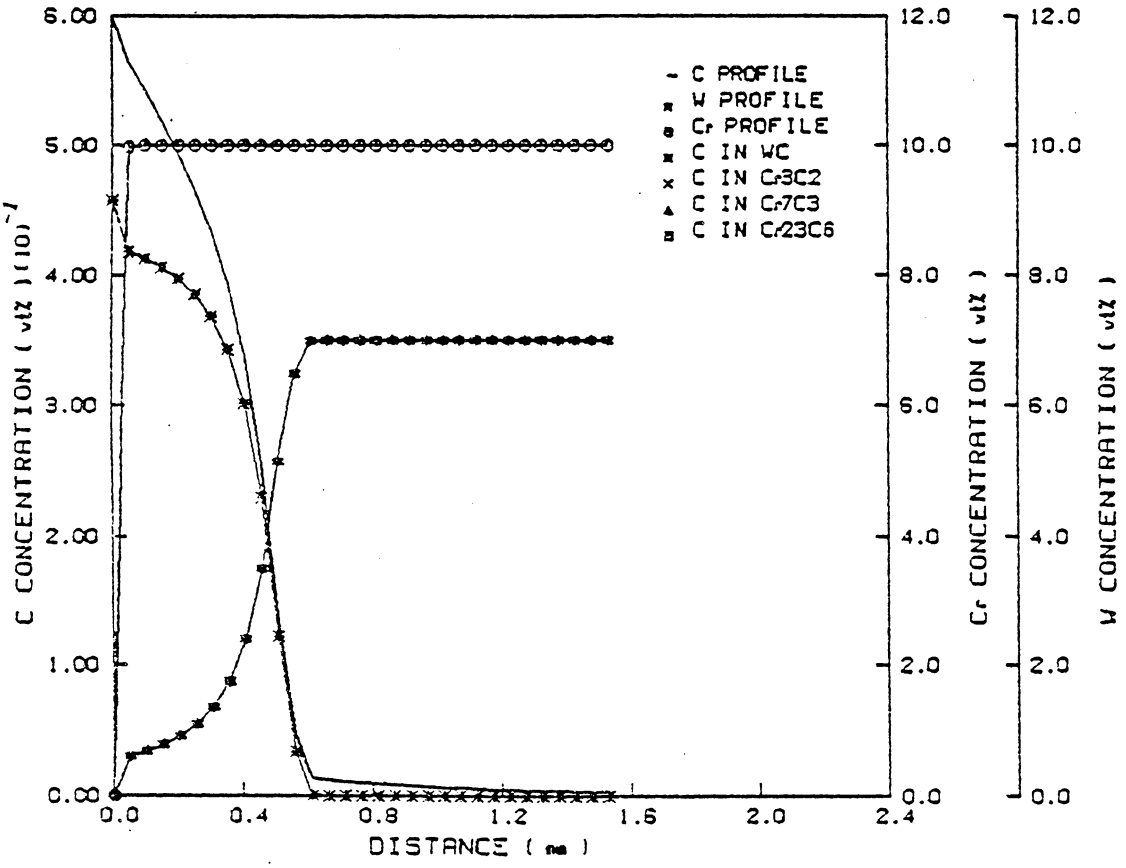

Figure 47. Carburization profiles of Ni-10Cr-7W alloys, 100 hrs, 850°C, oxidizing condition.

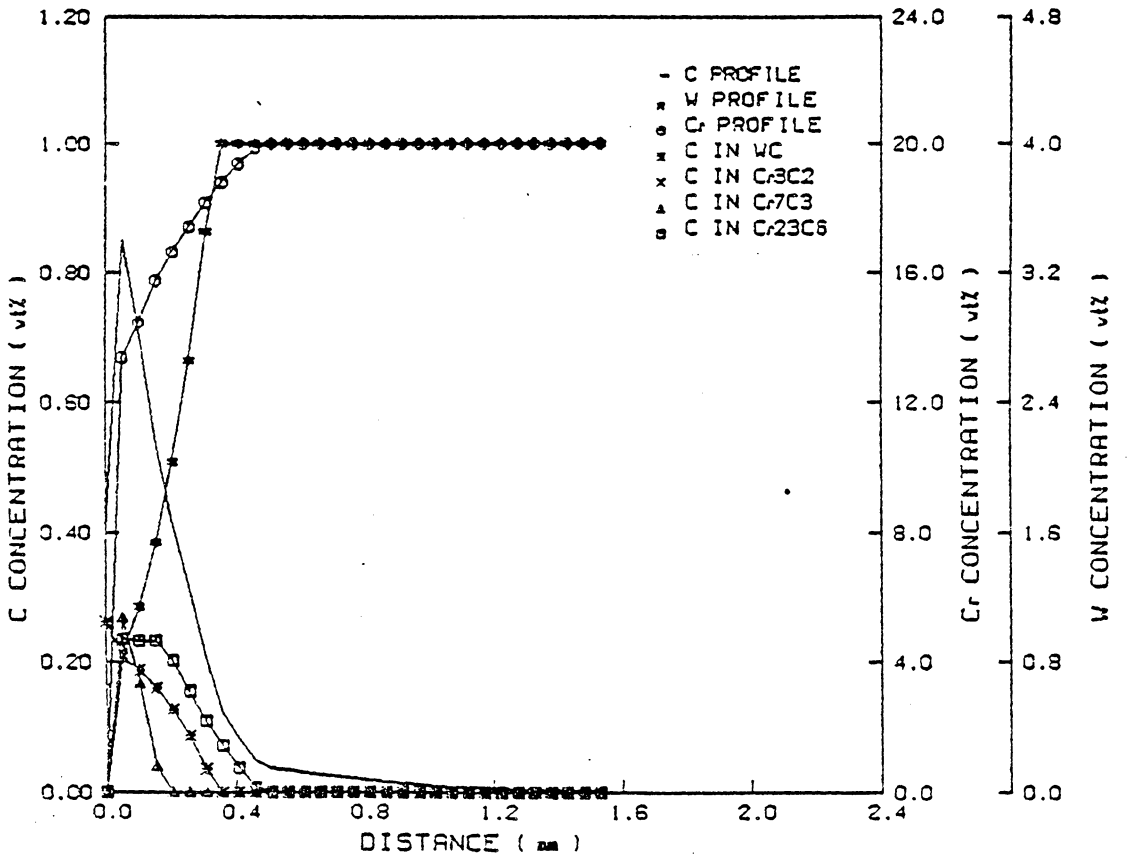

Figure 48. Carburization profiles of Ni-20Cr-4W alloys, 100 hrs, 850°C, oxidizing condition.

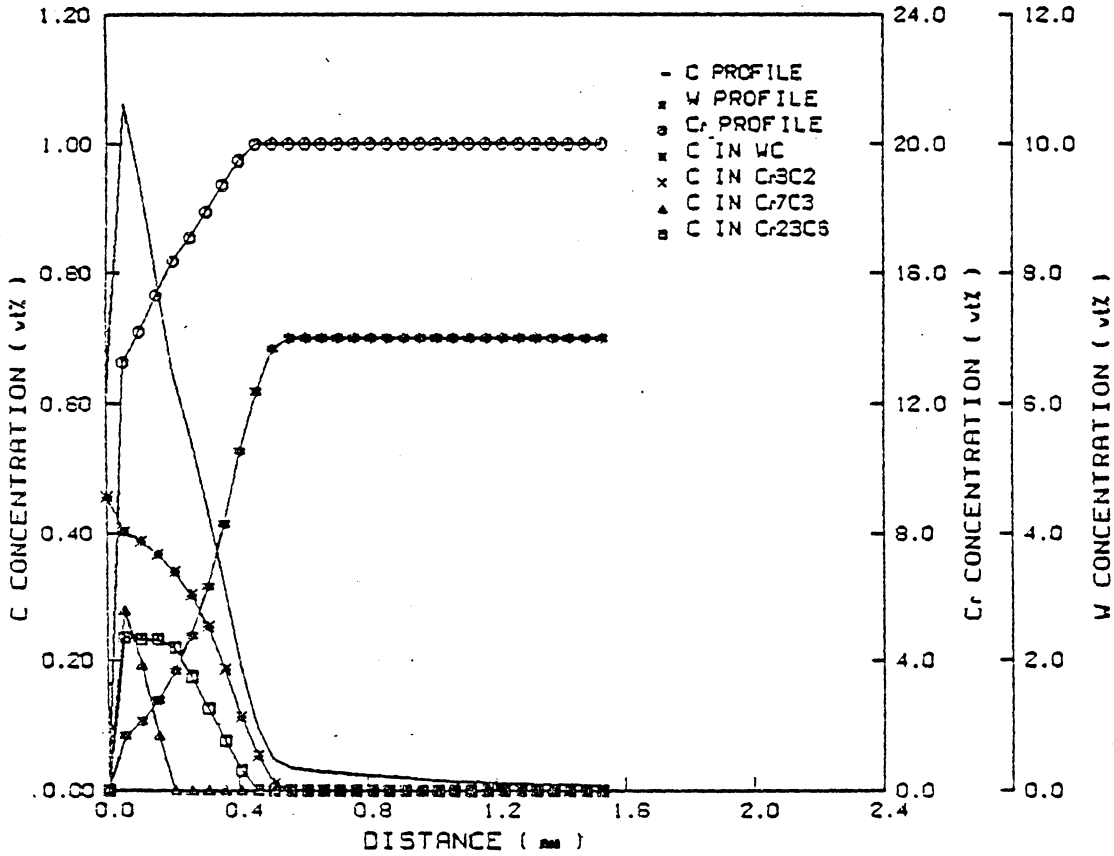

Figure 49. Carburization profiles of Ni-20Cr-7W alloys, 100 hrs, 850°C, oxidizing condition.

surface to almost 1.35 wt% in less than .045 mm.

For all the alloys considered, the solute element carbides such as, TiC, NbC, WC, Mo_2C, and Mo_6C were the only carbides formed for 10 wt% Cr. At higher percentages of Cr, Cr carbides become more stable, but this effect is not as pronounced as in non-oxidizing calculations.

Figures (50) through (53) show the corrosion rate behavior of the same alloys considered in figures (31) through (34) under oxidizing condition. The comparison of these figures suggests that the alloy with 1 wt% Nb was the most resistant alloy in carburizing environment.

Figure (54) shows the comparison of the corrosion behavior in oxidizing and non-oxidizing conditions. The effect of formation of a thin layer of oxide at the surface is evident, which decreases the corrosion rate considerably.

6.6 Experimental Results

Figures (55) through (60) show the microstructures of four alloys tested in H_2-2.7CH_4 gas mixture for 1.0 activity of carbon for different carburization times at 850°C. Figure (61) shows a weight gain plot for tests carried out. The iron base superalloy (i.e., Incoloy 800) showed the largest weight gains with Inconel x-750 showing slightly higher resistance to carburization than Inconel 600, and 601. The

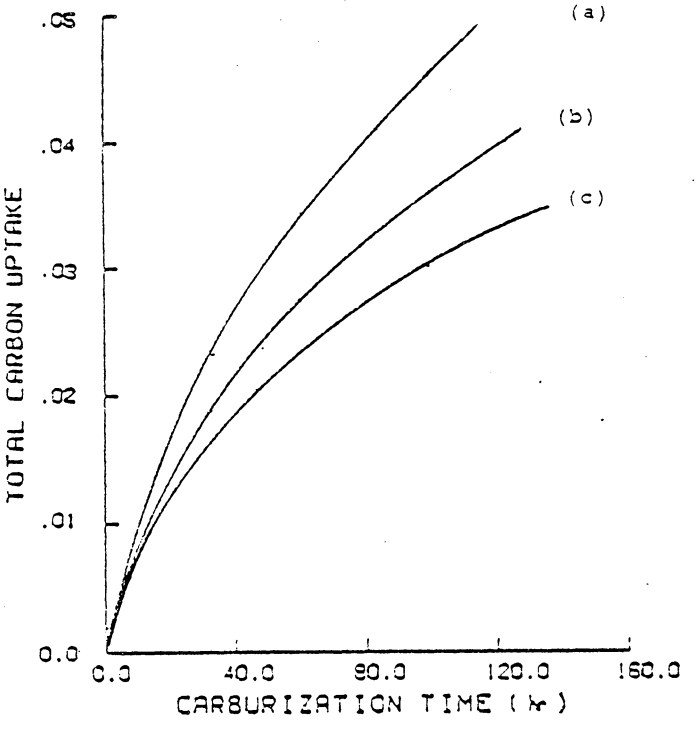

Figure 50. Total carbon uptake as a function of time, oxidizing condition. (a) Ni-30Cr-15Mo, (b) Ni-20Cr-15Mo, (c) Ni-10Cr-15Mo

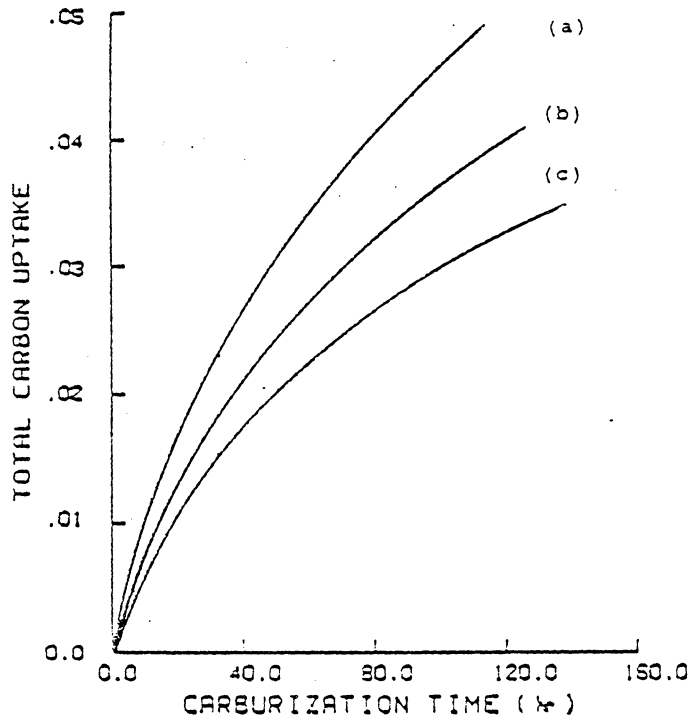

Figure 51. Total carbon uptake as a function of time, oxidizing condition. (a) Ni-30Cr-2.5Ti, (b) Ni-20Cr-2.5Ti, (c) Ni-10Cr-2.5Ti

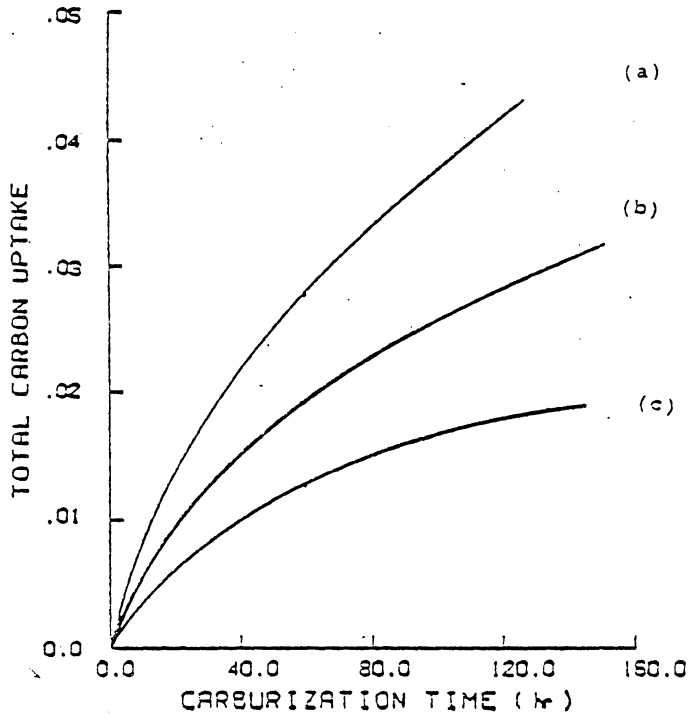

Figure 52. Total carbon uptake as a function of time, oxidizing condition. (a) Ni-30Cr-1Nb, (b) Ni-20Cr-1Nb, (c) Ni-10Cr-1Nb

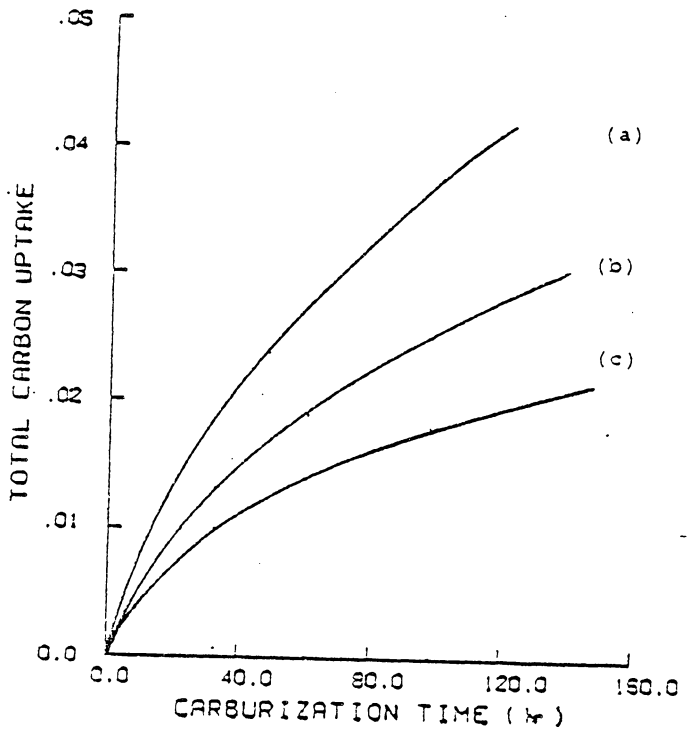

Figure 53. Total carbon uptake as a function of time, oxidizing condition. (a) Ni-30Cr-4W, (b) Ni-20Cr-4W, (c) Ni-10Cr-4W

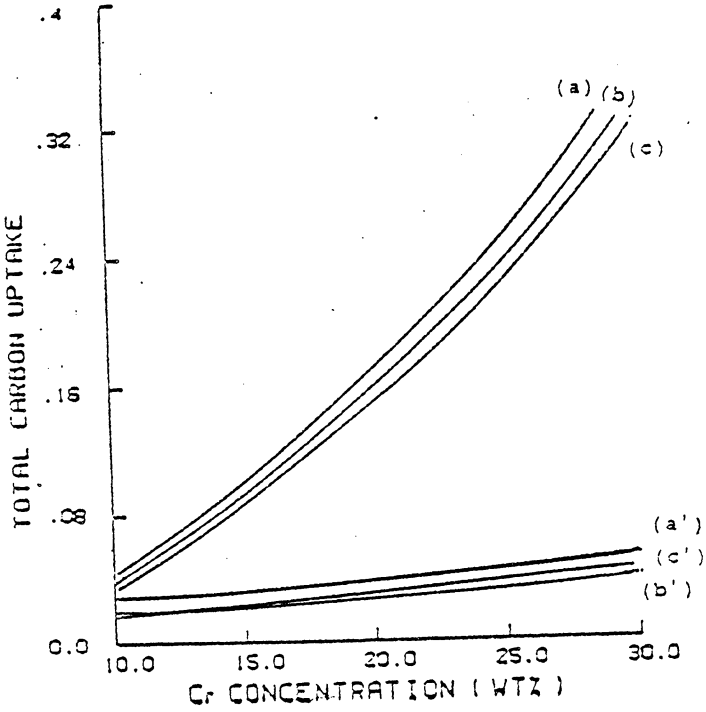

Figure 54. Total carbon uptake vs Cr contents.
(a) Cr and 2.5Ti, (b) Cr and 4W,
(C) Cr and 1Nb, non-oxidizing condition.
(a'), (b'), and (c') show the same alloys in oxidizing condition.

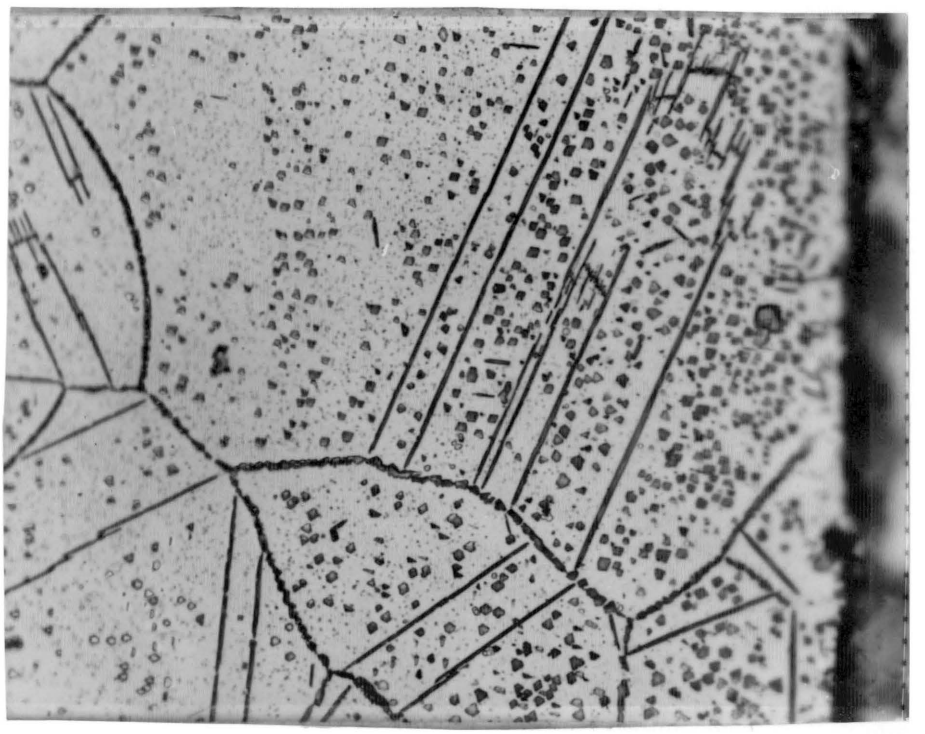

Figure 55. Microstructure showing carbide precipitates in Incoloy 800, 800x, 100hrs.

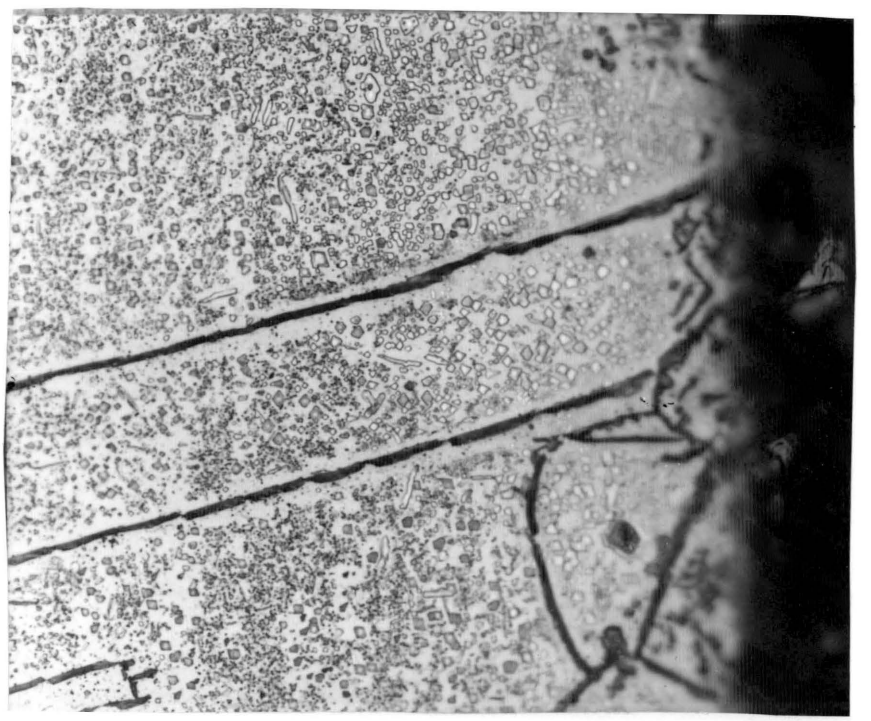

Figure 56. Microstructure showing carbide precipitates in Incoloy 800, 800x, 200hrs.

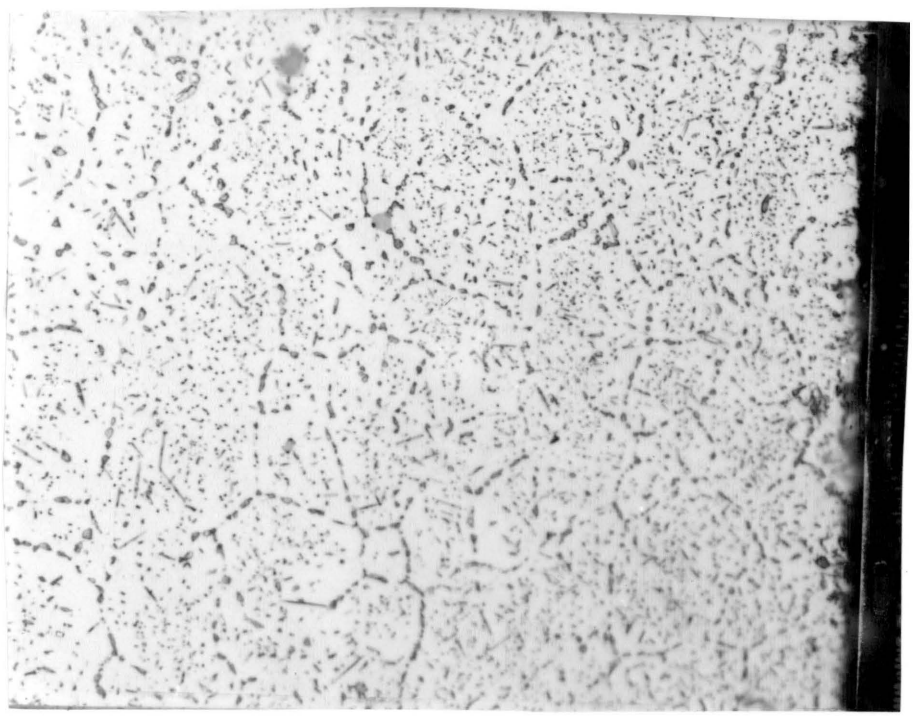

Figure 57. Microstructure showing carbide precipitates in Inconel 600, 800x, 200hrs.

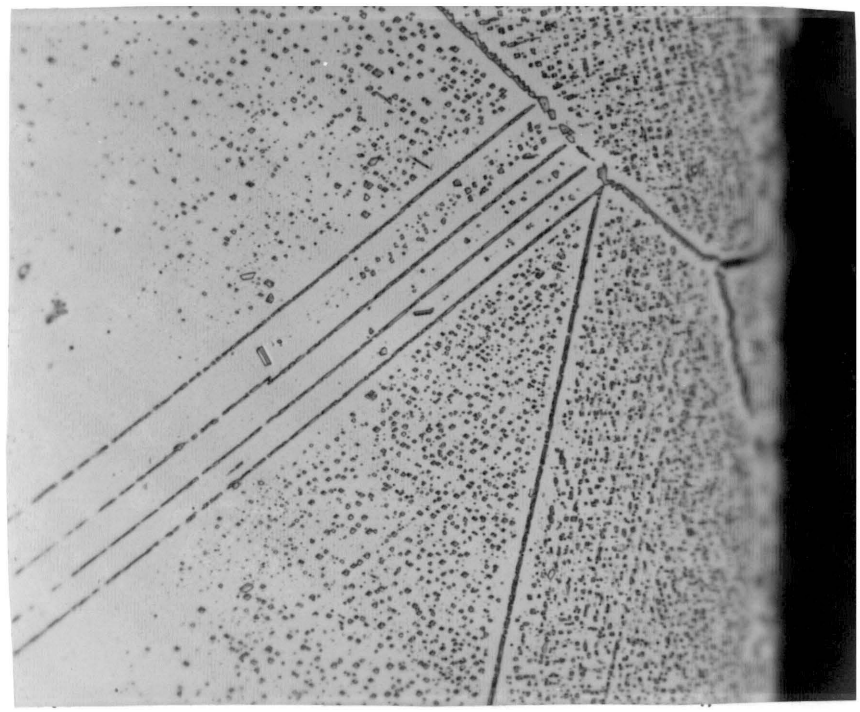

Figure 58. Microstructure showing carbide precipitates in Inconel 601, 800x, 100hrs.

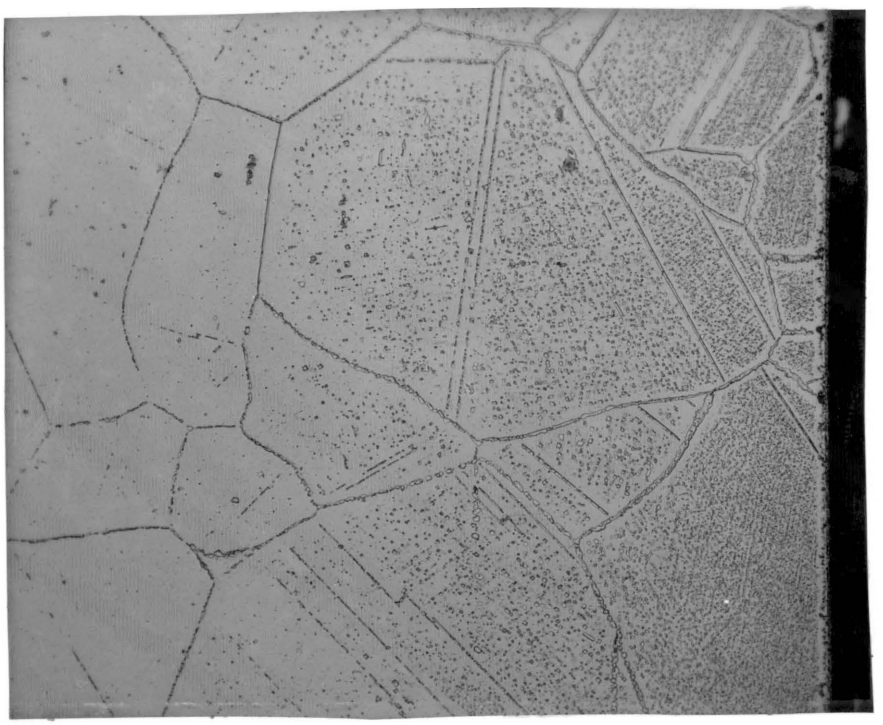

Figure 59. Microstructure showing carbide precipitates in Inconel 601, 400x, 200hrs.

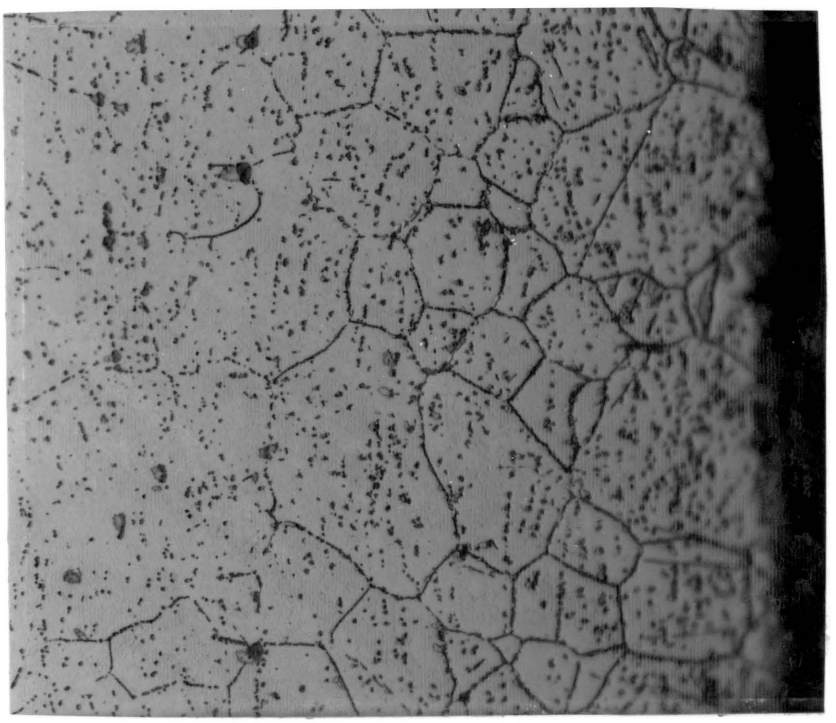

Figure 60. Microstructure showing carbide precipitates in Inconel X-750, 625x, 100hrs.

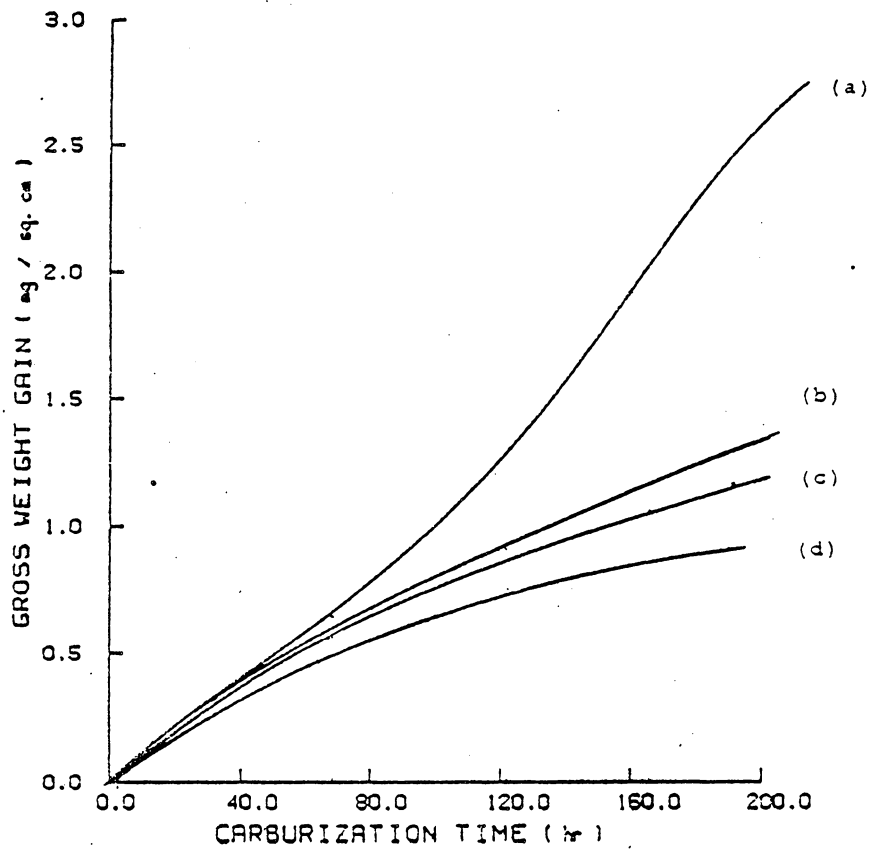

Figure 61. Weight gain determinations for the alloys exposed to H_2-CH_4 environment of 1.0 carbon activity at 850°C. (a) Incoloy 800, (b) Inconel 600, (c) Inconel 601, (d) Inconel X-750.

distribution of carbides through specimen has been measured using image analysis. Figures (62) and (63) show the change in carbide distribution for 100 and 200 hours, respectively.

There was no saturation of carbide observed for up to 200 hours of exposure. From the plots of (weight gain)^2 versus time shown in figure (64), Inconel 601, and X-750 show a good parabolic relationship. This suggests that the diffusion rate of carbon inwards is the rate controlling step in these alloys. Inconel 600 shows the same behavior for up to 160 hours of exposure to the gas test.

The rate of carburization for the alloys tested was found using equation (39) for the carburized samples:

$$X^2 = 4Dt \tag{73}$$

where X is the depth of carburization in centimeter, D is the apparent diffusivity of carbon, and t is the time in seconds. X was calculated metallographically. An average diffusivity of carbon can be obtained as follows:

$$D_{11(\text{Inconel 600})} = 2.5\text{x}10^{-10} \text{ cm}^2/\text{sec}$$

$$D_{11(\text{Inconel 601})} = .65\text{x}10^{-10} \text{ cm}^2/\text{sec}$$

$$D_{11(\text{Inconel x-750})} = 1.5\text{x}10^{-10} \text{ cm}^2/\text{sec}$$

$$D_{11(\text{Incoloy 800})} = 3.6\text{x}10^{-10} \text{ cm}^2/\text{sec}$$

The weight percent of carbon was calculated using

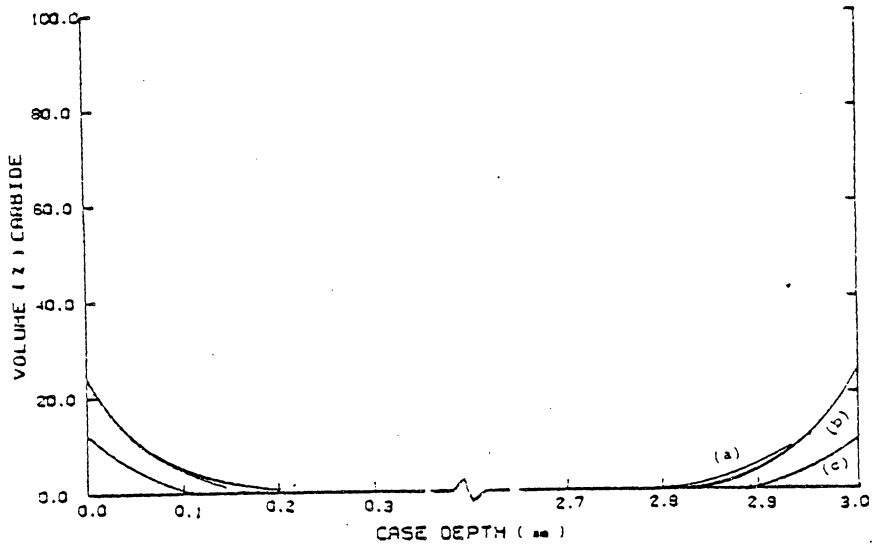

Figure 62. Plot showing amount of carbide present as a function of penetration distance for 100 hrs. (a) Inconel X-750, (b) Incoloy 800, (c) Inconel 600, and 601.

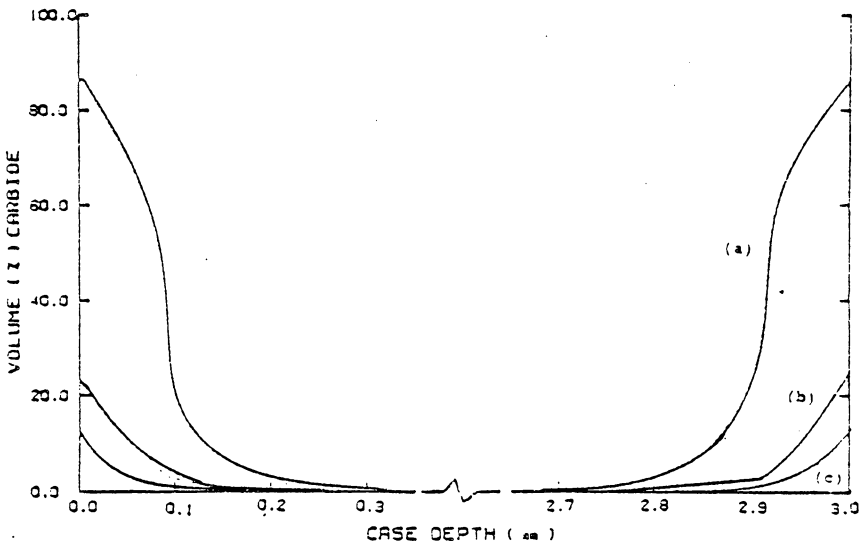

Figure 63. Plot showing amount of carbide present as a function of penetration distance for 200 hrs. (a) Incoloy 800, (b) Inconel 600, (c) Inconel 601.

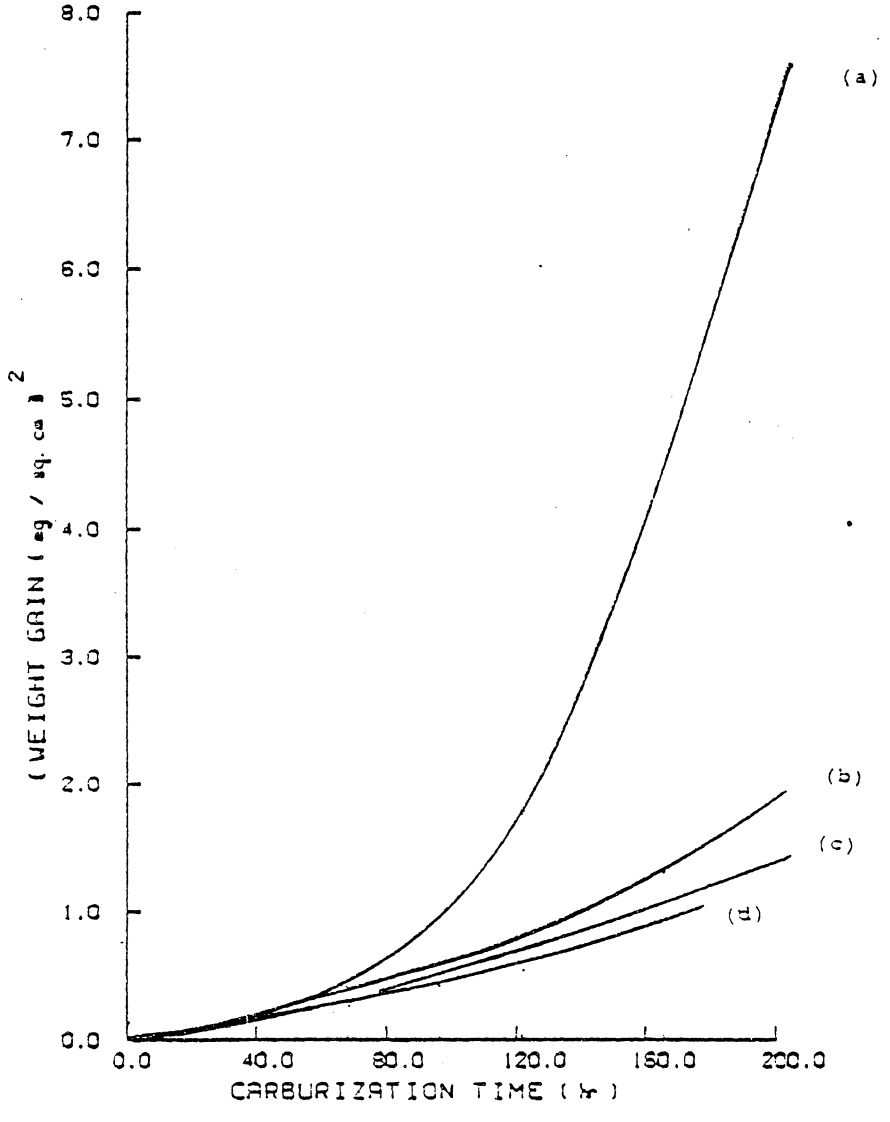

Figure 64. Relationship between the square of the weight gain and time.
(a) Incoloy 800, (b) Inconel 600,
(c) Inconel 601, (d) Inconel X-750.

equation (25) as follows:

$$\text{wt\% C} = V/(1 - V)\ (\text{Wt\% of C in carbides}) \tag{74}$$

Type of carbide assumed was based on our results shown in figure (12). Inconel 600 contains 15.5 wt% Cr, and Inconel 601 contains 23 wt% Cr as the major alloying elements. Therefore, the only carbides assumed to form were Cr_7C_3 in Inconel 600, and $Cr_{23}C_6$ in Inconel 600. Inconel X-750 contains 15.5 wt% Cr and 2.5 wt% Ti. The carbides that could be formed were TiC, and Cr_7C_3. An average carbon concentration was assumed for this alloy. The results were as follows:

$$\text{wt\% C in } Cr_7C_3 = 6.38$$

$$\text{wt\% C in } Cr_{23}C_6 = 4.4$$

$$\text{wt\% C in Tic, and } Cr_7C_3 = 8.5 \tag{75}$$

Table (5) summerizes the results. Table (5) also obtains the simulated calculations preformed for the alloy. These results showed good agreements with binary calculation as seen in table (5). The best agreement resulted for Incoloy 600 for 200 hours of exposure, and Incoloy X-750 for 100 hours of exposure as shown in figures (65), and (66).

The comparison of the weight gain and calculated carbon

Alloy	Max. C penetration (mm)			C at surface (wt%)			Total C Uptake (wt% cm)		
	exp.	cal.		Exp.	Cal.		Exp.	Cal.	
		B	T		B	T		B	T
Inconel 600									
32 hrs	.04	.051	0	.2	.98	0	.00057	.0035	0
100 hrs	.1	.1	.05	.64	.98	.028	.0015	.0066	.0001
200 hrs	.23	.2	.05	1.4	.98	.093	.0092	.0094	.005
$D_{11} = 2.5 \times 10^{-10}$									
$D_{13} = 5.4 \times 10^{-13}$									
Inconel 601									
32 hrs	.06	.051	.05	.34	1.38	.02	.00083	.003	.0001
100 hrs	.11	.1	.05	.45	1.38	.08	.0018	.0036	.0005
200 hrs	.175	.153	.1	.58	1.38	.18	.0023	.0094	.001
$D_{11} = .65 \times 10^{-10}$									
$D_{13} = 1.4 \times 10^{-13}$									
Inconel X-750									
32 hrs	.05	.1	.2	.39	1.6	.09	.0011	.0043	.0006
100 hrs	.21	.204	.36	1.7	1.6	.3	.0093	.008	.0018
$D_{11} = 1.5 \times 10^{-10}$									
$D_{13} = 3.2 \times 10^{-13}$									
$D_{12} = 2.4 \times 10^{-12}$									

Table 5. Calculated and experimental data for the alloys studied. B, T represent binary and ternary calculations, respectively.

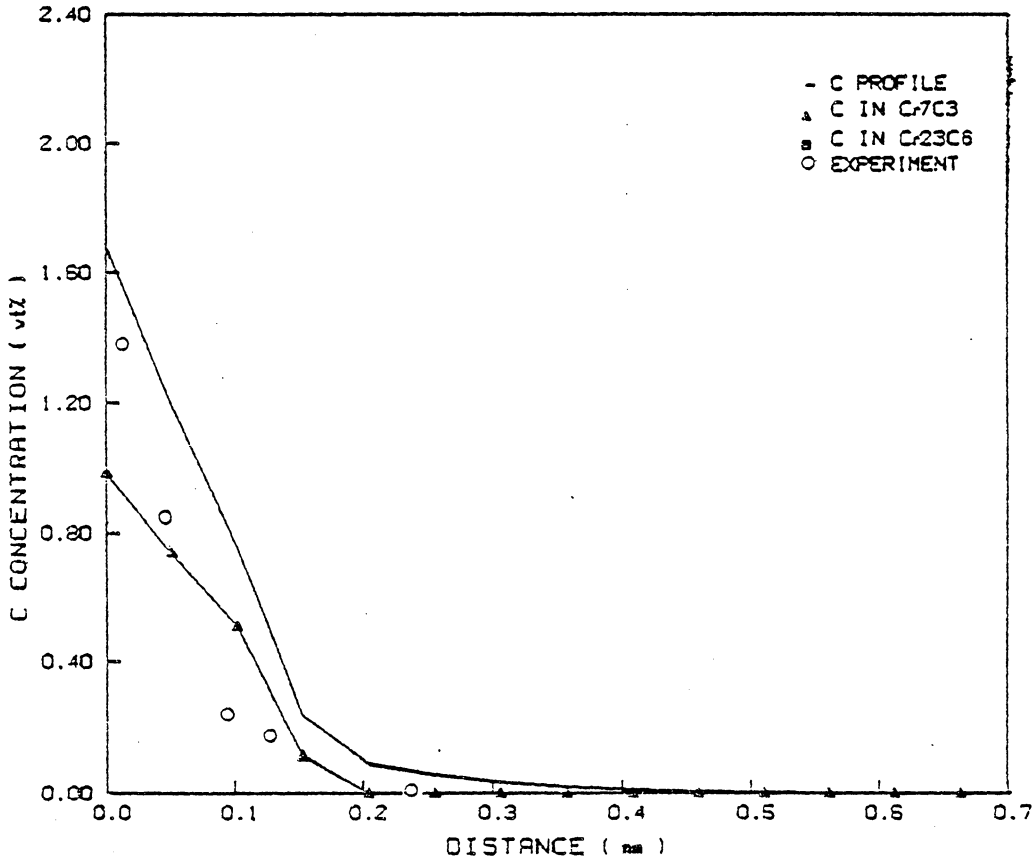

Figure 65. Carburization profile of Inconel 600, 200hrs 850°C.

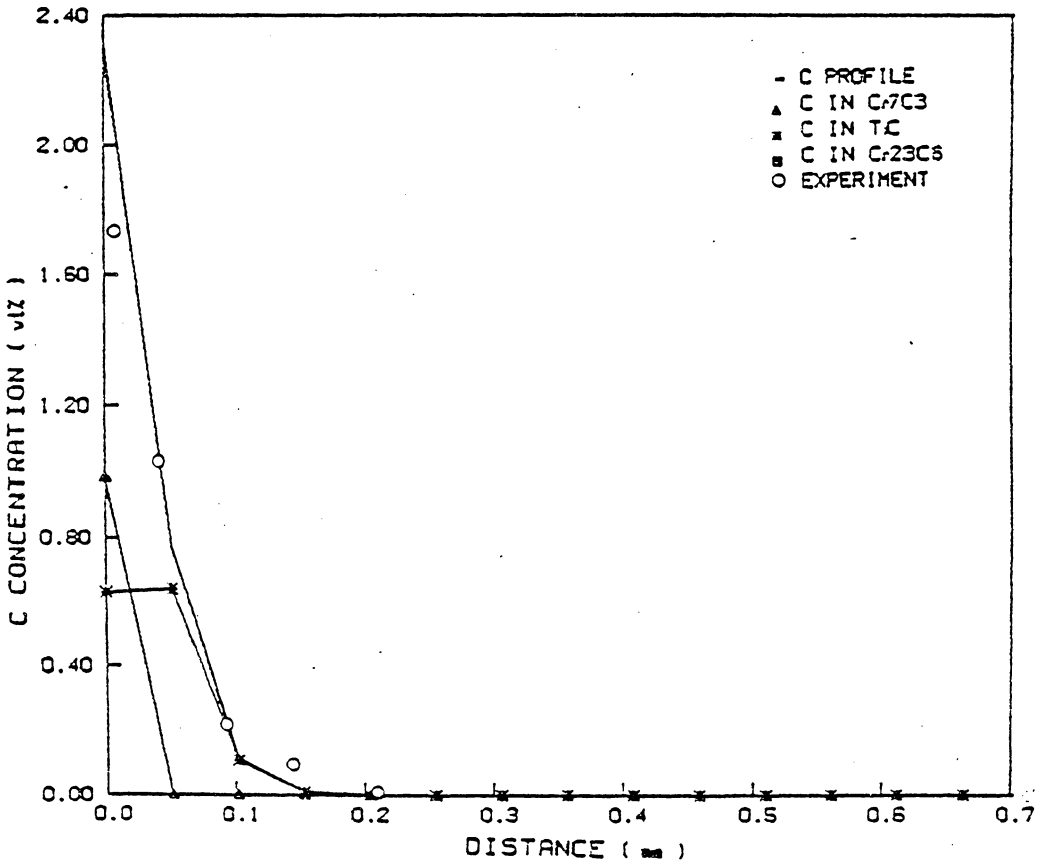

Figure 66. Carburization profile of Inconel X-750, 100hrs 850°C.

uptake was carried out. The weight gain can be related to tatal carbon uptake as follows:

Weight gain (g/cm^2) =

Density (Total carbon uptake/100.0) (76)

where the density of Ni-base alloys is about 8 (gr/cm^3). The calculated carbon uptake for the alloys tested are tabulated in table (5). The comparison of these data and figure (61) did not result in a good agreement between calculated and measured weight gains except for Inconel X-750. This is shown in figure (67). The disagreement could be due to the type of carbides that were assumed to form in the alloys. The alloying elements contained in the alloys could also affect these results. For example, iron content was high in some of the alloys, and the formation of iron carbide was not considered here. The experimental procedure was also carried out with a high carbon activity which could have a determental effect on the measured weight gains.

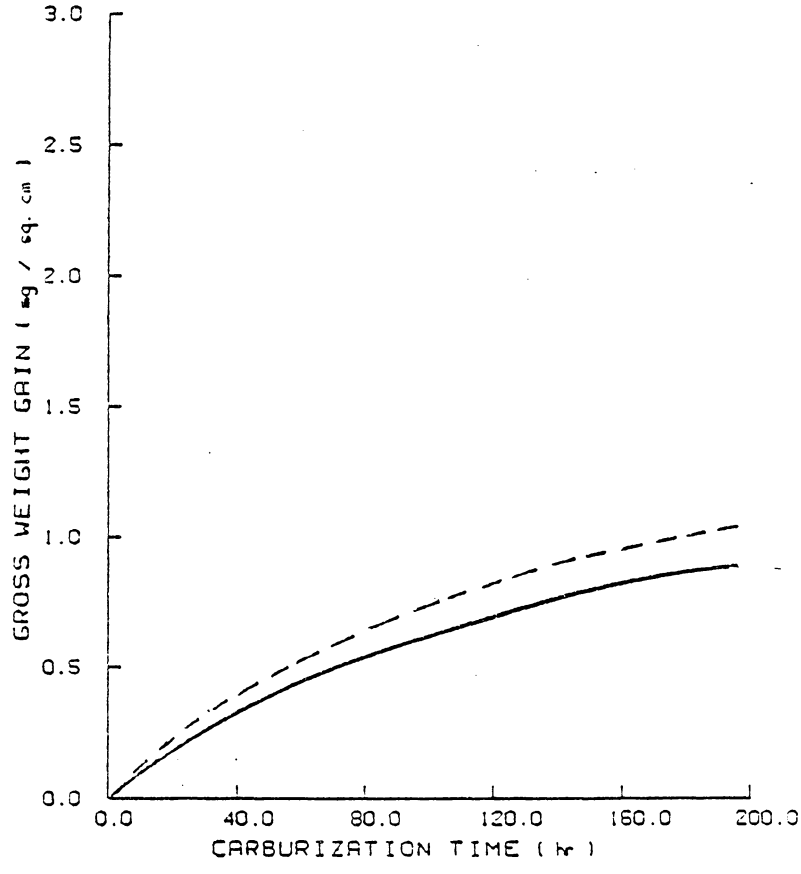

Figure 67. Plot showing calculated and measured weight gains in Inconel X-750. ___ Measured --- Calculated.

7 Discussion

The calculation of stability regions for the different carbides based on thermodynamic data agrees very well with the experimental results of Raghavan and co-workers (16). However, it should be noted that these data do not include alloys in the composition range where Mo_2C, Cr_7C_3 are predicted. Most commercial superalloys fall in the region where $Cr_{23}C_6$ and Mo_6C are stable. Nevertheless Cr_7C_3 is predicted for some superalloy compositions that have been studied experimentally (39,40). These experimental studies do not report Cr_7C_3. This discrepancy may be explained by the formation of Cr_2O_3 at the surface . This depletes the Cr surface content and therefore decreases C solubility. Since Cr_2O_3 will form at very low oxygen partial pressures, this is likely to be the case in the above mentioned experimental studies. In the present simulation it was found that under oxidizing conditions the formation of Cr_7C_3 is greatly diminished. Also, it only forms under complete saturation of the surface and after a certain time, when the alloy is depleted in Cr. Most experimental studies have been carried out in impure He or CH_4-H_2 mixture, with a lower C activity in the gas phase (13). Under those conditions only Mo_6C and $Cr_{23}C_6$ will form. However for higher C activities the pres-

ent simulation predicts that Cr_7C_3 will be also formed, as it has been shown experimentally for Incoloy 800 (47). This prediction has not been confirmed experimentally for Ni-base systems.

The numerical simulation method based on the finite difference solution of the diffusion equations is adequate to account for the simultaneous diffusion and precipitation of several different phases. However, some of the assumptions used in the present work are very crude approximations. In particular, mixed carbides have been observed in experimental studies mentioned above (16,17,40). It is also possible that the lower carbides (ie; $Cr_{23}C_6$) formed during the initial stages of the process will be converted to higher carbides (ie; Cr_7C_3) as the alloy becomes depleted in Cr. The present approach accounts for the formation of higher carbides when they are stable, but no dissolution of the existing carbides was allowed.

Comparison of binary and ternary diffusion calculations shows that in the ternary case the corrosion process is much slower. This means that the presence of small amounts of oxygen in the atmosphere can have a beneficial effect on the carburization behavior, even if a protective oxide layer is not formed. As suggested by previous works (3,24,48), multicomponent diffusion effects play an important role in car-

burization corrosion.

The apparent diffusivity of carbon in the alloys tested are about 25 times lower than the D_{11} used for calculations of figures (14) through (53). This could result in 5 times higher penetration depth, and higher carbon uptake as was expected in the calculated profiles. The apparent D_{11} used for calculation in non-oxidizing conditions resulted in good agreement with the measured profiles for two of the alloys tested. The data listed in table (5) suggest that for the same alloys, formation of a non-protective oxide layer would reduce the corrosion rate considerably. There has not been measurements on the type of carbides formed in Ni-based superalloys in non-oxidizing environments. A knowledge of this, could Lead to a better extrapolation of the calculated results.

Finally, it should be noted that although the present simulation can be very useful in understanding qualitatively the factors that determine resistance to carburization corrosion it can only yield quantitative predictions for simple cases. This is due to the simplifying assumptions that are necessary in the program, as well as the uncertainty in the available thermodynamic data.

8 Conclusions

Computer models have been developed to simulate the corrosion process during gas or pack carburization of nickel base superalloys. The computer models predict the resulting carbon and alloying element depth profiles for various times. Computer models were also developed to include the formation of oxides at the surface of the alloys, and their effects on the carburization process. Chromium and Titanium have large cross diffusivity effects and it is predicted that they have a large influence on the amount of carburization which will occur. Experimental data from Inconel 600, and Inconel X-750 curburization treatments are in excellent agreement with our calculations of effective surface carbon content and the formation of carbides in austenite at the carburization temperature.

Using the finite difference model, it is possible in principle to introduce more complex processes into the calculation without difficulty. The computer models developed in this study are easy to apply to the specific alloys and carburization treatments. They will allow complex carburizing treatments to be modeled and will significantly aid in designing corrosion-resistance alloys for use in carburizing or oxidizing-carburizing environments.

References

1. K. Bongartz, D. F. Lupton and H. Schuster, Met. Trans., 11A (1980), p.1883.
2. J. I. Goldstein and A. E. Moren, Met. Trans., 9A (1978), p.1515.
3. D. Farkas, K. Ohla, Oxidation Of Metals, 19 (1983), p.99.
4. T. Hirano, M. Okada, H. Yoshida and R. Watanabe, J. Nucl. Mat., 75 (1978), P.304.
5. S. Muraoka, H. Itani and S. Nomura, J. Nucl. Mat., 58 (1975), p18.
6. T. Hirano, H. Araki and H. Yoshida, j. Nuc. Mat., 97 (1981), p.272.
7. T. Hirano, H. Araki, T. Noda, H. Yoshida and R. Watanabe, Met. Trans., 12A (1981), p.451
8. F. N. Mazandarany and G. Y. Lai, Nucl. Tech., 43 (1979), P.349.
9. H. G. Bates, W. Betteridge, R. H. Cook, L. W. Graham and D. F. Lupton, Nucl. Tech., 28 (1976), P.424.
10. F. N. Mazandarany and P. L. Rittenhouse, Nucl. Tech., 28 (1976), P.406.
11. O. Demel, Nucl. Tech., 48 (1980), P.298.
12. K. Ledjeff, A. Rahmel and M. Schorr, Werk. Korr. 31 (1980), P.83.

13. T. Shikama, T. Tanabe, M. Fujitsuka, M. Kitajima, H. Yoshida, and R. Watanabe, Metall. Trans. A, 11A (1980), p.1589.

14. S. Muraoka, H. Itani and S. Nomura, J. Nucl. Mat., 58 (1975), p.18.

15. T. Shikama, T. Tanabe, M. Fujitsuka, H. Yoshida, and R. Watanabe,Iron Steel Inst., Japan, 66 (1980), P.112.

16. M. Raghavan, R. Muller, C. F. Klein and G. A. Vaughn, Scripta Met., 17 (1983), p.1189.

17. M. Raghavan, B. J. Berkowitz and J. C. Scanlon, Metall. Trans. A, 13A (1982), p.979.

18. R. A. Perkins, in "Behavior of High Temperature Alloys in Aggressive Environment", Proceeding of an International Conference, ED., N. H. Petten, The Netherland, 15-18 Oct., (1979), p.617.

19. A Schannaas, H. J. Grabke, Oxidation of Metals, 12 (1978), P.387.

20 J. S. Kirkaldy, Canad. Met. Quart. 8 (1969), p.35.

21. E. K. Ohriner and J. E. Morral, Scripta Met. 13 (1979), P.7.

22. L. Onsager, Ann. N. Y. Acad. Sci., 46 (1945) P.241.

23. L. C. Brown, and S. Kirkaldy, AIME, 230 (1964) P.223.

24. D. Farkas and J. Delgado, Scripta Met., 17 (1983), P.261.

25. W. Gurry, Trans. AIME, 180 (1950) P.671.

26. G. B. Gibbs, Oxid. of Met., 7(3) (1973), P.173.

27. M. Birks, in "Properties of High Temperature Alloys", Proceeding of a Symposium, ED., Z. A. Foroulis and F. S. Petti, Elec. Chem. Soc., 1976, P.215.

28. D. V. Von Rosenberg, Method for the Numerical Solution of Partial Differential Equation, Amer. Elsevier Publishing Co., new york, 1969.

29. A. R. Mitchel, Chap. 2, Computational Methods in Partial Differential Equations, Wily, New York, 1976.

30. Metals Handbook, ASM, Metals Park, OH, vol 8,

31. M. Small and E. Ryba, Met. Trans. 12A (1981), p.1389.

32. H. Kleykamp, Ber. Bunserges, Phys. Chem., 73 (1969), P.354

33. A. D. Kulkarni and W. L. Worrell, Metall. Trans.,3 (1972), p.2363.

34. K. Lobl, H. Tuma and M. Ciznerova, Memoires Scientifiques Rev. Metallurg., LXXI, No 5, (1974).

35. J. Tousek, J. Vrestal, and A. Rek, Kovove Materialy, 16 (1978). p.649.

36. R. O. Williams, Metall. Trans. A, 13A (1982), p.959.

37. P. J. Spencer, Private Communication.

38. M. Gleiser and J. Chipman, J. Phys. Chem., 66 (1962), p.1539.

39. B. Uhrenius and H. Harvig, Metal Science, 9 (1975), p.67.

40. T. Takahashi, J. Funjiwara, T. Matsushima, M. Kiyokawa,

41. O. Kubaschewski, Metallurgical Thermochem., Pergamon Press (1967), P.421

42. D. D. Pruthi, M. S. Anand and R. P. Agarwala, J. Nucl Mater., 64(1/2) (1977), p.206.

43. L. N. Burminskaya, Metalloved Proch. Mater., 3 (1971), P.251.

44. I. N. Frantsevich, D. F. Kalinovich, I. I. Kovenski, M. D. Smolin, in "Atomic Transport in Solids and Liquids" (Proc. Europhys, Conf.)., A. Lodding and T. Lagerwall Editors (Verlag Z. Natur Forschg., D-74 Tubingen, Germany, (1971), p.100.

45. P. Y. Muramatus, Trans. Japan Inst. Met., 16(2) (1975), P.61.

46. J. M. Walsh, Metal Sci. J., 3 (1969), P.68.

47. H. G. A. Bates, W. Betteridge, R. H. Cook, L. W. Graham, and D. F. Lupton, Nuclear Technology, 28 (1976), p.424.

48. D. Farkas, in "Materials In Nuclear Energy", Proceedings of an International Conference, ASM, Metals Park, Ohio, (1982), p.227.

Appendix

```
C    ------------------------------------------------------------
C     THIS PROGRAM DEVELOPS A FINITE DIFFERENCE CALCULATION FOR
C     CARBURIZATION PROFILES IN HIGH TEMPERATURE NI-CR ALLOYS.
C    ------------------------------------------------------------
     INTEGER R,S
     REAL*4 MATRIX,KM,KN,KP,KPS,KNS,NCM,NM,NCN,NCP,NN,NP,
     1NCT,NT,KT,KTS,KMS
     DIMENSION MATRIX(90,90)
     DIMENSION XA(31),XC(31),XM(31),XN(31),X(90)
     DIMENSION D(90)
     DIMENSION WKAREA(90),MAT(90,90)
     DIMENSION CI(30),CM(30),CN(30)
     DIMENSION CARM(30),CARN(30)
     DIMENSION A(3,3), B(3,3), C(3,3), T(3,3), LW(90), MW(90)
     DIMENSION CARP(30),CART(30)
     DIMENSION CAM(31),CAP(31),CAN(31),CAT(31)
C    CHANGE DIMENSIONS UP TO THIS POINT
     NX=30
     TK=.25
C    INCLUDE DIF FOR VARIABLE DIFFUSIVITIES HERE
C    READ CONDITIONS( INPUT DATA)
     TYPE 2
2    FORMAT(1X,'MAX. DIFFUSION DISTANCE IN CM AND TIME IN HRS')
     ACCEPT 4, XMAX, TMAX
4     FORMAT (F8.3,F8.3)
C    ------------------------------------------------------------------
C     XMAX IS THE MAX. DIFFUSION DISTANCE.TMAX IS THE MAX. TIME FOR
C     CURBURIZATION. EX; .153,1000. IN CM AND HOURS.
C    ------------------------------------------------------------------
C    GET DIFFUSIVITIES (FROM SUBROUTINE IN THE FUTURE)
     TYPE 6
6     FORMAT (1X,'DIFFUSIVITIES IN SQCM/SEC PLEASE')
     ACCEPT 8, D11, D12, D13, D22, D33
8     FORMAT (F10.3,F10.3,F10.3,F10.3,F10.3)
C    READ INITIAL CONDITIONS
C    ----------------------
     TYPE 10
10    FORMAT (1X,'INITIAL CONCENTRATIONS?')
     ACCEPT 12, CIS,CMS,CNS,CI0,CM0,CN0
```

```
12    FORMAT (F8.3,F8.3,F8.3,F8.3,F8.3,F8.3)
C     ------------------------------------------------------
C     CIS,CMS,CNS ARE THE INITIAL SURFACE CONCENTRATION.
C     CIO,CMO,CNO ARE THE INITIAL BULK CONCENTRATION.
C     CIS/O=SOLUBILITY OF CARBON.
C     CMS/O=THE THIRD ELEMENT (M) CONCENTRATION.
C     CNS/O= CR CONCENTRATION
C     ------------------------------------------------------
      TYPE 11
11    FORMAT (1X,'FLUX? 0 MEANS CONSTANT SURFACE CONCENTRATION')
C               ---------------------------------------
      ACCEPT 13,FLUX
13    FORMAT (F10.3)
      TYPE 24
24    FORMAT (1X,'REACTION PARAMETERS? K,N AND FACT')
      ACCEPT 26 ,KT,NCT,NT,FACTT
      TYPE 24
      ACCEPT 26 ,KM,NCM,NM,FACTM
C     ------------------------------------------------------------
C     KT AND KM ARE THE REACTION CONSTANT FOR THE THE THIRD ELEMENT
C     CARBIDE.SUPPOSE THE THIRD ELEMENT IS M,AND IT FORMS CARBIDES AS
C     MXCY. KT,OR KM=K*(ACTIVITY COEFF. OF M IN THE ALLOY)**X.AS FOR
C     MO2C X=2 AND K IS THE REACTION CONSTANT FOR THE CARBIDE FORMED.
C     NCT=Y, NT=X AND,
C     FACT'S=(X*ATOMIC WEIGHT OF M)/(Y*ATOMIC WEIGHT OFCARBON)
C     THIS IS THE PROCEDURE JUST FOR THE THIRD ELEMENT (M) CABIDE.
C     ------------------------------------------------------------
C     THE NEXT TWO READ STATEMENTS ARE FOR CR CARBIDES.
C     CRXCY, KP AND KN ARE JUST THE REACTION CONSTANT AND NEEDNOT TO
C     BE MULTIPLIED BY ACTIVITY COEFFICIENTS.
C     FACT'S=(X*ATOMIC WEIGHT OF CR)/(Y*ATOMIC WEIGHT OFCARBON)
C     ------------------------------------------------------------
      TYPE 24
      ACCEPT 26 ,KP,NCP,NP,FACTP
      TYPE 24
      ACCEPT 26 ,KN,NCN,NN,FACTN
 26    FORMAT (4F10.3)
 C     ***************************************************************************
 C     ------------------------------------------------------------
 C     TO RUN THE PROGRAM.
C     MAXIMUM DIFFUSION DISTANCE IN CM AND TIME IN HS PLEASE
C     .153,162.5
```

```
C   DIFFUSIVITIES IN SQCM/SEC PLEASE
C   .1E-07,0,0,2.35E-11,.198E-12
C   INITIAL CONCENTRATIONS?
C   .369,6.0,10.,0,6.0,10.
C   FLUX? 0 MEANS CONSTANT SURFACE CONCENTRATION
C   0
C   REACTION PARAMETERS? K,N AND FACT
C   .143E6,1.,2.,16.                    (MO2C)
C   REACTION PARAMETERS? K,N AND FACT
C   .798E10,1.,6.,48.                   (MO6C)
C   REACTION PARAMETERS? K,N AND FACT
C   .440E+07,3.,7.,10.1                  (CR7C3)
C   REACTION PARAMETERS? K,N AND FACT
C   .103E16,6.,23.,16.6                  (CR23C6)
C ***************************************************************************
C ---------------------------------------------------------------
C   PLEASE NOTICE:
C     FOR NI-CR ALLOYS IF D13=0 WE HAVE BINARY REACTION.
C     D13=-1.98E-11 WE HAVE TERNARY REACTION.
C     CIS IS THE SOLUBILITY OF C IN PURE NICKLE FOR TERNARY.
C     CMS=0 AND CNS=0 FOR TERNARY.
C    ---------------------------------------------------------------
C    CALCULATE INTERVALS IN X AND T
     DELX=XMAX/NX
     DELT=TK*(DELX**2)/D11
     NQ=3600*TMAX/DELT
     DELT=3600*TMAX/NQ
 C   FORM MATRIX
 C   FIRST A,B,C MATRICES
     A(1,1) = DELT*D11/(2*DELX**2)
     A(1,2) = DELT*D12/(2*DELX**2)
     A(1,3) = DELT*D13/(2*DELX**2)
     A(2,3) = 0
     A(2,1) = 0
     A(3,1) = 0
     A(3,2) = 0
     A(2,2) = DELT*D22/(2*DELX**2)
     A(3,3) = DELT*D33/(2*DELX**2)
     B(1,1) = -2*A(1,1) -1
     B(2,2) = -2*A(2,2) -1
     B(3,3) = -2*A(3,3) -1
     B(1,2) = -2*A(1,2)
```

```
      B(1,3) = -2*A(1,3)
      B(2,1) = 0
      B(2,3) = 0
      B(3,1) = 0
      B(3,2) = 0
      DO 460 R=1,3,1
      DO 460 S=1,3,1
      C(R,S)=A(R,S)
460   CONTINUE
 C    NOW FORM THE TRIDIAGONAL MATRIX OF A , B, AND C
      DO 100 L=1,NX,1
      DO 100 H=1,NX,1
      IF (H.EQ.L-1) GO TO 50
      IF (H.EQ.L)  GO TO 60
      IF (H.EQ.L+1) GO TO 70
      DO 45 I=1,3,1
      DO 45 J=1,3,1
      T(I,J) = 0
45    CONTINUE
      GO TO 80
50    CONTINUE
      DO 550 R=1,3,1
      DO 550 S=1,3,1
      T(R,S)=A(R,S)
550   CONTINUE
      GO TO 80
60    CONTINUE
      DO 570 R=1,3,1
      DO 570 S=1,3,1
      T(R,S)=B(R,S)
570   CONTINUE
      GO TO 80
70    CONTINUE
      DO 590 R=1,3,1
      DO 590 S=1,3,1
      T(R,S)=C(R,S)
590   CONTINUE
80    CONTINUE
      DO 100 I=1,3,1
      DO 100 J=1,3,1
      M = 3*(L-1)+I
      N = 3*(H-1)+J
```

```
      MATRIX(M,N) = T(I,J)
100   CONTINUE
C     INVERT MATRIX
C     INCLUDE INVERSION WITHIN LOOP
C     WHEN VARIABLE DIFFUSIVITIES ARE USED
      KL=3*NX
      CALL LINV1F (MATRIX,KL,90,MAT,0,WKAREA,IER)
C    FORM INITIAL CONCENTRATION VECTORS
      DO 200 I=1,NX,1
      CI(I) = CI0
      CM(I) = CM0
      CN(I) = CN0
 C    REACTION IN INITIAL CONDITION?
      IF(KT.EQ.0)GO TO 160
      IF(CM(I).EQ.0) GO TO 160
      KTS=KT*(10**((2.25-4.45*CN(I)/100)*NCT))
      CMAXT=21.8*(KTS**(-1/NCT))*((CM(I)/160.)**(-NT/NCT))
      IF (CI(I).LT.CMAXT) GO TO 160
      QT=FACTT*(CI(I)-CMAXT)
      IF(QT.LT.CM(I)) GO TO 140
      CART(I)=CART(I)+CM(I)/FACTT
      CI(I)=CI(I)-CM(I)/FACTT
      CM(I)=0
      GO TO 160
140   CONTINUE
      CART(I)=CART(I)+CI(I)-CMAXT
      CM(I)=CM(I)-FACTT*(CI(I)-CMAXT)
      CI(I)=CMAXT
160   CONTINUE
      IF(KM.EQ.0)GO TO 150
      IF(CN(I).EQ.0) GO TO 150
      KMS=KM*(10**((2.25-4.45*CN(I)/100)*NCM))
     1*((.7+5.33*CN(I)/100)**NM)
      FACTM=(NM*52.)/(NCM*12.)
      CMAXM=21.8*(KMS**(-1/NCM))*((CN(I)/100.)**(-NM/NCM))
      IF (CI(I).LT.CMAXM) GO TO 150
      QM=FACTM*(CI(I)-CMAXM)
      IF(QM.LT.CN(I)) GO TO 125
      CARM(I)=CARM(I)+CN(I)/FACTM
      CI(I)=CI(I)-CN(I)/FACTM
      CN(I)=0
      GO TO 150
```

```
125   CONTINUE
      CARM(I)=CARM(I)+CI(I)-CMAXM
      CN(I)=CN(I)-FACTM*(CI(I)-CMAXM)
      CI(I)=CMAXM
150   CONTINUE
      IF(KP.EQ.0) GO TO 202
      IF(CN(I).EQ.0) GO TO 202
      KPS=KP*(10**((2.25-4.45*CN(I)/100)*NCP))
     1*((.7+5.33*CN(I)/100)**NP)
      FACTP=(NP*52.)/(NCP*12.)
      CMAXP=21.8*(KPS**(-1/NCP))*((CN(I)/100.)**(-NP/NCP))
      IF(CI(I).LT.CMAXP) GO TO 202
      QN=FACTP*(CI(I)-CMAXP)
      IF(QN.LT.CN(I)) GO TO 201
      CARP(I)=CARP(I)+CN(I)/FACTP
      CI(I)=CI(I)-CN(I)/FACTP
      CN(I)=0
      GO TO 202
201   CONTINUE
      CARP(I)=CARP(I)+CI(I)-CMAXP
      CN(I)=CN(I)-FACTP*(CI(I)-CMAXP)
      CI(I)=CMAXP
202   CONTINUE
      IF(KN.EQ.0) GO TO 200
      IF(CN(I).EQ.0) GO TO 200
      KNS=KN*(10**((2.25-4.45*CN(I)/100)*NCN))
     1*((.7+5.33*CN(I)/100)**NN)
      FACTN=(NN*52.)/(NCN*12.)
      CMAXN=21.8*(KNS**(-1/NCN))*((CN(I)/100.)**(-NN/NCN))
      IF(CI(I).LT.CMAXN) GO TO 200
      QN=FACTN*(CI(I)-CMAXN)
      IF(QN.LT.CN(I)) GO TO 175
      CARN(I)=CARN(I)+CN(I)/FACTN
      CI(I)=CI(I)-CN(I)/FACTN
      CN(I)=0
      GO TO 200
175   CONTINUE
      CARN(I)=CARN(I)+CI(I)-CMAXN
      CN(I)=CN(I)-FACTN*(CI(I)-CMAXN)
      CI(I)=CMAXN
200   CONTINUE
      CIS0=CIS
```

```
      CIS=CIS0
C     FLUX OR SURFACE CONDITION?
      IF (FLUX.EQ.0)GO TO 210
      CIS = CI(1)+FLUX*DELX/D11
210   CONTINUE
C     REACTION AT SURFACE IN INITIAL CONDITION?
      IF(KT.EQ.0)GO TO 226
      IF(CMS.EQ.0) GO TO 226
      KTS=KT*(10**((2.25-4.45*CN(I)/100)*NCT))
      CMAXT=21.8*(KTS**(-1/NCT))*((CMS/160.)**(-NT/NCT))
      IF (CIS.LT.CMAXT) GO TO 226
      QM=FACTT*(CIS-CMAXT)
      IF(QM.LT.CMS) GO TO 216
      CARTS=CARTS+CMS/FACTT
      CIS=CIS-CMS/FACTT
      CMS=0
      GO TO 226
216   CONTINUE
      CARTS=CARTS+CIS-CMAXT
      CMS=CMS-FACTT*(CIS-CMAXT)
      CIS=CMAXT
226   CONTINUE
      IF(KM.EQ.0)GO TO 225
      IF(CNS.EQ.0) GO TO 225
      KMS=KM*(10**((2.25-4.45*CNS/100)*NCM))*((.7+5.33*CNS/100)**NM)
      FACTM=(NM*52.)/(NCM*12.)
      CMAXM=21.8*(KMS**(-1/NCM))*((CNS/100.)**(-NM/NCM))
      IF (CIS.LT.CMAXM) GO TO 225
      QM=FACTM*(CIS-CMAXM)
      IF(QM.LT.CNS) GO TO 215
      CARMS=CARMS+CNS/FACTM
      CIS=CIS-CNS/FACTM
      CNS=0
      GO TO 225
215   CONTINUE
      CARMS=CARMS+CIS-CMAXM
      CNS=CNS-FACTM*(CIS-CMAXM)
      CIS=CMAXM
225   CONTINUE
      IF(KP.EQ.0) GO TO 290
      IF(CNS.EQ.0) GO TO 290
      P=23.*SQRT(CNS)
```

```
      IF(P.GT.100.) P=100.
      KPS=KP*(10**((2.25-4.45*CNS/100)*NCP))*((.7+5.33*CNS/100)**NP)
      FACTP=(NP*52.)/(NCP*12.)
      CMAXP=21.8*(KPS**(-1/NCP))*((CNS/100.)**(-NP/NCP))
      IF(CIS.LT.CMAXP) GO TO 290
      QN=FACTP*(CIS-CMAXP)
      IF(QN.LT.CNS) GO TO 275
      CARPS=CARPS+CNS/FACTP
      CIS=CIS-CNS/FACTP
      CNS=0
      GO TO 290
275   CONTINUE
      CARPS=CARPS+CIS-CMAXP
      CNS=CNS-FACTP*(CIS-CMAXP)
      CIS=CMAXP
290   CONTINUE
      IF(KN.EQ.0) GO TO 250
      IF(CNS.EQ.0) GO TO 250
      KNS=KN*(10**((2.25-4.45*CNS/100)*NCN))*((.7+5.33*CNS/100)**NN)
      FACTN=(NN*52.)/(NCN*12.)
      CMAXN=21.8*(KNS**(-1/NCN))*((CNS/100.)**(-NN/NCN))
      IF(CIS.LT.CMAXN) GO TO 250
      QN=FACTN*(CIS-CMAXN)
      IF(QN.LT.CNS) GO TO 235
      CARNS=CARNS+CNS/FACTN
      CIS=CIS-CNS/FACTN
      CNS=0
      GO TO 250
235   CONTINUE
      CARNS=CARNS+CIS-CMAXN
      CNS=CNS-FACTN*(CIS-CMAXN)
      CIS=CMAXN
250   CONTINUE
 C    START LOOP
      DO 400 LT=1,NQ,1
 C    FORM D
      D(1)=(DELT*D11/(2*DELX**2))*(2*CI(1)-CI(2)-2*CIS)-CI(1)
     1+(DELT*D12/(2*DELX**2))*(2*CM(1)-CM(2)-2*CMS)
     1+(DELT*D13/(2*DELX**2))*(2*CN(1)-CN(2)-2*CNS)
      D(2)=(DELT*D22/(2*DELX**2))*(2*CM(1)-CM(2)-2*CMS)-CM(1)
      D(3)=(DELT*D33/(2*DELX**2))*(2*CN(1)-CN(2)-2*CNS)-CN(1)
      DO 300 I=2,NX-1,1
```

```
      D(3*I-2) = (DELT*D11/(2*DELX**2))*(2*CI(I)-CI(I+1)-CI(I-1))
     1-CI(I)+(DELT*D12/(2*DELX**2))*(2*CM(I)-CM(I-1)-CM(I+1))+
     1(DELT*D13/(2*DELX**2))*(2*CN(I)-CN(I-1)-CN(I+1))
      D(3*I-1)=(DELT*D22/(2*DELX**2))*(2*CM(I)-CM(I+1)-CM(I-1))-
     1CM(I)
      D(3*I) = ((DELT*D33/(2*DELX**2))*(2*CN(I)-CN(I+1)-CN(I-1)))-
     1CN(I)
300   CONTINUE
      D(3*NX-2)=(DELT*D11/(2*DELX**2))*(-CI(NX-1))-CI(NX)
     1+(DELT*D12/(2*DELX**2))*(-CM(NX-1))
     1+(DELT*D13/(2*DELX**2))*(-CN(NX-1))
      D(3*NX-1)=(DELT*D22/(2*DELX**2))*(
     1-CM(NX-1))-CM(NX)
      D(3*NX)=(DELT*D33/(2*DELX**2))*
     1(-CN(NX-1))-CN(NX)
C     SOLVE SYSTEM OF EQUATIONS
      CALL VMULFF (MAT,D,90,90,1,90,90,X,90,IERR)
C     FROM X FORM CONCENTRATION VECTORS
      DO 400 I=1,NX,1
      CI(I) = X(3*I-2)
      CM(I) = X(3*I-1)
      CN(I) = X(3*I)
      IF(I.NE.1) GO TO 320
      CIS=CIS0
C     FLUX OR SURFACE CONDITION?
      IF (FLUX.EQ.0)GO TO 302
      CIS = CI(1)+FLUX*DELX/D11
302   CONTINUE
C     REACTION AT SURFACE?
      IF(KT.EQ.0)GO TO 311
      IF(CMS.EQ.0) GO TO 311
      KTS=KT*(10**((2.25-4.45*CNS/100)*NCT))
      CMAXT=21.8*(KTS**(-1/NCT))*((CMS/160.)**(-NT/NCT))
      IF (CIS.LT.CMAXT) GO TO 311
      QM=FACTT*(CIS-CMAXT)
      IF(QM.LT.CMS) GO TO 306
      CARTS=CARTS+CMS/FACTT
      CIS=CIS-CMS/FACTT
      CMS=0
      GO TO 311
306   CONTINUE
      CARTS=CARTS+CIS-CMAXT
```

```
      CMS=CMS-FACTT*(CIS-CMAXT)
      CIS=CMAXT
311   CONTINUE
      IF(KM.EQ.0)GO TO 310
      IF(CNS.EQ.0) GO TO 310
      KMS=KM*(10**((2.25-4.45*CNS/100)*NCM))*((.7+5.33*CNS/100)**NM)
      FACTM=(NM*52.)/(NCM*12.)
      CMAXM=21.8*(KMS**(-1/NCM))*((CNS/100.)**(-NM/NCM))
      IF (CIS.LT.CMAXM) GO TO 310
      QM=FACTM*(CIS-CMAXM)
      IF(QM.LT.CNS) GO TO 305
      CARMS=CARMS+CNS/FACTM
      CIS=CIS-CNS/FACTM
      CNS=0
      GO TO 310
305   CONTINUE
      CARMS=CARMS+CIS-CMAXM
      CNS=CNS-FACTM*(CIS-CMAXM)
      CIS=CMAXM
310   CONTINUE
      IF(KP.EQ.0) GO TO 322
      IF(CNS.EQ.0) GO TO 322
      KPS=KP*(10**((2.25-4.45*CNS/100)*NCP))*((.7+5.33*CNS/100)**NP)
      FACTP=(NP*52.)/(NCP*12.)
      CMAXP=21.8*(KPS**(-1/NCP))*((CNS/100.)**(-NP/NCP))
      IF(CIS.LT.CMAXP) GO TO 322
      QN=FACTP*(CIS-CMAXP)
      IF(QN.LT.CNS) GO TO 317
      CARPS=CARPS+CNS/FACTP
      CIS=CIS-CNS/FACTP
      CNS=0
      GO TO 322
317   CONTINUE
      CARPS=CARPS+CIS-CMAXP
      CNS=CNS-FACTP*(CIS-CMAXP)
      CIS=CMAXP
322   CONTINUE
      IF(KN.EQ.0) GO TO 320
      IF(CNS.EQ.0) GO TO 320
      KNS=KN*(10**((2.25-4.45*CNS/100)*NCN))*((.7+5.33*CNS/100)**NN)
      FACTN=(NN*52.)/(NCN*12.)
      CMAXN=21.8*(KNS**(-1/NCN))*((CNS/100.)**(-NN/NCN))
```

```
      IF(CIS.LT.CMAXN) GO TO 320
      QN=FACTN*(CIS-CMAXN)
      IF(QN.LT.CNS) GO TO 315
      CARNS=CARNS+CNS/FACTN
      CIS=CIS-CNS/FACTN
      CNS=0
      GO TO 320
315   CONTINUE
      CARNS=CARNS+CIS-CMAXN
      CNS=CNS-FACTN*(CIS-CMAXN)
      CIS=CMAXN
320   CONTINUE
 C    REACTION?
      IF(KT.EQ.0)GO TO 351
      IF(CM(I).EQ.0) GO TO 351
      KTS=KT*(10**((2.25-4.45*CN(I)/100)*NCT))
      CMAXT=21.8*(KTS**(-1/NCT))*((CM(I)/160.)**(-NT/NCT))
      IF (CI(I).LT.CMAXT) GO TO 351
      QM=FACTT*(CI(I)-CMAXT)
      IF(QM.LT.CM(I)) GO TO 326
      CART(I)=CART(I)+CM(I)/FACTT
      CI(I)=CI(I)-CM(I)/FACTT
      CM(I)=0
      GO TO 351
326   CONTINUE
      CART(I)=CART(I)+CI(I)-CMAXT
      CM(I)=CM(I)-FACTT*(CI(I)-CMAXT)
      CI(I)=CMAXT
351   CONTINUE
      IF(KM.EQ.0)GO TO 350
      IF(CN(I).EQ.0) GO TO 350
      KMS=KM*(10**((2.25-4.45*CN(I)/100)*NCM))
     1*((.7+5.33*CN(I)/100)**NM)
      FACTM=(NM*52.)/(NCM*12.)
      CMAXM=21.8*(KMS**(-1/NCM))*((CN(I)/100.)**(-NM/NCM))
      IF (CI(I).LT.CMAXM) GO TO 350
      QM=FACTM*(CI(I)-CMAXM)
      IF(QM.LT.CN(I)) GO TO 325
      CARM(I)=CARM(I)+CN(I)/FACTM
      CI(I)=CI(I)-CN(I)/FACTM
      CN(I)=0
      GO TO 350
```

```
325   CONTINUE
      CARM(I)=CARM(I)+CI(I)-CMAXM
      CN(I)=CN(I)-FACTM*(CI(I)-CMAXM)
      CI(I)=CMAXM
350   CONTINUE
      IF(KP.EQ.0) GO TO 450
      IF(CN(I).EQ.0) GO TO 450
      KPS=KP*(10**((2.25-4.45*CN(I)/100)*NCP))
     1*((.7+5.33*CN(I)/100)**NP)
      FACTP=(NP*52.)/(NCP*12.)
      CMAXP=21.8*(KPS**(-1/NCP))*((CN(I)/100.)**(-NP/NCP))
      IF(CI(I).LT.CMAXP) GO TO 450
      QN=FACTP*(CI(I)-CMAXP)
      IF(QN.LT.CN(I)) GO TO 425
      CARP(I)=CARP(I)+CN(I)/FACTP
      CI(I)=CI(I)-CN(I)/FACTP
      CN(I)=0
      GO TO 450
425   CONTINUE
      CARP(I)=CARP(I)+CI(I)-CMAXP
      CN(I)=CN(I)-FACTP*(CI(I)-CMAXP)
      CI(I)=CMAXP
450   CONTINUE
      IF(KN.EQ.0) GO TO 400
      IF(CN(I).EQ.0) GO TO 400
      KNS=KN*(10**((2.25-4.45*CN(I)/100)*NCN))
     1*((.7+5.33*CN(I)/100)**NN)
      FACTN=(NN*52.)/(NCN*12.)
      CMAXN=21.8*(KNS**(-1/NCN))*((CN(I)/100.)**(-NN/NCN))
      IF(CI(I).LT.CMAXN) GO TO 400
      QN=FACTN*(CI(I)-CMAXN)
      IF(QN.LT.CN(I)) GO TO 375
      CARN(I)=CARN(I)+CN(I)/FACTN
      CI(I)=CI(I)-CN(I)/FACTN
      CN(I)=0
      GO TO 400
375   CONTINUE
      CARN(I)=CARN(I)+CI(I)-CMAXN
      CN(I)=CN(I)-FACTN*(CI(I)-CMAXN)
      CI(I)=CMAXN
400   CONTINUE
C     END LOOP
```

```
C    FORM OUTPUT VECTORS
     DO 600 I=1,NX,1
     XA(I+1)=I*DELX
     XC(I+1)=CI(I)+CARM(I)+CARN(I)
    1+CARP(I)+CART(I)
     XM(I+1)=CM(I)
     CAT(I+1)=CART(I)
     CAM(I+1)=CARM(I)
     CAP(I+1)=CARP(I)
     CAN(I+1)=CARN(I)
     XN(I+1)=CN(I)
600  CONTINUE
     XC(1)=CIS+CARMS+CARNS
    1+CARPS+CARTS
     XM(1)=CMS
     XN(1)=CNS
     CAT(1)=CARTS
     CAM(1)=CARMS
     CAP(1)=CARPS
     CAN(1)=CARNS
     WRITE(21,103)
103 FORMAT(4X,'XA',7X,'XC',7X,'XM',7X,'XN',
    17X,'1ST&2ND M CARB.',3X,'1ST&2ND CR CARBIDE',/)
     WRITE(21,14)(XA(I),XC(I),XM(I),XN(I),CAT(I),CAM(I),CAP(I),
    1CAN(I),I=1,NX+1)
     ARC=0
     ART=0.
     ARM=0.
     ARP=0.
     ARN=0.
     DO 1111 I=1,30
     ARC=ARC+XC(I)*DELX+.5*(XC(I+1)-XC(I))*DELX
     ART=ART+CAT(I)*DELX+.5*(CAT(I+1)-CAT(I))*DELX
     ARM=ARM+CAM(I)*DELX+.5*(CAM(I+1)-CAM(I))*DELX
     ARP=ARP+CAP(I)*DELX+.5*(CAP(I+1)-CAP(I))*DELX
     ARN=ARN+CAN(I)*DELX+.5*(CAN(I+1)-CAN(I))*DELX
1111 CONTINUE
     ARTC=ART+ARM+ARP+ARN
     WRITE(21,18)TMAX,FLUX,NUM
     WRITE(21,111)
     WRITE(21,20) D11,D12,D13,D22,D33
     WRITE(21,211)
```

```
      WRITE(21,22) CIS,CMS,CNS,CI0,CM0,CN0
      WRITE(21,3) KT,NCT,NT,FACTT
      WRITE(21,19) KM,NCM,NM,FACTM
      WRITE(21,21) KP,NCP,NP,FACTP
      WRITE(21,23) KN,NCN,NN,FACTN
      IF(D13.EQ.0.) GO TO 61
      WRITE(21,63)
63    FORMAT(1X,'TERNARY')
      GO TO 399
61    WRITE(21,64)
64    FORMAT(1X,'BINARY')
399   WRITE(21,36)ARC,ART,ARM
36    FORMAT(1X,'ARC=',F6.4,4X,'ART=',F6.4,4X,'ARM=',F6.4)
      WRITE(21,37)ARP,ARN,ARTC
37    FORMAT(1X,'ARP=',F6.4,4X,'ARN=',F6.4,4X,'ARTC=',F6.4)
111   FORMAT(1X,'DIFFUSION COEFFICIENT;D11,D12,D13,D22,D33')
211   FORMAT(1X,'INITIAL CONDITIONS')
3     FORMAT(1X,'FOR REACTION 1',4E12.3)
19    FORMAT(1X,'FOR REACTION 2',4E12.3)
21    FORMAT(1X,'FOR REACTION 3',4E12.3)
23    FORMAT(1X,'FOR REACTION 4',4E12.3)
14    FORMAT(1X,8F9.4)
18    FORMAT(1X,'TIME=',F12.3,3X,'FLUX=',E12.3,3X,'INPUT #',I3)
20    FORMAT(1X,5E12.3)
22    FORMAT(1X,6E11.3)
      STOP
      END
```

The vita has been removed from the scanned document